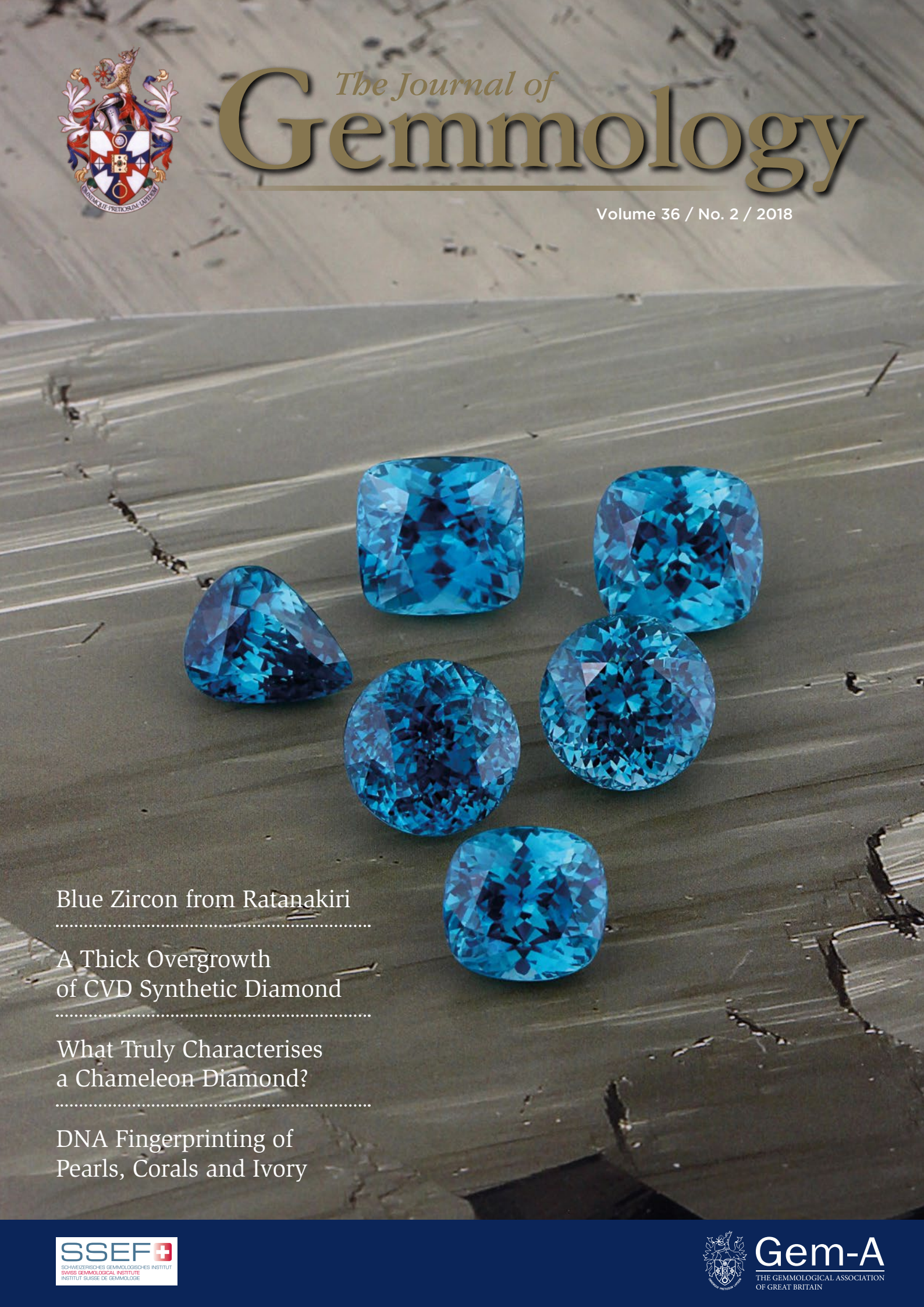

The Journal of
Gemmology

Volume 36 / No. 2 / 2018

Blue Zircon from Ratanakiri

A Thick Overgrowth of CVD Synthetic Diamond

What Truly Characterises a Chameleon Diamond?

DNA Fingerprinting of Pearls, Corals and Ivory

SSEF
SCHWEIZERISCHES GEMMOLOGISCHES INSTITUT
SWISS GEMMOLOGICAL INSTITUTE
INSTITUT SUISSE DE GEMMOLOGIE

Gem-A
THE GEMMOLOGICAL ASSOCIATION OF GREAT BRITAIN

SSEF

SCHWEIZERISCHES GEMMOLOGISCHES INSTITUT
SWISS GEMMOLOGICAL INSTITUTE
INSTITUT SUISSE DE GEMMOLOGIE

ORIGIN DETERMINATION · TREATMENT DETECTION

DIAMOND GRADING · PEARL TESTING

EDUCATION · RESEARCH

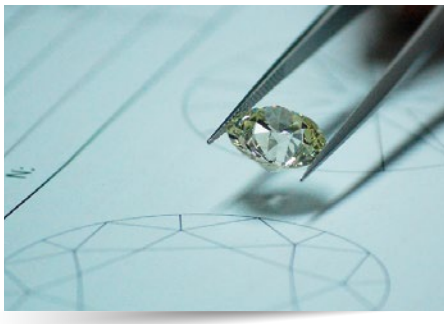

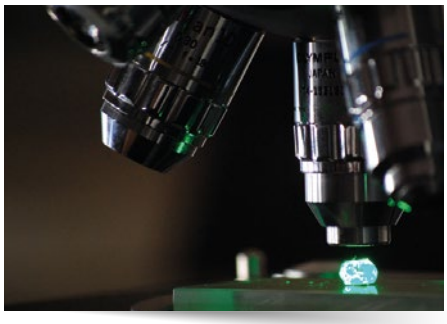

THE SCIENCE OF GEMSTONE TESTING™

Aeschengraben 26, 4051 Basel, Switzerland Tel. +41 61 262 06 40 Fax + 41 61 262 06 41 admin@ssef.ch www.ssef.ch

The Journal of Gemmology

Volume 36 / No. 2 / 2018

COLUMNS

Cover photo: *Zircon from Cambodia (here, 8.92–15.17 ct) is prized for its bright blue colour after undergoing heat treatment. The properties of this zircon are described in an article by Manuela Zeug and co-authors on pp. 112–132 of this issue. Photo by Prasit Prachagool, Thai Lanka Trading Ltd Part., Bangkok, Thailand.*

ARTICLES

Photo by M. Zeug

The Journal is published by Gem-A in collaboration with SSEF and with the support of AGL.

Gem-A THE GEMMOLOGICAL ASSOCIATION OF GREAT BRITAIN

SSEF SCHWEIZERISCHES GEMMOLOGISCHES INSTITUT SWISS GEMMOLOGICAL INSTITUTE INSTITUT SUISSE DE GEMMOLOGIE

AGL AMERICAN GEMOLOGICAL LABORATORIES

The Journal of Gemmology

CONTENT SUBMISSION

The Editor-in-Chief is glad to consider original articles, news items, conference/excursion reports, announcements and calendar entries on subjects of gemmological interest for publication in *The Journal of Gemmology*. A guide to the various sections and the preparation of manuscripts is given at www.gem-a.com/index.php/news-publications/publications/journal-of-gemmology/submissions, or contact the Editor-in-Chief.

SUBSCRIPTIONS

Gem-A members receive *The Journal* as part of their membership package, full details of which are given at www.gem-a.com/membership. Laboratories, libraries, museums and similar institutions may become direct subscribers to *The Journal*.

ADVERTISING

Enquiries about advertising in *The Journal* should be directed to advertising@gem-a.com. For more information, see https://gem-a.com/index.php/news-publications/publications/journal-of-gemmology/advertising.

DATABASE COVERAGE

The Journal of Gemmology is covered by the following abstracting and indexing services: Australian Research Council academic journal list, British Library Document Supply Service, Chemical Abstracts (CA Plus), Copyright Clearance Center's RightFind application, CrossRef, EBSCO (Academic Search International, Discovery Service and TOC Premier), Gale/Cengage Learning Academic OneFile, GeoRef, Index Copernicus ICI Journals Master List, Mineralogical Abstracts, Cambridge Scientific Abstracts (ProQuest), Scopus and the Thomson Reuters' Emerging Sources Citation Index (in the Web of Science).

COPYRIGHT AND REPRINT PERMISSION

Design & production by Zest Design, www.zest-uk.com

Printed by DG3 Group (Holdings) Ltd

ISSN: 1355-4565

Gem-A
THE GEMMOLOGICAL ASSOCIATION OF GREAT BRITAIN

21 Ely Place
London EC1N 6TD
UK
t: +44 (0)20 7404 3334
f: +44 (0)20 7404 8843
e: information@gem-a.com
w: www.gem-a.com

Registered Charity No. 1109555
A company limited by guarantee and registered in England No. 1945780
Registered office: Palladium House, 1–4 Argyll Street, London W1F 7LD

What's New

INSTRUMENTATION

GemTrue Veritas

Released in early 2018, the GemTrue Veritas is the latest diamond tester from DiKai Industrial (Shenzhen, China), a compact unit designed to distinguish natural diamond from CVD/HPHT synthetics and synthetic moissanite. The tester operates on four AAA batteries or USB, calibrates automatically upon start-up, and indicates results via an LED display. Limited information is available at www.dikaitools.com/en/Diamond_Testers_Moissanite_Testers/20170909/636.html. *CMS*

Synthetic Diamond Identification Kit

In January 2018, the Mediterranean Gemmological and Jewellery Conference store began offering its Synthetic Diamond Identification Kit, a zippered, fitted pouch with three instruments and two booklets assembled to provide everything the gemmologist-on-the-go needs to separate synthetic, treated and natural diamonds. The kit contains a Gemetrix PL-Inspector UV lamp (see *The Journal*, Vol. 35, No. 5, 2017, p. 373), a miniature folding polariscope and a portable light. Accompanying these is a handbook titled *Fluorescence as a Tool for Diamond Origin Identification—a Guide* (see *The Journal*, Vol. 35, No. 5, 2017, p. 374), along with tweezers, a loupe and a stone-cleaning cloth. Visit www.gemconference.com/store/instruments/synthetic-diamond-identification-kit. *CMS*

NEWS AND PUBLICATIONS

11th International Kimberlite Conference Abstracts and Field Trip Guidebooks

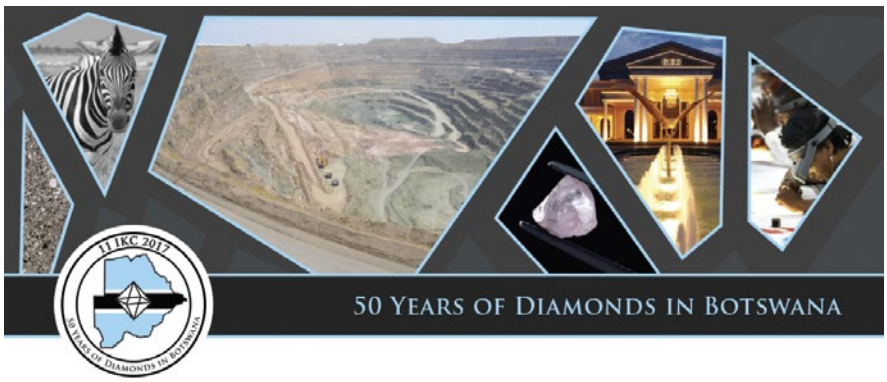

Extended abstracts of oral and poster presentations from the 11th International Kimberlite Conference (held 18–22 September 2017 in Gaborone, Botswana) are available for individual download at http://11ikc.com/long_abstract/oral.htm and http://11ikc.com/long_abstract/poster.htm. In addition, field trip guidebooks for two of the excursions (Trip 2—Kimberley region, South Africa and Trip 4—Lesotho) can be downloaded at http://11ikc.com/showcontent.aspx?MenuID=1998. *CMS*

ASEAN Gem & Jewelry Review

Issue 1, 2018, of this English-language gem and jewellery trade publication for the Association of Southeast Asian Nations (ASEAN) focuses on trade developments in Thailand, Malaysia and Myanmar, as well as export statistics and trade news for the ASEAN area. A centrefold map highlights the major gem and jewellery production sources for member countries in Southeast Asia. Download the issue at www.git.or.th/thai/info_center/trade_review/2018/ASEAN_Gem_Review_issue1.pdf. *CMS*

De Beers Diamond Insight Report 2017

This De Beers Group report profiles the diamond industry value chain (downstream, midstream and upstream segments, as well as focusing on China) and then examines three key trends pertaining to the female consumer (increased participation of women in the economy, changing family and personal relationships, and femininity redefined). Global consumer demand for diamond jewellery in 2017 was mainly driven by the USA market and climbed to a total of US$82 billion, an all-time high and a 2% increase on the previous year. The document concludes with an outlook for 2018. View or download the report at www.debeersgroup.com/en/reports/insight/insight-reports/insight-report-2017/overview.html. *BML*

GIT Lab Update: Rare Poudretteite


LAB UPDATE

RARE PINK POUDRETTEITE

In April 2018, The Gem and Jewelry Institute of Thailand (GIT) in Bangkok released a report titled 'Rare Pink Poudretteite'. It describes a 1.38 ct faceted pink stone that was submitted to GIT's laboratory for identification. The sample's RI and SG distinguished it from similar-appearing gems such as tourmaline, kunzite and morganite, and its Raman spectrum matched poudretteite. The pink colour is rare for facet-quality material; poudretteite is usually colourless. Download this and previous GIT lab updates at www.git.or.th/articles_technic_en.html. *CMS*

Inhorgenta 2018 Presentations

Videos of seminar presentations and/or speaker interviews from the February 2018 Inhorgenta Munich show can now be accessed at http://inhorgenta.com/events-news/inhorgenta-forum/program/index.html, and a list of the presentations is available at http://jlm-guides.de/INHORGENTA_MUNICH/en/seminar-programme. The topics include pearls, coloured stones, diamond, watches, online sales and future trends. *BML*

PDAC 2018 THE WORLD'S PREMIER MINERAL EXPLORATION & MINING CONVENTION

PDAC 2018 Diamond Abstracts

The Prospectors & Developers Association of Canada convention held March 2018 featured a special session titled 'The 25th Anniversary of Canadian Diamond Mining: The Next Generation'. The session featured six presentations that covered various Canadian diamond deposits, including Renard in Quebec, Chidliak in Nunavut, Star and Orion South in Saskatchewan, and three mines in the Northwest Territories: Gahcho Kué, Ekati, and Diavik. Abstracts of all but the Diavik presentation are available at http://tinyurl.com/ycx8xqto.

CMS

OTHER RESOURCES

Diamond Terminology Guideline

Nine diamond industry organisations (AWDC, CIBJO, DPA, GJEPC, IDI, IDMA, USJC, WDC and WFDB) have worked together to develop the Diamond Terminology Guideline, which was released in January 2018. The Guideline is intended to be a reference document for the diamond and jewellery trade to encourage the use of clear, fair, and effective terminology pertaining to natural and synthetic diamonds and diamond simulants. The Guideline is based on the ISO 18323 standard *Jewellery – Consumer Confidence in the Diamond Industry* and the *CIBJO Diamond Blue Book*. It is available on the Diamond Producers Association website at www.diamondproducers.com/diamond-industry/diamond_terminology. *CMS*

Gemworld Pricing Calculator

Recently, Gemworld International released a new diamond and gem pricing calculator called GemGuide Pricing, which is freely available for desktop computers and also can be downloaded as an app for iOS and Android mobile devices. To access pricing information, users must have a current subscription to *GemGuide*.

The calculator works for both diamonds and coloured stones. For diamonds, enter any set of parameters and the weight, and the calculator returns a wholesale price or a retail price using your mark-up. Parameters that will automatically adjust the price include cut grade and fluorescence. For coloured stones, the user can input a colour from any grading system including Gemworld's own World of Color. When using World of Color, and entering the clarity and cut features, the calculator will automatically price the gem, again at wholesale or retail. The calculator interactively determines gem pricing, and when using colour grading systems other World of Color, the user can override the grade and the software will then calculate a price. By selecting other attributes of clarity and cut, the grade will automatically adjust by taking appropriate deductions. When finished, an estimated price is provided, both per carat and per stone. More than 70 coloured stone varieties are priced. In addition, the calculator will convert to any of 33 international currencies.

To access GemGuide Pricing, visit https://app.gemguide.com. To download the app, search the app stores for 'GemGuide Pricing'. For more information, visit www.gemguide.com/the-gemguide/pricing-app-tutorial.

Richard B. Drucker
Gemworld International Inc.
Glenview, Illinois, USA

What's New provides announcements of new instruments/technology, publications, online resources and more. Inclusion in What's New does not imply recommendation or endorsement by Gem-A. Entries were prepared by Carol M. Stockton (CMS) or Brendan M. Laurs (BML), unless otherwise noted.

Gem Notes

COLOURED STONES

Figure 1: Some of the aragonites from the Czech Republic displayed during the 2018 Tucson gem shows include these stones (12.61–15.94 ct) that were faceted by Luigi Mariani. Photo by Mauro Pantò.

Aragonite from the Czech Republic

The gem and mineral shows that take place every February in Tucson, Arizona, USA, are an excellent place to see rare and collectable gemstones. Among the many items on display at the 2018 shows was an attractive array of faceted aragonite from the Czech Republic (e.g. Figure 1). The stones were shown by Mauro Pantò (The Beauty in the Rocks, Sassari, Italy), who had 12 gems weighing up to 21.83 ct that were cut from two pieces of rough material he had purchased in Tucson in 2016. They ranged from near-colourless to pale yellow or brownish yellow, and showed colourful dispersion.

Figure 2: Weighing an impressive 74.31 ct, this pale yellowish brown aragonite is an example of the larger stones obtained from Cicov Hill in the Czech Republic. Photo by J. Hyršl.

Faceted aragonite is rather rare in the gem trade, and cut stones usually weigh up to several carats. The most significant production of gem-quality rough material has come from the Czech Republic, where it has been mined since the early 19th century (Hyrsl, 1996). The most important locality is Cicov Hill near Horenec, in the Bílina region of north-western Czech Republic (Filippi and Hyrsl, 2004). Gem-quality portions of crystals from this locality may occasionally attain dimensions of 1–2 cm, yielding faceted stones that are quite large (e.g. Figure 2). Cicov Hill is the source of some of the world's largest faceted aragonites (some exceeding 100 ct), but they are very rare.

It is not known when the rough material was found that was faceted into the stones seen recently in Tucson, but these attractive gems show that good-quality aragonite from the Czech Republic still occasionally becomes available in the marketplace.

Brendan M. Laurs FGA

Dr Jaroslav Hyršl
Prague, Czech Republic

References

Filippi M. and Hyrsl J., 2004. Aragonite from Cicov Hill in the Czech Republic. *Mineralogical Record*, **35**, 137–142.

Hyrsl J., 1996. Gem aragonite from the Czech Republic. *Canadian Gemmologist*, **17**(3), 76–77.

Large Green Beryls from Pancas, Brazil

For decades, the Pancas area of Espírito Santo State in eastern Brazil has been known as a source of gem-quality chrysoberyl and beryl (Cassedanne and Roditi, 1993; Reys, 2017). Recently a significant discovery of green beryl occurred there, and in January 2017 the crystals were brought to the Tucson gem shows, where they were purchased by Joe Jelks (Horizon Mineral Lapidary, Lewes, Delaware, USA). The parcel weighed a total of 3.83 kg, and the largest crystal was 1.24 kg and approximately 14 cm long. The colour of the beryl varied from 'mint' green to yellow-green (e.g. Figure 3). The crystals were heavily etched, and contained portions that were 'silky' as well as large clean facet-grade areas.

Jelks partnered with gem cutter Frank Schaffer (FGS Gems, Philadelphia, Pennsylvania, USA), who had experience with faceting larger stones for the collector market (Figure 4). After mapping each piece and sawing out the cleanest areas, the first stone was produced: a 104 ct Portuguese-cut round measuring 63 mm in diameter (Figure 5, left). Over the course of a one-year period, cutting of the rest of the parcel yielded a total of approximately 3,400 carats. The largest stones consisted of a 747 ct cushion, 499 ct teardrop, 487 ct cushion and 363 ct trilliant (Figure 5, right). A number of smaller stones in the 60–100 ct range were also produced. In addition, several cabochons were cut that exhibited strong chatoyancy. Rather than heating the material to obtain a bluer hue, Jelks and Shaffer retained the natural green colour of the beryl. The stones were exhibited for the first time at the 2018 Tucson gem shows.

Although mining in Brazil has slowed in recent years (Reys, 2017), this find shows that significant gems are still occasionally produced there.

Brendan M. Laurs FGA

Figure 3: Some of the large green beryl crystals produced recently from the Pancas area of Brazil are shown here. The largest crystal is ~9 cm long. Photo by Joe Jelks.

Figure 4: A 363 ct 'mint'-green beryl from Pancas is shown being cut by Frank Schaffer. The stone measures approximately 70 × 55 mm. Photo by Joe Jelks.

References

Cassedanne J. and Roditi M., 1993. The location, geology, mineralogy and gem deposits of alexandrite, cat's-eye and chrysoberyl in Brazil. *Journal of Gemmology*, **23**(6), 333–354, https://dx.doi.org/10.15506/jog.1993.23.6.333.

Reys A., 2017. Coloured stone mining and trade in Brazil: A brief history and current status. *Journal of Gemmology*, **35**(8), 708–726, http://dx.doi.org/10.15506/JoG.2017.35.8.708.

Figure 5: The Portuguese-cut green beryl on the left (named 'The Headlight') weighs 104 ct, while the green beryl trilliant on the right is 363 ct. Photos by Joe Jelks.

Chrysocolla Chalcedony with Native Copper Inclusions

Chrysocolla chalcedony, or 'gem silica', is a blue-to-green gem material that is commonly polished into cabochons and beads, and is known mainly from Peru (Hyršl, 2001). Its attractive colouration is caused by dispersed inclusions of chrysocolla within the chalcedony host. Fine-quality material typically has a rather homogeneous colour appearance, but at the February 2018 Tucson gem shows a distinctive cabochon with obvious metallic inclusions was seen among many samples of 'gem silica' that were displayed by Larry Woods (Jewels from the Woods, Blanco, Texas, USA). Woods obtained the rough material several years ago, when it reportedly came from a new deposit in northern India. The ~20 kg of mixed-quality rough material ranged from light blue to deep greenish blue. Cutting has yielded dozens of stones, but the metallic inclusions were retained in only one of them that has been polished so far (39.05 ct; see Figure 6).

Woods loaned the 39.05 ct specimen for examination, and energy-dispersive X-ray fluorescence (EDXRF) chemical analysis of the inclusions by author NDR yielded a strong signal for Cu, as expected for their

Figure 6: Weighing 39.05 ct, this 'gem silica' cabochon contains obvious inclusions of native copper. Photo by Robison McMurtry, © GIA.

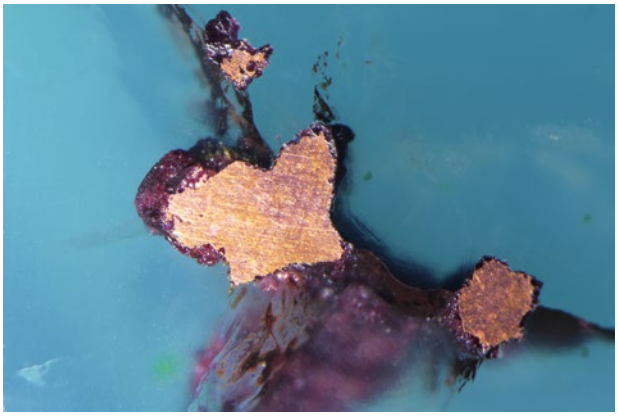

Figure 7: The native copper inclusions in the gem silica are surrounded by a thin coating of cuprite. The coppery metallic lustre is only seen where the inclusions intersect the polished surface of the cabochon. Photomicrograph by N. D. Renfro, © GIA; image width 3.86 mm.

appearance resembling native copper where they intersected the polished surface of the cabochon (Figure 7). The copper inclusions were surrounded by a thin opaque reddish purple coating that was identified as cuprite by Raman analysis.

While it is not uncommon for native copper, cuprite and chrysocolla to be associated with one another in copper deposits, it is rather unusual for copper/cuprite inclusions to occur in otherwise pure gem-quality chrysocolla chalcedony. The only similar occurrence known to the authors is blue chalcedony from Bolivia (see www.gemstonemagnetism.com/overview_p_4-_the_magnetic_metals_that_color_gems.html).

Brendan M. Laurs FGA

Nathan D. Renfro
Gemological Institute of America
Carlsbad, California, USA

Reference

Hyršl J., 2001. Gemstones of Peru. *Journal of Gemmology*, **27**(6), 328–334, http://dx.doi.org/10.15506/jog.2001.27.6.328.

Colourless Cordierite—and Quartz—from Tanzania

Cordierite, often referred to as *iolite* by gemmologists, is typically encountered in the gem trade as a blue stone that may resemble sapphire and, therefore, is also called 'water sapphire'. In addition, very rare colourless cordierite has been documented from Sri Lanka (Bank, 1985; Zwaan, 1986, 1996), and is also known to occur in Tanzania and Madagascar (Hanus et al., 2016). The properties of the Sri Lankan samples examined by Bank (1985) were: RIs—1.527–1.536, birefringence—0.009 and SG—2.55. Zwaan (1996) obtained RI readings from a group of stones that ranged from 1.520 (lowest) to 1.541 (highest), and an SG of 2.57. Compared to typical blue cordierite, the very low RI and SG values—as

Figure 8: These rough and cut stones all originated from the same parcel that was represented as colourless cordierite. Despite their similar overall appearance, the two samples on the left proved to be quartz while the other three are cordierite. The faceted stones weigh 1.08–5.85 ct. Photo by Robison McMurtry, © GIA.

well as the lack of pleochroic blue colouration—are consistent with depleted Fe and high Mg contents, and Zwaan (1986, 1996) further mentioned that the Sri Lankan material had up to 95 mol.% occupancy of the Mg sites. In addition, Johnson and Koivula (1998) documented a colourless cordierite from an unspecified locality with slightly higher properties that were indistinguishable from plagioclase (RIs—1.531–1.541, birefringence—0.010, optic character—biaxial positive, and SG—2.62).

During the February 2017 Tucson gem shows, Adam Pearl (East African Gem Traders Ltd, Nairobi, Kenya and Cleveland, Ohio, USA) showed one of the authors (BML) a small parcel of colourless rough material that his supplier represented as cordierite, and this identity was subsequently confirmed for one of the pieces by Raman analysis. The stones reportedly came from central Tanzania, and about 300 g of rough material were produced. All of the pieces showed evidence of chemical etching, and were transparent with a slightly hazy appearance (e.g. Figure 8). Pearl faceted the largest stone in the parcel, but when he submitted it for a laboratory report he was surprised to learn that it was quartz. Pearl then faceted two more stones, and Raman analysis by author NDR showed that one of them was quartz and the other was cordierite (again, see Figure 8). Two pieces of rough from the parcel were also identified as cordierite by Raman analysis. The gemmological properties of the faceted cordierite were as follows: RIs—1.529–1.540, birefringence—0.011, optic character—biaxial positive, and SG—2.52.

Despite the very similar colourless hazy appearance of both the cordierite and quartz to the unaided eye, microscopic examination of the samples showed that their inclusions were very different. While the quartz contained fine needles throughout the stones, the cordierite displayed some discernible etch tubes along with finely textured, linear patterned clouds that gave the stones an overall slightly milky appearance (Figure 9). These features were consistent in both of the faceted quartzes and in the three cordierites (two rough and one cut) that were examined.

It is an interesting coincidence that cordierite and quartz with quite similar appearances were mixed in the same parcel of rough material, and this is particularly unusual given the rarity of colourless cordierite. Nevertheless, they can be readily separated by their optic character, SG values and inclusions.

Brendan M. Laurs FGA and Nathan D. Renfro

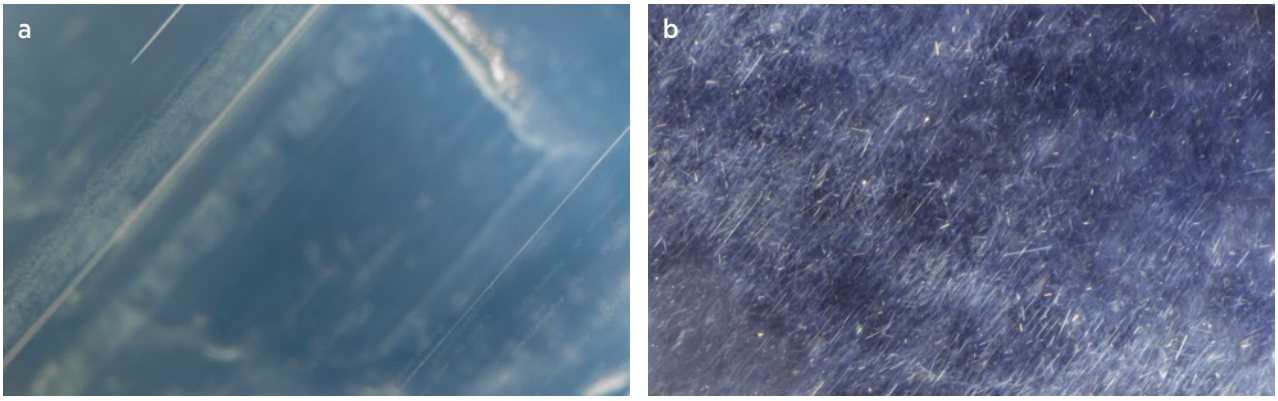

Figure 9: (a) The slightly milky appearance of the cordierite is due to fine linear clouds, seen here with a few etch tubes. **(b)** The hazy appearance of the quartz is caused by the presence of fine needles throughout the stone. Photomicrographs by N. D. Renfro, © GIA; image widths 4.10 mm.

References

Bank H., 1985. Farblose Cordierite und Cordierit-Katzenaugen aus Sri Lanka (Colourless cordierite and cat's-eye cordierite from Sri Lanka). *Zeitschrift der Deutschen Gemmologischen Gesellschaft*, **34**(1/2), 79–80.

Hanus R., Kusá I. and Kasíková J., 2016. Gem-quality sekaninaite from the Czech Republic. *Journal of Gemmology*, **35**(2), 148–154, http://dx.doi.org/10.15506/JoG.2016.35.2.148.

Johnson M.L. and Koivula J.I., Eds., 1998. Gem News: Iolite gemologically indistinguishable from feldspar. *Gems & Gemology*, **34**(4), 290–302.

Zwaan P.C., 1986. Gem minerals from the Embilipitiya and Kataragama areas in Sri Lanka. *Australian Gemmologist*, **16**(2), 35–40.

Zwaan P.C., 1996. Enstatite, cordierite, kornerupine, and scapolite with unusual properties from Embilipitiya, Sri Lanka. *Gems & Gemology*, **32**(4), 262–269, https://dx.doi.org/10.5741/gems.32.4.262.

Faceted Blue Dumortierite from Madagascar

Since late 2016, the authors have seen blue faceted stones from Madagascar weighing up to approximately 2.3 ct that ranged from light to dark violetish blue, often with a hint of grey in the lighter colours (e.g. Figure 10). Such material has been sold in Madagascar as 'tanzanite' (reportedly with identification reports from a Malagasy lab), and in December 2016 a few of these rough and cut stones were brought to the Mineral Expo show in Paris, France.

Four rough pieces were loaned to the authors for identification by two different traders, including Patrick Lefebvre (Aix-en-Provence, France), who specialises in Madagascar minerals. Fourier-transform Raman spectra were obtained using a Bruker MultiRam spectrometer equipped with a 1064 nm Nd:YAG laser (300 mW power, 4 cm^{-1} resolution and 100 scans). The spectra clearly identified the four stones as dumortierite, with main peaks at 204, 508 and 970 cm^{-1} (Figure 11). A similar-looking light violet-blue, 2.36 ct faceted oval was submitted to the Laboratoire Français de Gemmologie (LFG) in January 2017 (again, see Figure 10), and was also identified as dumortierite with Raman spectroscopy.

Figure 10: Weighing 2.36 ct, this faceted dumortierite from Madagascar was submitted to the Laboratoire Français de Gemmologie (LFG) in January 2017. Photo courtesy of LFG.

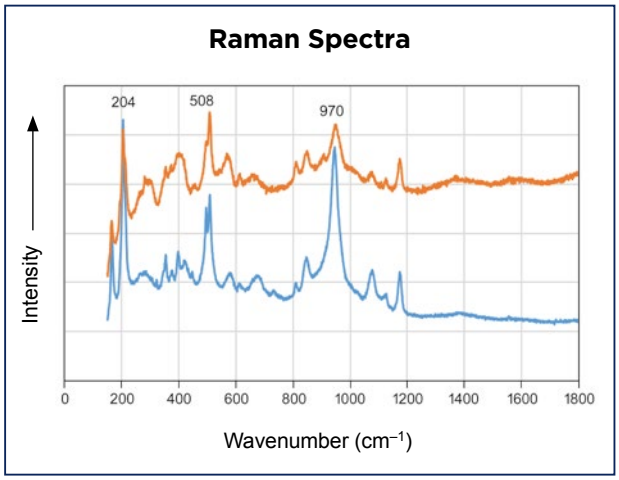

Figure 11: Raman spectra are shown here for two of the rough blue dumortierites from Madagascar. They show peaks at 204, 508 and 970 cm^{-1} that are typical of dumortierite.

RI measurements obtained by the spot method on flat areas of the rough pieces were 1.67–1.69, with a biaxial negative character. The hydrostatic SG ranged from 3.17 to 3.40. All of the samples showed very strong pleochroism from near-colourless to dark violetish blue (Figure 12), which is reportedly due to Fe^{2+}–Fe^{3+} intervalence charge transfer (Rossman, 2015). By contrast, Fe^{2+}–Ti^{4+} charge transfer is believed to give a different (pink) colour in dumortierite (Goreva et al., 2001).

The RI values are somewhat low for tanzanite, and also for dumortierite, probably due to the imperfect surface of the rough samples. The SG measurements span the range for both tanzanite and dumortierite, and the strong pleochroism is also common to both gems. This makes confusion between tanzanite and dumortierite likely.

The stones were inert to long-wave UV radiation but fluoresced a strong whitish blue to short-wave UV. This

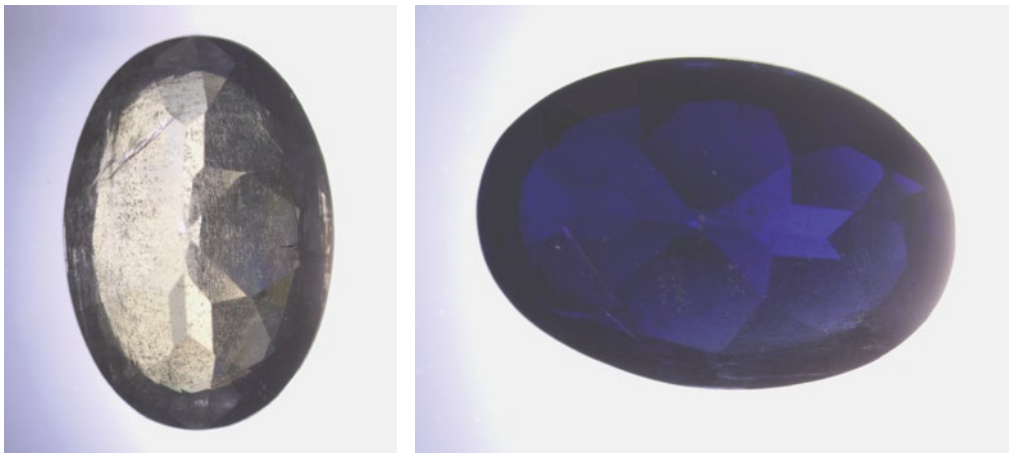

Figure 12: The 2.36 ct dumortierite displays very strong pleochroism from near-colourless to dark violetish blue, attributed to Fe^{2+}–Fe^{3+} charge transfer. Photos courtesy of LFG.

property, together with the biaxial negative character, helps differentiate tanzanite from dumortierite when using classical gemmological methods.

A strong blue short-wave fluorescence is often related to titanium (probably TiO_6 groups, i.e. in sapphire, benitoite and elbaite; Fritsch and Waychunas, 1994). Indeed, a semi-quantitative X-ray fluorescence spectrum obtained with a Rigaku Nex CG instrument revealed, besides the expected Al and Si, a fair amount of Ti (possibly ~1 wt.%), traces of Fe (also related to the colour), Ga and Ge (common substituents of Al and Si), and traces of As. The presence of Ti is consistent with our hypothesis for the origin of the short-wave-only strong whitish blue fluorescence. Further, the dumortierite supergroup contains species with As and Ti as main components (Pieczka et al., 2013), making both elements likely impurities in this species.

Two of the pieces of rough contained many blue, near-parallel, rounded and somewhat elongated inclusions (Figure 13), which were identified with Raman spectroscopy as lazulite. A similar inclusion was seen in the 2.36 ct stone, along with many fluid inclusions and other, unidentified crystal inclusions. The blue lazulite inclusions are reminiscent of those seen in 'blue' quartzite from Mt Bity, also in Madagascar (Rondeau et al., 2016), which is coloured by such inclusions.

Facet-grade blue dumortierite is not common but has been reported previously: Ostwald (1964) mentioned a 4 ct faceted stone (no further details) with Madagascar among the possible localities. Hänni (2007) reported both brownish pink (2.06 ct) and violetish grey (up to 1.18 ct) dumortierite from Tunduru, Tanzania. These gems were also Ti-bearing and fluoresced 'white' in short-wave UV only. Rossman (2015) provided spectra and a photograph of near-gem violetish blue dumortierite from Sahirina, Madagascar. So this 'new' discovery might originate from an area where sporadic finds of such gem dumortierite occurred previously in Madagascar.

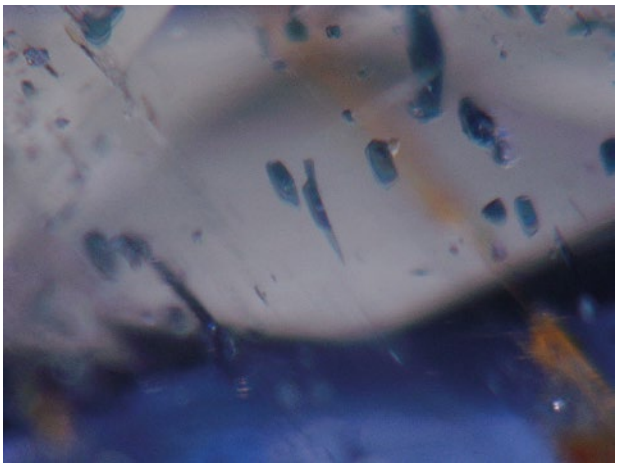

Figure 13: Inclusions of blue lazulite were clearly visible in some of the samples of dumortierite from Madagascar. Photomicrograph by A. Delaunay; magnified 160×.

Dr Emmanuel Fritsch
(emmanuel.fritsch@cnrs-imn.fr)
University of Nantes and CNRS Nantes, France

Aurélien Delaunay and Sophie Leblan
Laboratoire Français de Gemmologie, Paris, France

References

Fritsch E. and Waychunas G.A., 1994. Chapter 15: Gemstones. In M. Robbins, Ed., *Fluorescence: Gems and Minerals Under Ultraviolet Light*, Geoscience Press, Phoenix, Arizona, USA, 149–174.

Goreva J.S., Ma C. and Rossman G.R., 2001. Fibrous nanoinclusions in massive rose quartz: The origin of rose coloration. *American Mineralogist*, **86**(4), 466–472, http://dx.doi.org/10.2138/am-2001-0410.

Hänni H., 2007. Gem News International: Transparent dumortierite and sapphirine from Tanzania. *Gems & Gemology*, **43**(4), 379.

Ostwald J., 1964. Some rare blue gemstones. *Journal of Gemmology*, **9**(5), 182–184, http://dx.doi.org/10.15506/JoG.1964.9.5.182.

Pieczka A., Evans R.J., Grew E.S., Groat L.A., Ma C. and Rossman G.R., 2013. The dumortierite supergroup. I. A new nomenclature for the dumortierite and holtite groups. *Mineralogical Magazine*, **77**(6), 2825–2839, http://dx.doi.org/10.1180/minmag.2013.077.6.09.

Rondeau B., Fritsch E., Stéphant N., Boulet C. and Chauviré B., 2016. Gem lazulite-bearing blue quartzite from Itremo, Madagascar: A potential for new mineral species. *EMC2016*, Rimini, Italy, 11–15 September, 501.

Rossman G.R., 2015. Dumortierite visible spectra (350 – 1000 nm). http://minerals.gps.caltech.edu/FILES/Visible/dumortierite/Index.html, accessed 25 March 2018.

Blue Gahnite from Nigeria

Gahnite ($ZnAl_2O_4$) is the zinc-rich member of the spinel group, and forms solid-solution series with spinel *sensu stricto* ($MgAl_2O_4$) and hercynite ($Fe^{2+}Al_2O_4$). Gem-quality gahnite is rarely encountered, although pale blue to dark blue stones up to approximately 1 cm of near end-member composition have been characterised from pegmatite deposits located near Jemaa, central Nigeria (e.g. Jackson, 1982; Batchelor and Kinnaird, 1984; D'Ippolito et al., 2013; Fregola et al., 2014). The blue colour of this material was attributed by D'Ippolito et al. (2013) to a combination of Fe^{2+} spin-forbidden electronic transitions and Fe^{2+}–Fe^{3+} intervalence charge transfer, while Fregola et al. (2014) proposed traces of cobalt (≤200 ppm).

During the June 2017 JCK show in Las Vegas, Nevada, USA, gem dealer Eric Braunwart (Colombia Gem House, Vancouver, Washington, USA) showed these authors some small blue 'spinels' from Nigeria. They reportedly came from south-eastern Nigeria near the border with Cameroon, which is quite far from the Jemaa area referenced above. The crystals typically ranged from slightly worn euhedral octahedra to waterworn subhedral and rounded crystals indicating possible secondary (eluvial or alluvial) deposition. The rough material showed a consistent deep blue colour, which was retained even when cutting melee down to 1 mm in diameter. Production has consisted of sporadic small parcels weighing 10–50 g. Most of the rough is quite small, yielding 1–3 mm melee; the largest gem cut to date is a round brilliant of 0.30 ct (4 mm in diameter).

Figure 14: Three octahedral crystals (0.11–0.20 g) and two faceted samples (0.17 and 0.19 ct) of blue gahnite from Nigeria were examined for this report. Photo by E. Boehm.

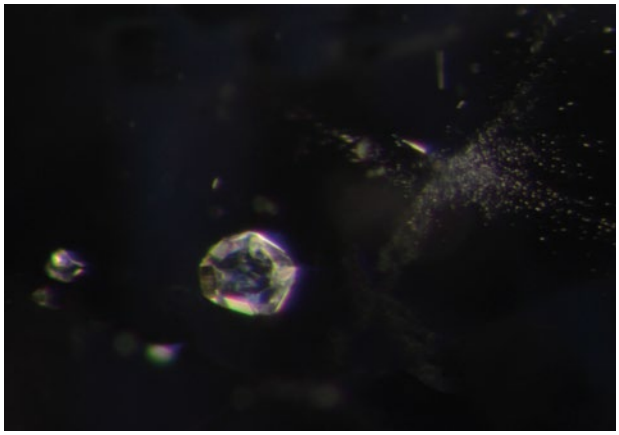

Figure 15: Internal features in the Nigerian gahnite shown here consist of a rounded transparent colourless crystal, a smaller colourless crystal on its left side and a cloud of particles. Photomicrograph by E. Boehm, magnified 45×.

Braunwart loaned some rough and cut samples (Figure 14) to one of the authors (EB) for examination. Two of the faceted gems, weighing 0.17 and 0.19 ct, showed an RI reading of 1.795 consistent with gahnite. (A third faceted stone yielded RIs of 1.762–1.770 and displayed hexagonal growth zoning; it was therefore identified as a sapphire.) A spot RI reading of 1.78 was also obtained from one of the crystals. The faceted gems were too small to provide an accurate hydrostatic SG reading, but the SG of the crystals varied from 4.40 to 4.65, which also falls within the range of gahnite. The RI and SG data from these samples were similar to those obtained by Jackson (1982): 1.793–1.794 and 4.40–4.59, respectively.

Microscopic examination of the rough and cut samples revealed rounded transparent colourless crystals

with the appearance of apatite, euhedral transparent colourless crystals with rectangular cross-sections, flat transparent hexagonal crystals, negative crystals and clouds of fine particles (e.g. Figure 15). The samples showed a moderate red reaction in the Chelsea filter, and a digital spectroscope revealed a strong absorption band in the blue region from 460 to 465 nm and a weak band in the yellow range from 570 to 590 nm. Similar features were documented in the Nigerian gahnite characterised by Jackson (1982), together with some additional absorptions.

Industry demand for the new Nigerian gahnite reportedly has been robust, even considering the small size of the stones, and the market will likely continue to absorb all of the material that is produced.

Edward Boehm FGA (edward@raresource.com)
RareSource, Chattanooga, Tennessee, USA

Brendan M. Laurs FGA

References

Batchelor R.A. and Kinnaird J.A., 1984. Gahnite compositions compared. *Mineralogical Magazine*, **48**(348), 425–429, http://dx.doi.org/10.1180/minmag.1984.048.348.13.

D'Ippolito V., Andreozzi G.B., Bosi F., Hålenius U., Mantovani L., Bersani D. and Fregola R.A., 2013. Crystallographic and spectroscopic characterization of a natural Zn-rich spinel approaching the endmember gahnite ($ZnAl_2O_4$) composition. *Mineralogical Magazine*, **77**(7), 2941–2953, http://dx.doi.org/10.1180/minmag.2013.077.7.05.

Fregola R.A., Skogby H., Bosi F., D'Ippolito V., Andreozzi G.B. and Halenius U., 2014. Optical absorption spectroscopy study of the causes for color variations in natural Fe-bearing gahnite: Insights from iron valency and site distribution data. *American Mineralogist*, **99**(11–12), 2187–2195, http://dx.doi.org/10.2138/am-2014-4962.

Jackson B., 1982. Gem quality gahnite from Nigeria. *Journal of Gemmology*, **18**(4), 265–276, http://dx.doi.org/10.15506/jog.1982.18.4.265.

Garnet from Eldorado Bar, Montana, USA

The alluvial sapphire deposits of the Eldorado Bar area on the Missouri River near Helena, Montana, USA (Hsu et al., 2017) have yielded small quantities of garnets as a by-product of mining for gem corundum. Although much research has focused on sapphires from this area, little is published on the garnets. During the February 2017 Tucson gem shows, some rough and cut samples of Eldorado Bar garnet were loaned for examination by Todd Wacks (Tucson Todd's Gems, Tucson, Arizona, USA). The stones consisted of two pieces of rough (0.83 and 0.87 g) and one faceted trilliant (0.94 ct; see Figure 16). He had obtained the rough material from Farooq Hashmi (Intimate Gems, Glen Cove, New York, USA), who in 2016–2017 saw 200–300 g of facetable stones of mostly sub-gram size; the largest pieces weighed 2–3 g.

Gemmological characterisation was performed by authors CW and BW. The rough stones consisted of waterworn dodecahedral crystals that were deep orangey red. The faceted stone was deep reddish orange, and its RI was 1.750 and hydrostatic SG was 3.80. It showed patchy anomalous double refraction in the polariscope. A rare-earth magnet was able to lift and hold the faceted stone. An ultraviolet-visible (UV-Vis) spectrum (Figure 17) obtained with an Ocean Optics USB4000 spectrometer recorded features corresponding to both almandine (Fe^{2+}) and spessartine (Mn^{2+}), and Raman spectroscopy with a GemmoRaman-532SG instrument showed the closest match to pyrope-almandine reference spectra. EDXRF chemical analysis indicated major Si, Al, Fe and Mg, and moderate Ca and Mn.

Figure 16: These rough (0.83 and 0.87 g) and cut (0.94 ct) garnets from Eldorado Bar, Montana, were examined for this report. Photo by B. M. Laurs.

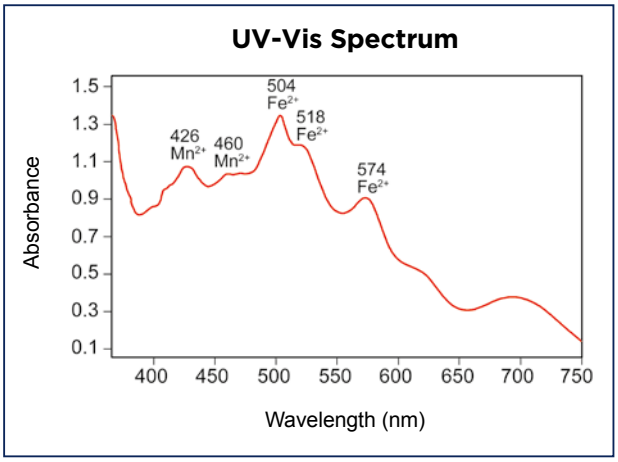

Figure 17: UV-Vis spectroscopy of the faceted Montana garnet showed absorptions at 426 and 460 nm attributed to spessartine (Mn^{2+}), and at 504, 518 and 574 nm attributed to the almandine (Fe^{2+}) component.

Chemical analysis of one of the rough stones and the faceted garnet by laser ablation inductively coupled plasma mass spectrometry (LA-ICP-MS) was performed by author ZS using a Thermo Fisher Scientific iCAP Qc ICP-MS, coupled with an ESI NWR-213 laser ablation system with a frequency-quintupled Nd:YAG laser (213 nm wavelength). The data showed the samples were pyrope-almandine (~$Pyr_{62}Alm_{30}$) with minor grossular and spessartine components (Table I). The data were quite consistent within each stone, indicating that they contained very little chemical zoning. Among the trace elements, Y was most abundant (Table II).

Garnet from Eldorado Bar is sometimes referred to as 'malaya' (or 'malaia') because of its colour, but this term should be reserved for pyrope-spessartine rather than pyrope-almandine.

Cara Williams FGA and Bear Williams FGA
(info@stonegrouplabs.com)
Stone Group Laboratories
Jefferson City, Missouri, USA

Ziyin (Nick) Sun FGA
Gemological Institute of America
Carlsbad, California, USA

Brendan M. Laurs FGA

Reference

Hsu T., Lucas A., Kane R.E., McClure S.F. and Renfro N.D., 2017. Big Sky Country sapphire: Visiting Montana's alluvial deposits. *Gems & Gemology*, **53**(2), 215–227, http://dx.doi.org/10.5741/GEMS.53.2.215.

Table I: Average chemical composition of two Montana garnets by LA-ICP-MS.*

Composition	Faceted	Rough
Oxide (wt.%, converted)		
SiO_2	40.16	39.85
Al_2O_3	23.45	23.07
FeO	15.34	15.67
MnO	0.85	1.88
MgO	18.00	16.48
CaO	2.02	2.98
Total	99.83	99.93
Ions per 12 oxygens		
Si	2.93	2.93
Total tet.	2.93	2.93
Al	2.02	2.00
Total oct.	2.02	2.00
Mg	1.96	1.81
Fe^{2+}	0.94	0.96
Mn	0.05	0.12
Ca	0.16	0.23
Total dodec.	3.10	3.13
Mol.% end members		
Almandine	30.1	30.4
Grossular	5.1	5.9
Pyrope	63.1	61.3
Spessartine	1.7	2.4

* Analytical parameters: 55 µm diameter laser spot size, fluence (energy density) ~10–12 J/cm^2 and 15 Hz repetition rate. Argon was used as nebuliser gas (0.95 L/min), auxiliary gas (0.8 L/min) and cooling gas (14 L/min). Helium, used as part of the carrier gas, had a flow rate of 0.8 L/min. Argon and He gas flow, torch position, sampling depth and lens voltage were optimised to achieve maximum sensitivity (counts per concentration) and low oxide production rates ($^{232}Th^{16}O/^{232}Th$ <1%). Ablated material was vaporised, atomised and ionised with a plasma power of 1,550 W. Data acquisition was performed in time-resolved mode. Dwell time of each isotope was 0.01 s except ^{27}Al and ^{28}Si, which were measured for 0.005 s. Gas background was measured for 20 s, while dwell time of each laser spot was 40 s. Only the second half (20 s ablation) of the laser profile was used to calculate concentrations, which eliminated surface contamination. ^{29}Si was used as an internal standard and GSD-1G, GSE-1G and NIST 610 were used as external standards. Three spots on each sample were analysed. V and Cr were not detected.

Table II: Average trace-element composition of two Montana garnets by LA-ICP-MS.*

Element (ppmw)	Faceted	Rough
Li	4.38	2.90
Na	104	45.8
P	92.2	54.4
Sc	91.6	36.5
Ti	52.0	59.5
Co	27.5	23.4
Ni	0.775	0.786
Zn	35.0	38.1
Ga	4.61	5.32
Ge	3.08	2.94
Y	515	84.5
Zr	19.3	34.1
Sn	1.17	0.350
Ce	0.088	0.123
Pr	nd	0.091
Nd	1.60	2.05
Sm	5.21	5.235
Eu	1.04	1.77
Gd	28.7	13.5
Tb	8.90	2.37
Dy	86.1	16.0
Ho	18.8	3.01
Er	55.2	9.13
Tm	7.42	1.31
Yb	50.8	9.46
Lu	6.70	1.27
Hf	0.508	0.664

* Abbreviations: ppmw = parts per million by weight; nd = not detected.

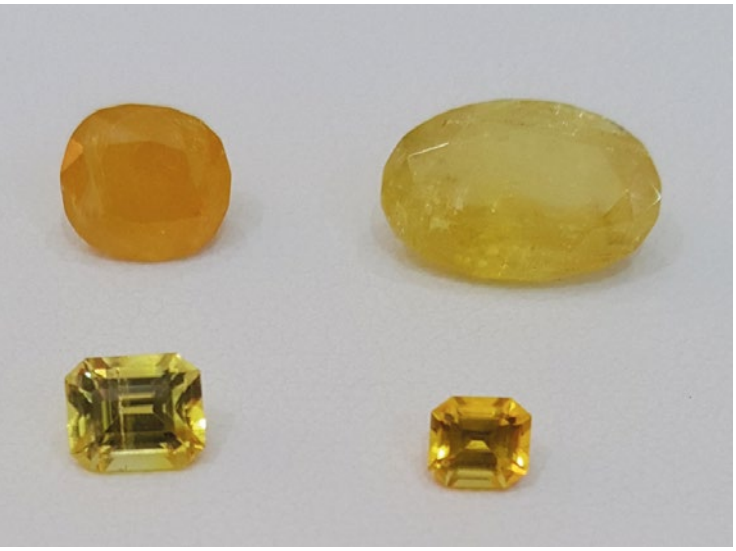

Figure 18: Some of the faceted legrandites studied for this report include a 2.15 ct translucent yellowish orange oval modified brilliant, a 5.15 ct moderately included 'canary' yellow oval modified brilliant, a 1.07 ct slightly included 'canary' yellow emerald cut and a 0.43 ct eye-clean orangey yellow emerald cut. Photo by D. Gravier.

Legrandite from Mapimí, Mexico

Legrandite is a hydrated zinc arsenate, $Zn_2(AsO_4)(OH) \cdot H_2O$, with a Mohs hardness of 4½, which is rarely encountered in faceted form (e.g. Liddicoat, 1967). It ranges from colourless to yellow to orange, and the best-known localities are in Mexico: the Ojuela mine, Mapimí, Durango State and the Flor de Peña mine in Nuevo León State.

Facetable legrandite is rare due to its natural scarcity and its brittleness. The included crystals tend to break apart parallel to their longest direction, and clean pieces are seldom seen. In late 2017, a small quantity of facetable legrandite entered the market, reportedly from Mapimí. From approximately 20 kg of matrix material, one of the authors (DG) recovered ~100 g of rough from which about 40 stones were cut. The gems weighed 0.15 ct to approximately 5 ct, although clean stones were less than 1 ct. They ranged from an intense yellow (transparent) to yellowish orange (semi-transparent; see, e.g., Figure 18).

Some of the faceted stones were characterised for this report. RI values of four samples showed they were biaxial positive with n_α = 1.699–1.701, n_β = 1.706 and n_γ = 1.738–1.739, yielding a birefringence of 0.037–0.040. These results are comparable with those reported by Anthony et al. (2001): n_α = 1.702, n_β = 1.709 and n_γ = 1.740. Hydrostatic SG values of 4.08–4.12 were obtained for a 5.15 ct stone, and these values are somewhat higher than the 3.98–4.01 range given by Anthony et al. (2001). No distinctive absorption features were seen with a handheld spectroscope. Typical inclusions consisted of feathers and incipient fissures (Figure 19a). Also present were 'fingerprints', and one stone contained a tiny cluster of orangey brown material with the appearance of iron oxide or hydroxide (Figure 19b). The larger gems showed obvious doubling (Figure 19c).

Few gems show the intense yellow colour of legrandite, but its rarity and low hardness classify it as a collector's stone.

Denis Gravier (dgravier@aol.com)
Gravier & Gemmes, Poncin, France

Brendan M. Laurs FGA

References

Anthony J.W., Bideaux R.A., Bladh K.W. and Nichols M.C., Eds., 2001. *Handbook of Mineralogy*, Vol. 4, Mineralogical Society of America, Chantilly, Virginia, USA, www.handbookofmineralogy.org/pdfs/legrandite.pdf.

Liddicoat R.T., 1967. Developments and Highlights at the Gem Trade Lab in Los Angeles: Unusual gem materials. *Gems & Gemology*, **12**(5), 151.

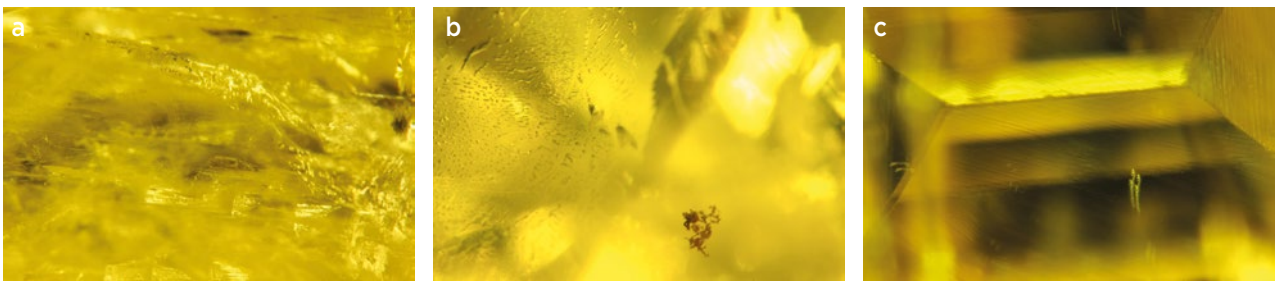

Figure 19: Internal features in the legrandite gemstones examined for this report include **(a)** feathers and incipient fissures, **(b)** 'fingerprints' and a tiny cluster of orangey brown material, and **(c)** obvious doubling displayed by the larger stones. Photomicrographs by D. Gravier; image widths 4.0 mm (a), 1.8 mm (b) and 3.2 mm (c).

Figure 20: 'Manakarra' quartz is typically purple (i.e. amethyst; left), although some of the stones show bluish green colouration (right). Photos courtesy of Joel Ivey.

Grape-like 'Manakarra' Quartz from Sulawesi, Indonesia

In 2014, a new quartz gem material was discovered near the town of Mamuju on Sulawesi Island, Indonesia. According to geologist Joel Ivey (IndoAgate.com, Bangkok, Thailand), it was initially found on a beach, and then was traced up streambeds into the nearby jungle, where local miners have dug narrow tunnels into the steep hillsides (see www.indoagate.com/manakarra.html for more information). The original production consisted of friable, pale grey to brown material with a dull lustre, but by 2016 much higher quality stones were found *in situ* that consisted of grape-like purple or bluish green clusters with a sparkling lustre (e.g. Figure 20). The material commonly has been sold as 'grape' chalcedony or 'grape' agate, and is also called *Batu Manakarra* or simply *Manakarra* (e.g. Thompson, 2016), which refers to the name of a beach near the initial discovery.

According to Ivey, who has visited the mining area, the specimens are hosted by clay-filled areas associated with submarine pillow lavas that form part of a Miocene-age volcanic sequence dominated by mafic lavas, volcanic breccias and tuffs. Ivey estimates that well over 500 tonnes of mixed-quality stones have been recovered, with the largest clusters weighing up to 80 kg. However only about 10% of the material is colourful, and the ratio of specimen- to lapidary-grade stones is approximately 60/40. The quartz typically shows purple (amethyst) or grey-green to bluish green colouration, and less commonly is pale pink, yellow or colourless. Approximately 80% is purple, 15% is green and other colours constitute 5% or less of the production. Individual spheres or 'orbs' range up to 18 mm, but are mostly 3–6 mm in diameter. Orbs measuring 6–10 mm are rare, and larger ones are very seldom encountered. Freeform drusy pieces are cut from the material (Figure 21), and many of the smaller orb-like clusters are wire-wrapped for jewellery use. The larger single or double orbs are commonly drilled and used for beads, or polished and set into pins, brooches and other items. Those showing a low lustre are tumble-polished to produce a shiny fibrous appearance.

Figure 21: Drusy pieces of the Manakarra amethyst have been cut into various shapes for jewellery use. The stones shown here range from 26 × 18 mm to 45 × 28 mm. Photo by Joe Jelks.

Figure 22: A thin slice (0.56 mm thick) of a 4.1-mm orb of Manakarra amethyst displays radial cracks and grain boundaries that are most visible toward its interior **(a, b)**. In cross-polarised light, the radiating growth habit of the quartz is obvious **(c)**. The individual quartz domains are generally about 20 µm wide. Photomicrographs by G. R. Rossman; image widths 1.97 mm (b and c).

Ivey donated some purple and grey-green samples to one of the authors (GRR), and Raman analysis confirmed that the material was quartz. Optical absorption spectroscopy of a doubly polished slice of a purple sphere matched the spectrum of amethyst. EDXRF chemical analysis showed that the purple spheres were mostly Si with about 150 ppm Fe and around 10 ppm Ga and Zn. EDXRF spectroscopy of the green spheres also showed mostly Si, but they contained a much broader array of minor components including nearly 1% Mg, 0.2% Ca, about 1,000 ppm Fe, and traces of Ga, Rb, Sr, Mn, Ge, Y and U.

Internal features in the purple spheres consisted of a radial aggregate of pervasive cracks and grain boundaries (Figure 22a,b) that may host some of the Fe detected in the material. The radiating growth structure was also seen in a thin section of an orb when viewed in cross-polarised light (Figure 22c). The green spheres contained numerous green inclusions (Figure 23).

The amethyst colouration of the quartz is apparently related to the background radiation of the host rock. According to a geological map produced by the Indonesian government, the basaltic rocks that host the amethyst overlie a large granitic body with the potential for uranium mineralisation. Remobilisation of radioactive components could have deposited them into the amethyst host rocks. Indeed, gamma-ray spectroscopy by author GRR showed that the low-level radioactivity of the host rock is mostly from the thorium decay series. As is the case with typical crystals of amethyst, heating the spheres to 400°C resulted in a loss of the amethyst colour.

Although the bulbous appearance of the orbs is reminiscent of some chalcedony or agate (both of which consist of cryptocrystalline quartz), the Manakarra material consists of much coarser-grained radiating micro-crystals. The grape-like form of the quartz is due to its radial growth pattern, with multiple nucleation points producing the clusters of spheres associated with its distinctive appearance.

Brendan M. Laurs FGA

Dr George R. Rossman
California Institute of Technology
Pasadena, California, USA

Reference

Thompson S.E., 2016. Manakarra chalcedony aka grape. *Lapidary Journal/Jewellery Artist*, **20**(6), 16–17.

Figure 23: Numerous inclusions cause the colour of the green orbs of Manakarra quartz, as shown here in a slice of a sphere cluster measuring 5.1 mm wide and 1.75 mm thick. Photomicrograph by G. R. Rossman.

Green Aventurescent Quartzite from a New Find in Tanzania

Figure 24: Green aventurescent quartzite from a relatively new deposit in Tanzania was polished by Jürgen Christmann into this egg (765 ct) and drop-shaped cabochon (82 ct). Collection of Robert Myers; photo by T. Stephan.

A relatively new deposit of green aventurescent quartzite has been discovered in northern Tanzania, and the material is being marketed as 'Emerald quartz', 'Green Tanzurine' or 'Emerald Tanzurine' (e.g. White and Dickson, 2018). The latter two names are being used by USA-based supplier Jonathan Bartky (Ariel Treasures, Livingston, New Jersey), who has exported ~2 tonnes of rough material. He introduced the green aventurescent quartzite to the USA market at the September 2016 Denver Gem & Mineral Show. Since then, various items have been manufactured from this material, including spheres, eggs, cabochons, tumbled stones, pendants and beaded strands.

Two pieces of rough (~30 g each) and three polished stones (25–750 ct) were examined for this report. One of the rough pieces was then polished, and a portion of it was used to prepare thin sections. Additionally, for comparison two samples of aventurine quartz from India (15 g rough and 122.5 ct polished) were also examined, and a thin section was prepared.

The rough material from Tanzania was predominantly opaque, but appeared translucent in strong transmitted light. The translucency was better in the polished samples (e.g. Figure 24), and macroscopically it was obviously an aggregate material coloured by flecks of green inclusions. An aggregate appearance was also seen in the polariscope, which further revealed that the individual grains were doubly refractive. The RI and hydrostatic SG values were consistent with quartz: n_o = 1.543, n_e = 1.552, birefringence = 0.009 and SG = 2.65. Microscopic observation revealed numerous round, partially pseudo-hexagonal, green platy inclusions (Figure 25, left). Raman analysis with a Renishaw inVia spectrometer identified the inclusions as fuchsite, the same chromian mica that colours green aventurine quartz (i.e. quartzite that shows a schiller effect).

Nevertheless, we noted some significant differences

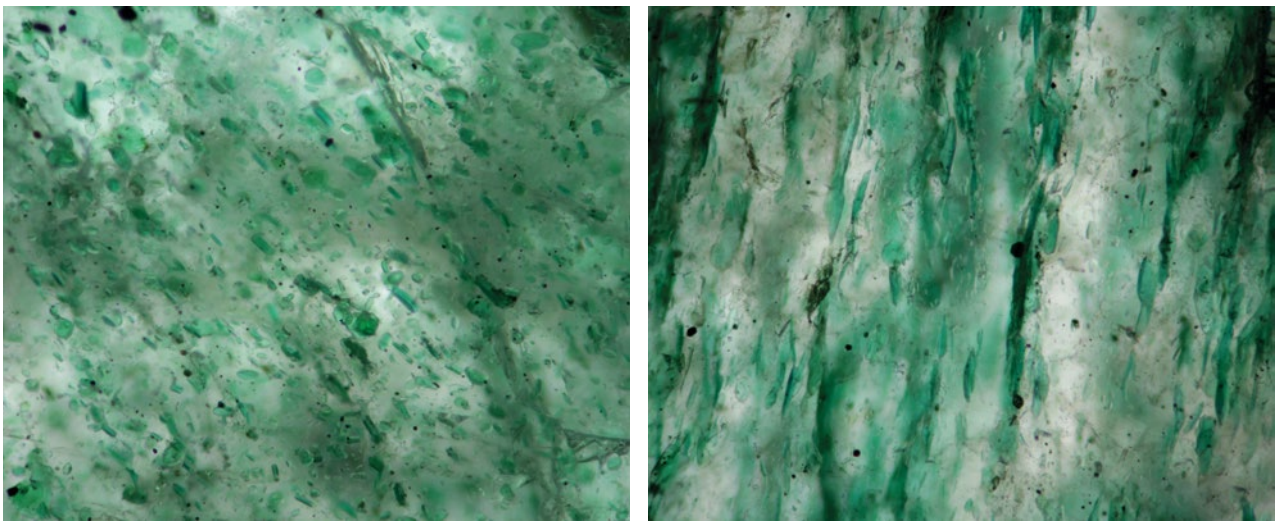

Figure 25: Viewed in transmitted light, the distribution of fuchsite inclusions is shown in the new green aventurescent quartzite from Tanzania (left, image width 3.46 mm), as compared to typical green aventurine from India (right, image width 3.37 mm). Photomicrographs by T. Stephan.

between typical aventurine quartz and this new material from Tanzania. India is the major producer of green aventurine quartz and a detailed mineralogical study of this material was reported by Monroe (1986). Fuchsite-bearing quartzite is commonly rather fine grained (i.e. up to 1–2 mm), with even smaller grains of fuchsite that are incorporated as an accessory constituent along the boundaries between the quartz grains. The fuchsite is mainly oriented in one direction along the foliation of the rock (e.g. Figure 25, right). By contrast, the Tanzanian material consists of coarser grains of quartz (1–5 mm), and the fuchsite forms inclusions within the quartz. Furthermore, the material lacks schistosity, which implies a lower-grade metamorphism. The textural differences between this new green aventurescent quartzite and typical aventurine are particularly evident in thin sections viewed with crossed polarisers (Figure 26).

Acknowledgements: Samples of the green aventurescent quartzite from Tanzania were kindly donated by Impexco (Idar-Oberstein, Germany).

Tom Stephan (t.stephan@dgemg.com),
Dr Ulrich Henn FGA and Fabian Schmitz
German Gemmological Association
Idar-Oberstein, Germany

Brendan M. Laurs FGA

References

Monroe E.A., 1986. Green aventurine quartz: Mineralogical characterization. *Journal of Gemmology*, **20**(2), 83–86, http://dx.doi.org/10.15506/JoG.1986.20.2.83.

White J.S. and Dickson L.D., 2018. Tanzurine, cherry-red and emerald-green quartz from Tanzania. *Rocks & Minerals*, **93**(3), 250–257, http://dx.doi.org/10.1080/00357529.2018.1428863.

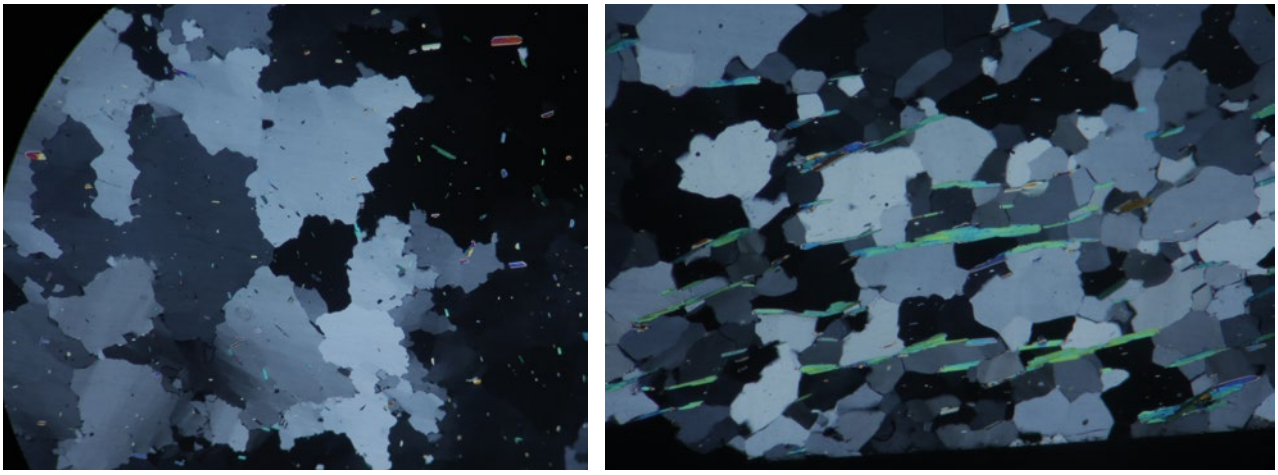

Figure 26: Obvious textural differences are seen between the Tanzanian green aventurescent quartzite and Indian aventurine when thin sections of these materials are viewed with cross-polarised light. The quartz grains display low-order grey-to-black interference colours, while the fuchsite appears highly birefringent. In the material from Tanzania, randomly oriented fuchsite grains are included within coarse interlocked quartz (left, image width 6.62 mm). By contrast, aventurine from India contains subparallel fuchsite laths that are aligned between grain boundaries in relatively fine-grained quartz aggregates (right, image width 3.73 mm). Photomicrographs by T. Stephan.

Blue-to-Violet Spinels from Mozambique

Mozambique was recently noted as a source of pink spinel (Boehm, 2016), and at approximately the same time rough stone dealer Farooq Hashmi reported seeing purple and blue spinels from Mozambique while on a buying trip to Africa. He first encountered them in mid-November 2015 in Arusha, Tanzania, where he saw several kilograms of rough material as broken pieces that were mostly below 3 g each. He was offered more of this spinel while visiting Arusha in May and June 2016. From the rough stones he obtained, Hashmi selected one piece to be faceted for testing, and it was cut into a 1.36 ct round brilliant (Figure 27). Characterisation of this stone by one of the authors (EB) revealed the following properties: colour—slightly violetish blue, RI—1.718, hydrostatic SG—3.66, Chelsea filter reaction—inert, and no absorption features were discernible with a handheld spectroscope. In addition, no inclusions were visible with the gemmological microscope.

Figure 27: This 1.36 ct violetish blue spinel is from Mozambique. The stone was faceted by Marvin M. Wambua (Safigemscutters Ltd, Nairobi, Kenya). Photo by E. Boehm.

More recently, at the 2018 Tucson gem shows, a range of greyish to greenish blue to violet to purple spinels from Mozambique were displayed by one of the authors (MS) and Kobi Sevdermish (Advanced Quality, Ramat Gan, Israel). They started cutting the material in early 2017, and produced faceted stones from 2 mm in diameter up to 8 ct. About 3,000 carats of the larger stones have been cut. Seven spinels weighing 1.20–3.83 ct (Figure 28) were characterised by one of the authors (GB). Five of them were violetish purple to reddish purple with medium-to-dark tone and moderate-to-vivid saturation, and two of them were greenish blue to blue with dark tone and high saturation. The RI was 1.718 ± 0.001 and hydrostatic SG values were 3.58–3.62. Internal features consisted of fine needles showing various patterns, including short silk-like inclusions and elongate networks with a partially dissolved appearance (Figure 29). Intersecting networks of needles created a spiderweb-like appearance in some samples.

Figure 28: Weighing 1.20–3.83 ct, these spinels from Mozambique show various purple-to-blue hues. Photo by Maria Shpak.

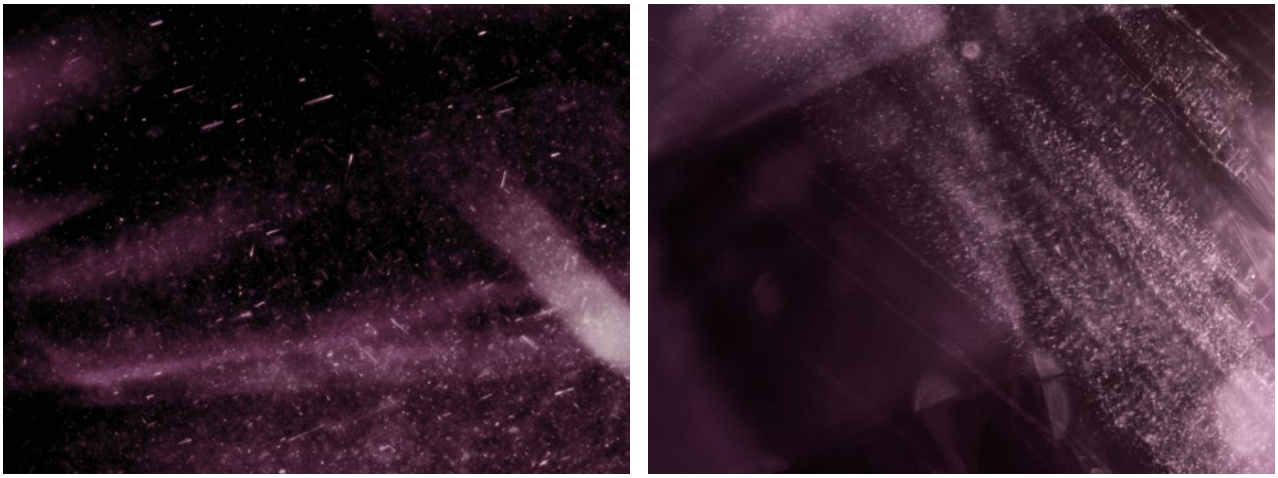

Figure 29: Some of the Mozambique spinels contained fine silk-like needles that were dispersed (left, magnified 60×) or present in elongate networks with a partially dissolved appearance (right, magnified 50×). Photomicrographs by G. Borenstein.

Figure 30: Colourless hexagonal prisms with the appearance of apatite also formed inclusions in the Mozambique spinels. Photomicrograph by Idan Shaulov; magnified 60×.

Also present were 'fingerprints' and small transparent hexagonal prisms that were doubly refractive and had the appearance of apatite (Figure 30).

The specific locality (or localities) for these spinels in Mozambique is presently unknown to the authors, but given the differences in the colour appearance and SG of the stones examined by each author, it is possible that they came from more than one deposit.

Guy Borenstein FGA and Menahem Sevdermish FGA
(smenahem@gemewizard.com)
Gemewizard Gemological Laboratory
Ramat Gan, Israel

Edward Boehm FGA

Reference

Boehm E., 2016. Gem Notes: Pink spinel from Mozambique. *Journal of Gemmology*, **35**(2), 109–111.

Violet Tourmaline from Democratic Republic of Congo

Gem-quality tourmaline is known in virtually every colour, but violet is rather uncommon. While on a buying trip to Africa in the first part of 2017, rough stone dealer Farooq Hashmi obtained an unusual violet tourmaline from his supplier in Rwanda. The crystal was taken from a small parcel of rough tourmaline that reportedly came from a new mine in the Democratic Republic of Congo (DRC). The crystal measured ~1.2 cm long (Figure 31), and the bottom part of it was subsequently faceted into a 1.42 ct round modified brilliant for this report (Figure 32).

The faceted stone and crystal section were examined by authors CW and BW. The crystal exhibited a hexagonal cross section, and the prism faces were lightly striated parallel to the c-axis. The crystal termination was composed of three near-equal rhomboid pyramidal faces. Both the rough and cut samples were greyish violet and were inert to UV radiation. The RIs of the faceted stone were 1.620–1.640, yielding a birefringence of 0.020. The SG of the faceted stone was measured hydrostatically as 3.06. The main inclusions in both samples were fluid-filled partially healed fissures. In addition, the crystal hosted numerous growth tubes oriented parallel to the c-axis that were filled with a reddish brown epigenetic material (Figure 33), while the

Figure 31: This violet tourmaline crystal (~1.2 cm long) was reportedly produced from a new mine in the DRC. Photo by Farooq Hashmi.

faceted stone contained some fine frosted 'fingerprint' inclusions and some reddish brown solid inclusions with no discernible crystal form. Raman analysis with the GemmoRaman-532SG instrument gave the closest match to elbaite, and EDXRF spectroscopy gave strong peaks for Mn, Fe, Ca and Zn. Although Zn is somewhat unusual in gem tourmaline, a significant amount of this element was likewise detected (together with the other elements mentioned above) in a chemical analysis of the crystal by John Attard (Attard's Minerals, San Diego, California, USA) using EDXRF spectroscopy.

Energy-dispersive chemical analysis of the faceted stone with a scanning electron microscope by author AUF showed that the tourmaline was elbaite with Mn as the principal chromophoric element.

It remains to be seen whether additional production of this unusually coloured gem tourmaline from DRC will enter the market.

Cara Williams FGA and Bear Williams FGA

Alexander U. Falster and
Dr William 'Skip' B. Simmons
Maine Mineral & Gem Museum
Bethel, Maine, USA

Brendan M. Laurs FGA

Figure 32: A portion of the tourmaline crystal in Figure 31 was faceted into a 1.42 ct gemstone by Todd Wacks (Tucson Todd's Gems). The remaining part of the crystal is 6.54 mm long. Photo by B. Williams.

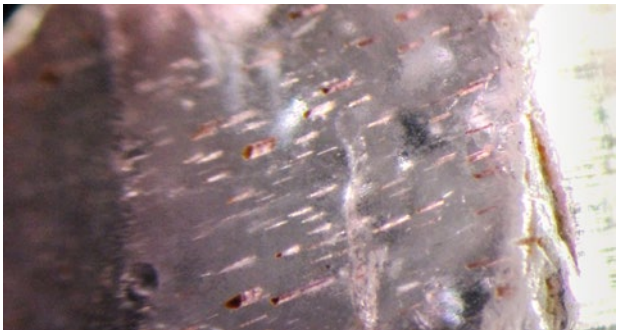

Figure 33: An array of growth tubes oriented parallel to the c-axis are located just under the pyramidal termination of the tourmaline crystal, and are filled with a reddish brown epigenetic material. Photomicrograph by B. Williams; magnified 25×.

ORGANIC MATERIALS

Burmese Amber from Khamti, Sagaing Region

Burmese amber, also called *burmite* (or *pa-yin* in Burmese), is a Cretaceous fossilised resin. Most commercial extraction of burmite has focused on several important sites in the Hukawng Valley of Kachin State in northern Myanmar (Figure 34). In recent years, political instability in Kachin State forced many amber (and gold) miners to flee the area and search for deposits in other regions of Myanmar. For example, in 2010–2011 a new locality for Burmese amber was discovered near Hti Lin, Magway Region, central Myanmar (Figure 34; Tay Thye Sun et al., 2015).

In addition, many local miners (who are mainly farmers) from Kachin State started searching for new gem deposits to the west along the Chindwin River. In 2012–2013, another amber mining area was found near Khamti (or Hkamti) Township, which is located 180 km northwest of Myitkyina, in the Sagaing Region of north-western Myanmar (Figure 34). Currently more than 1,000 miners are active there in both open-pit and underground workings (Figure 35). The amber-bearing seams form in strata with coal and calcite that are hosted within shale layers, typically ~20–30 m below the surface. The overlying soil is around 3–5 m thick. In addition to producing amber, the miners also recover *fei cui* (Burmese jadeite) and gold in this area.

Thirty-two Khamti amber samples were examined using standard gemmological instruments and Fourier-transform infrared (FTIR) spectroscopy. All were polished cabochons or free-forms of gem quality, weighing 0.72–55.67 ct. They displayed a wide range of colours, from pale 'lemon' yellow, 'honey' yellow and brownish yellow to dark brown, as well as some unusual colours such as 'cherry' red and 'tea-leaf' green to dark greenish brown (e.g. Figure 36, left). Some brownish yellow, reddish brown and cherry-red samples showed a bluish

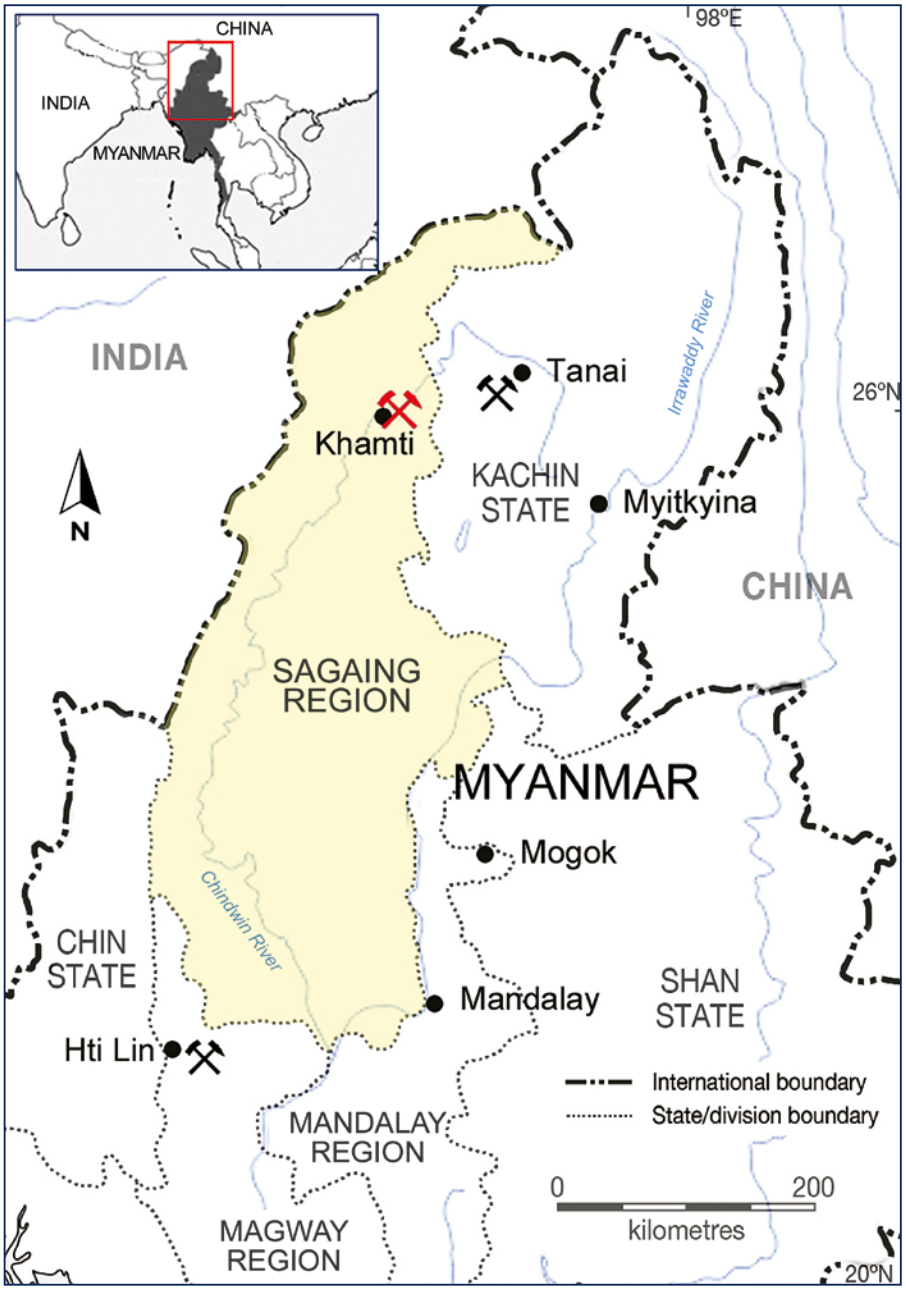

Figure 34: There are three main amber-mining areas in Myanmar. The Khamti deposits (red symbol) are located in Sagaing Region (yellow shading) of north-western Myanmar, while the famous Hukawng Valley mines are located south-west of Tanai in Kachin State. The Hti Lin area is in Magway Region, central Myanmar.

green surface colour in daylight that may be attributed to Tyndall scattering of light by clouds of very fine gas bubbles. The spot RI ranged from 1.54 to 1.55, and the hydrostatic SG was 1.03–1.06. Most samples showed chalky blue to light purple fluorescence (Figure 36, right), which was strong in long-wave and weak under short-wave UV radiation. However, some of the samples luminesced moderate-to-strong pink (sometimes with blue veins or patches corresponding to plant debris), and this fluorescence was likewise stronger under long-wave than short-wave UV radiation (again, see Figure 36, right). The pink UV luminescence helps explain why some brown to dark brown samples (i.e. lower left in Figure 36) displayed a purple surface colour in reflected daylight.

Most of the amber samples were clean and transparent, and only a few were translucent to opaque. Microscopic observation revealed many tiny, flattened, oval gas bubbles and swirled flows of brownish coloured debris. Inclusions consisting of a cockroach and a cricket were found in two different brownish yellow samples, while samples with more unusual body colours were typically free of insects. Other inclusions—such as fern leaves, scorpions, lizards and feathers—have also been discovered in Khamti amber (Maung Muang Minn, pers. comm., 2017).

Specular reflectance FTIR spectroscopy showed that most of the Khamti amber samples had spectra similar to those of burmite from the Hukawng Valley (cf. Beck et al., 1964; Wang et al., 2015). However, some cherry-red

Figure 35: In the Khamti area, amber is mined from open pits (left) and from hand-dug shafts (right). Photo by Ben Sim.

Figure 36: These 0.72–55.67 ct samples of Khamti amber (left) display variable fluorescence (right), consisting mostly of pink in the left column and blue-to-purple in the right column. The fluorescence is shown here under long-wave UV radiation. Photos by S.I Liu.

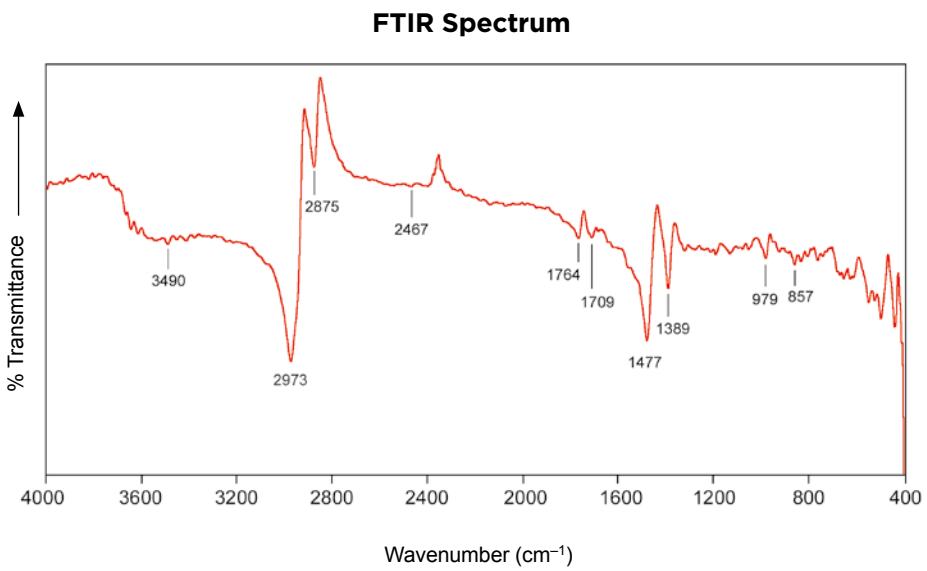

Figure 37: Some unusual features for Burmese amber are shown in this FTIR spectrum of a cherry-red sample from Khamti, including weak-to-absent absorptions at 1734 cm^{-1} and in the 1250–1050 cm^{-1} region, and an additional band at 1764 cm^{-1}.

and light yellow samples had somewhat different infrared spectra. The significant absorption band in Burmese amber at 1734 cm^{-1} corresponding to the C=O stretching vibration of carboxylic esters and acid groups was very weak (or sometimes absent), and an additional absorption at 1764 cm^{-1} was present in these Khamti ambers (Figure 37). The C–O stretching vibrations in the 1250–1050 cm^{-1} region were also relatively weak. Further investigations should be undertaken to better characterise such Khamti samples using Raman and mass spectroscopy, as well as FTIR spectroscopy of pressed KBr pellets in transmission mode.

The presence of these relatively recently discovered amber deposits in the Khamti area of the Sagaing Region suggests that there might be more as-yet undiscovered burmite deposits in Myanmar, which could provide additional new amber varieties and help ensure a sufficient supply of Burmese amber to the growing international market.

Acknowledgements: The author thanks Maung Muang Minn for providing samples and discussions of Hkamti amber, Ben Sim for photographs of the mining area, and Kin Wah (Tommy) Tsui and Chun Kit Lau (China Gems Laboratory Ltd, Hong Kong) for FTIR spectroscopy.

Dr Shang I (Edward) Liu FGA (edwardliu@gahk.org)
The Gemmological Association of Hong Kong

References

Beck C.W., Wilbur E. and Meret S., 1964. Infra-red spectra and the origin of amber. *Nature*, **201**(4916), 256–257, http://dx.doi.org/10.1038/201256a0.

Tay Thye Sun, Kleišmantas A., Thet Tin Nyunt, Zheng Minrui, Krishnaswamy M. and Loke Hui Ying, 2015. Burmese amber from Hti Lin. *Journal of Gemmology*, **34**(7), 606–615, http://dx.doi.org/10.15506/JoG.2015.34.7.606.

Wang Y., Shi G.H., Shi W. and Wu R.H., 2015. Infrared spectral characteristics of ambers from three main sources (Baltic, Dominica and Myanmar). *Spectroscopy and Spectral Analysis*, **35**(8), 2164–2169 (in Chinese with English abstract).

MISCELLANEOUS

Opal Master Reference Sets

In light of numerous developments concerning opals during the past two decades—including new deposits, varieties and synthetics—a series of comprehensive opal master reference sets were recently released by Andrew and Damien Cody (Cody Opal, Melbourne, Australia). A total of 60 sets have been assembled after more than two years of research and development.

Designed to be used as a tool for education, identification, classification and grading, each set comprises nine acrylic boards (e.g. Figure 38) containing a total of 216 reference samples. The specimens were assembled from more than 200,000 pieces, with nearly 13,000 of them selected for the sets. Natural opals were sourced from several significant localities worldwide, and synthetics were acquired from leading manufacturers.

The nine boards in each set consist of the following:

- **Board 1**—*Natural Precious Solid Opal*: Body Tone Scale (black to light; Munsell N1–N9) and Australian Black Opal Grading Scale (red-multi, orange-green, green and blue; AAA–D)
- **Board 2**—*Natural Precious Solid Opal*: Diaphaneity Scale (transparent–opaque), Australian Light Opal Grading Scale (red-multi and green-blue; AAA–F) and Light Opal of the World
- **Board 3**—*Natural Precious Opal on Host Rock*: Australian Boulder Opal Grading Scale (AAA–C), Opal on Host Rock Examples and Host Rock Types
- **Board 4**—*Natural Precious Opal in Host Rock (Matrix)*: Queensland (Australia) Boulder Matrix Opal Examples, Andamooka (Australia) Matrix Opal Examples and Matrix Opal of the World
- **Board 5**—*Natural Precious Hydrophane Opal*: Ethiopian Light Opal Grading Scale (AAA–C), Wollo (Ethiopia) Opal Examples, and Other Hydrophane Opal
- **Board 6**—*Natural Common Opal*: Mexican Fire Opal Grading System (cherry red–orange-yellow), Brazilian Fire Opal Grading System (orange–yellow) and Other Common Opal
- **Board 7**—*Composite Opal*: Doublet Grading Scale (red-multi and green), Triplet Grading Scale (red-multi, green and blue) and Other Composites
- **Board 8**—*Artificial Opal*: Kyocera (both mineral-type and resin-impregnated synthetics), Fuji (resin-impregnated synthetic and resin hybrid), Sterling (resin-impregnated synthetic) and Imitations
- **Board 9**—*Opal Specimens*: Opalized Fossils (molluscs, worm burrows and wood) and Formation Examples (hyalite, nobby and seam)

Each set is individually numbered, and the boards are secured with tamper-proof screws and holographic security labels. A loose-leaf handbook of explanatory notes on the samples accompanies each set. As opal nomenclature is currently under review, both the handbook and the boards themselves can be updated as necessary by Cody Opal.

The opal sets were initially displayed in early 2018 at the International Jewellery Tokyo show in Japan and the GJX show in Tucson. This is the first time that comprehensive opal master sets have been assembled, and the majority of them have already been acquired by most of the world's important gemmological laboratories and institutions, including Gem-A. It is hoped that these sets will help educate the gem trade and facilitate the consistency of opal grading, classification and terminology throughout the industry.

Brendan M. Laurs FGA

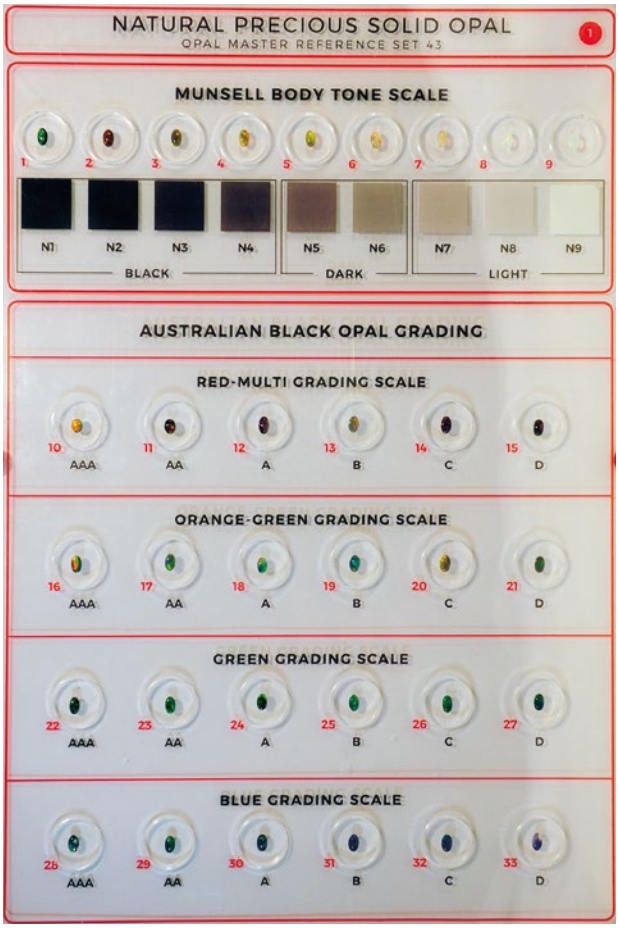

Figure 38: Comprehensive opal master reference sets have been released, with each consisting of nine boards. Shown here is board no. 1, which displays a body tone scale and an Australian black opal grading scale. The board measures 30 × 21 cm, and the samples are mounted within an assemblage of three acrylic plates. Photo courtesy of Cody Opal.

Figure 1: These zircons (10.45–20.51 ct) from Ratanakiri, Cambodia, show the attractive blue colouration of heat-treated material from this locality. Photo by Mark H. Smith, Thai Lanka Trading Ltd Part., Bangkok, Thailand.

Blue Zircon from Ratanakiri, Cambodia

Manuela Zeug, Lutz Nasdala, Bhuwadol Wanthanachaisaeng, Walter A. Balmer, Fernando Corfu and Manfred Wildner

ABSTRACT: Zircon from Ratanakiri Province, north-eastern Cambodia, is well known in the gem trade for its vivid blue colour that results from heat treatment. The untreated brown material turns blue under reducing conditions at ~900–1,000°C. Ratanakiri zircon is characterised by remarkably low contents of trace elements. In particular, the actinides have low concentrations (e.g. approximately 120 ppm U and 95 ppm Th). Together with the very young age of the zircon (< 1 million years [Ma]), this results in an extremely low self-irradiation dose, which in turn is in agreement with its non-radiation-damaged, nearly perfectly crystalline state. The heat treatment, therefore, does not result in detectable changes in the zircon's structural state. The cause of the blue colour, presumably related to a valence change upon heating in the reducing environment, is still under debate. The absorption of the treated Ratanakiri zircon is decidedly different from that of blue U^{4+}-doped and blue V^{4+}-doped synthetic $ZrSiO_4$. Absorption spectra show a strongly pleochroic band at 18,200–13,000 cm^{-1} (corresponding to ~550–770 nm wavelength) that is clearly responsible for the treated blue colour; however, its assignment remains unresolved.

The Journal of Gemmology, **36**(2), 2018, pp. 112–132, http://dx.doi.org/10.15506/JoG.2018.36.2.112

Zircon has been used as a gem material for thousands of years. This is not least because of the mineral's high refractive index and optical dispersion. Transparent colourless zircon nearly approaches diamond in fire and brilliance, and therefore has been used as a diamond imitation for centuries. Colourless zircon is occasionally known in the gem market by its misnomer 'Matara (or Matura) diamond', named after the city of Matara on the southern coast of Sri Lanka (Roskin, 2003). In addition to being colourless, zircon occurs in a wide range of hues including slightly smoky or pale yellow ('jargoon' or 'jargon'), orange to reddish brown ('hyacinth' or 'jacinth'), yellowish to brownish green, dull dark brown to nearly black (often belonging to metamict varieties such as 'cyrtolith' or 'malacon') and purple and pink (Faulkner and Shigley, 1989; Nasdala et al., 2003; Kempe et al., 2016). Natural untreated blue zircon, however, is extremely rare. For example, small dipyramidal crystals of 'sky'-blue colour (occasionally with a greyish, greenish or purplish tint) are known from the San Vito quarry on the western slope of the Somma-Vesuvius volcanic complex in Italy (Russo and Punzo, 2004; see also Kempe et al., 2016).

Besides Sri Lanka, gem-quality zircon was, and still is, produced in Cambodia, Vietnam, Thailand, Myanmar, India, Pakistan, China, Russia, France, Tanzania, Madagascar, the USA, Canada, Australia and other countries (Faulkner and Shigley, 1989; Roskin, 2003; Watson, 2007; Smith and Balmer, 2009; Shigley et al., 2010; Chen et al., 2011; Sutherland et al., 2016). The reddish brown to brown zircon from Ratanakiri (or Ratanak Kiri), Cambodia, has become increasingly important in the gem trade, since it is known that this material turns into different shades of blue upon heat treatment, including a significant fraction that is vivid blue (Figure 1; Smith and Balmer, 2009). In addition to 'Starlite', the term 'Ratanakiri zircon' has developed into a common trade name for gem-quality blue zircon. The proliferation of 'Ratanakiri zircon' is somewhat comparable to the term 'Paraiba tourmaline', which has developed into a general trade name for vivid blue-to-green Cu-bearing tourmaline that is used regardless of a stone's geographical origin. Additional locations known to produce zircon that in some cases can be enhanced to (rather light) blue include Shan State in north-western Myanmar; Bang Kacha and Tok Prom near Chanthaburi, Thailand; Bo Phloi near Kanchanaburi, Thailand; and the Central Highlands of Vietnam (e.g. Roskin, 2003; Satitkune et al., 2013; Huong et al., 2016). However, none of these locations produces zircon that can be treated to such an intense, vivid blue colour as the Ratanakiri material. Here we present recent research regarding blue Ratanakiri zircon.

BACKGROUND

Zircon ($ZrSiO_4$) has a tetragonal structure (space group $I4_1/amd$) with a unit cell composed of four SiO_4^{4-} and four ZrO_8^{12-} groups (formula unit Z = 4). Non-formula cations incorporated in the zircon structure include trivalent rare-earth elements (REE^{3+}) as well as Hf^{4+}, Ti^{4+}, Th^{4+}, U^{4+}, U^{5+}, P^{5+}, Nb^{5+} and Ta^{5+} (Hoskin and Schaltegger, 2003; Kempe et al., 2016; and references therein). Although REEs are considered incompatible elements because of their large ionic radii, they commonly substitute in small amounts for Zr^{4+}, which has dodecahedral coordination in the zircon lattice (Hanchar and van Westrenen, 2007). The incorporation of trivalent REE for tetravalent Zr, however, requires charge compensation. This is mostly realised by combined incorporation of REE^{3+} along with a pentavalent ion, either P^{5+} (for Si^{4+}) or Nb^{5+}/Ta^{5+} (for Zr^{4+}; see Hoskin et al., 2000; Hoskin and Schaltegger, 2003; and references therein). Even though zircon has occasionally been reported to contain 10–30 wt.% Hf (Ma and Rossman, 2005; Pérez-Soba et al., 2007; Van Lichtervelde et al., 2009) or up to 13 wt.% U (Zamyatin et al., 2017), non-formula elements normally have low concentrations in this mineral. Other than Hf (with HfO_2 typically in the range 0.6–2.0 wt.%), all non-formula elements are well below the weight-percent level in gem-quality zircon.

Zircon is a common accessory mineral that occurs in many igneous and metamorphic rocks. Relatively large, gem-quality crystals grow predominantly in felsic pegmatites and more rarely in metasomatic rocks. Because of its hardness, remarkable physical stability and chemical resistance, zircon also is a common detrital component in sediments; hence this mineral often occurs in gravel deposits. Its susceptibility to weathering and other fluid-driven alteration, however, is appreciably increased upon the accumulation of radiation damage (e.g. Ewing et al., 2003; Hay and Dempster, 2009; Xu et al., 2012; Malusà et al., 2013). That is, alpha-decay events of U, and to a lesser extent Th (and their unstable daughter nuclei), result in structural damage, with the final, amorphous state being called *metamict* (Ewing, 1994). The accumulation of radiation damage in zircon is connected with a range of property changes, including a decrease in refractive index and birefringence (Sahama, 1981). Also, the density decreases from ~4.7 g/cm^3 to well below 3.9 g/cm^3 (Holland and Gottfried, 1955). Highly radiation-damaged zircon (that nevertheless might have some gem quality areas, usually showing a green colour) is therefore often referred to as 'low zircon' in the gemmological community.

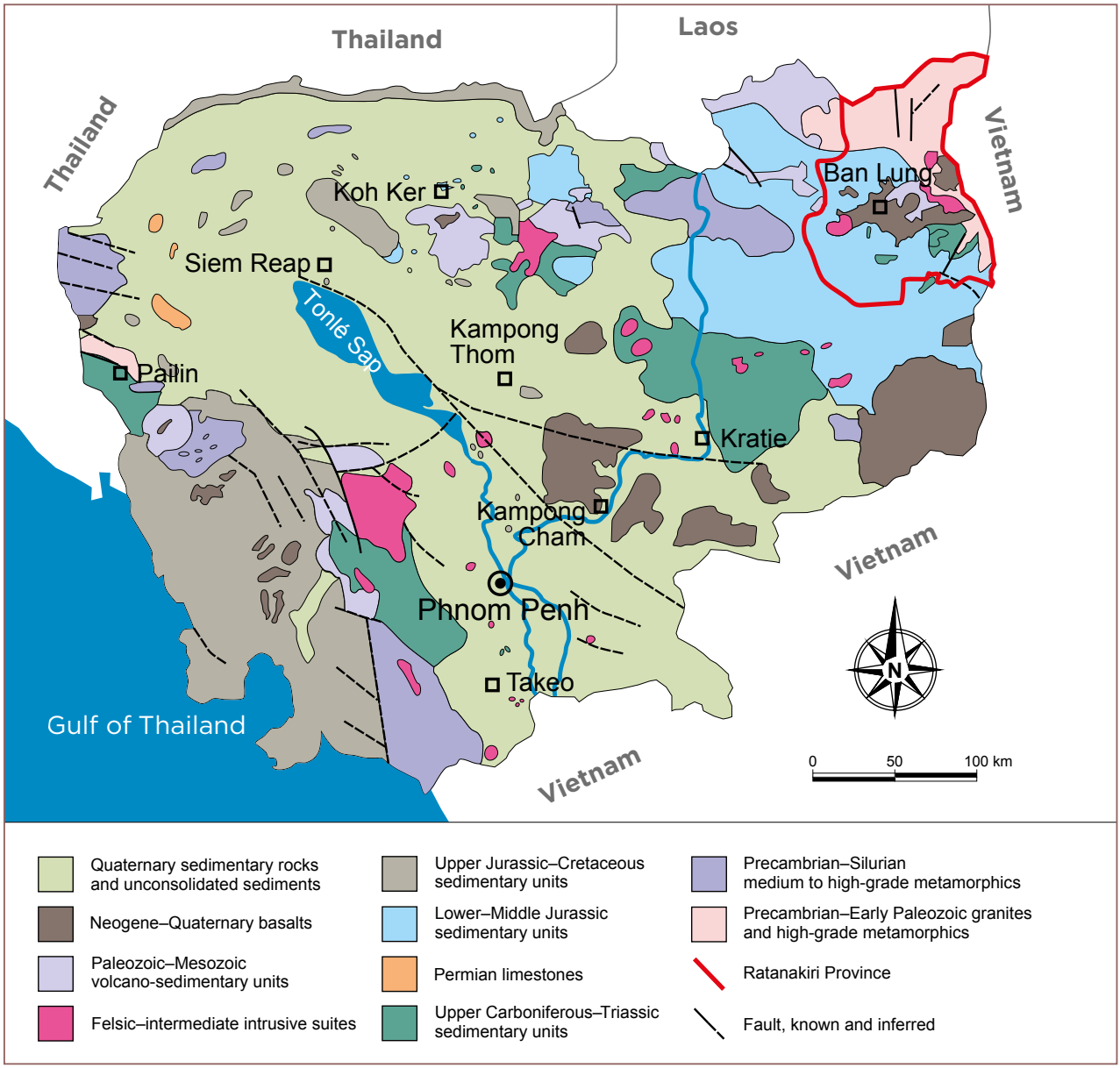

Figure 2: Ratanakiri Province, located in north-eastern Cambodia, is outlined in red on this simplified geological map of the country (modified after United Nations, 1993; Douglas et al., 2008). The zircon deposits are associated with the weathering of Neogene–Quaternary basaltic rocks (shown in dark brown).

The large variety of zircon colours depends on the content of transition metals and radiation-induced colour centres (Burns, 1993; Anderson and Payne, 1998; Nasdala et al., 2003), and might also involve crystal-field or charge-transfer transitions (Klinger et al., 2012; Kempe et al., 2016). However, the causes of most zircon colours remain unclear, or at least seem controversial to date. The only comprehensive summary of the literature, along with original spectroscopic results, was recently published by Kempe et al. (2016). The trace-element-related interpretations of colour causes proposed by these authors, however, remain unsupported as they did not present chemical data for their samples.

It should be added that doped synthetic $ZrSiO_4$ of various colouration is used as high-temperature stable and chemically inert pigments. These include, for instance, yellow Pr^{3+}-doped $ZrSiO_4$ (Stiebler et al., 1992; Del Nero et al., 2004), 'lemon'-yellow Tb^{3+}-doped $ZrSiO_4$ (Kar et al., 2004), blue V^{4+}-doped $ZrSiO_4$ (Demiray et al., 1970; Niesert et al., 2002; Pyon et al., 2011) and pink-to-red Fe-doped $ZrSiO_4$ (Cappelletti et al., 2005). It is, however, well known that the colours of natural zircon have different causes than those of the synthetic pigments, the latter of which contain dopant levels several orders of magnitude above the concentrations of the same elements in natural zircon.

ZIRCON MINING IN RATANAKIRI

Geological Setting

Ratanakiri is the north-easternmost province of Cambodia. Here, zircon crystals are found in numerous alluvial deposits that formed from the weathering of Cenozoic (Neogene–Quaternary) basaltic rocks. The Ratanakiri volcanic province belongs to the Indochina Cratonic Terrane that covers eastern Thailand, Laos, Cambodia and southern Vietnam. The development of the Ratanakiri volcanic province heralds the start of the collision of the Eurasian and Indian continents during the Himalayan orogeny (55–45 Ma ago; Gibbons et al., 2015). Extensive volcanic activity occurred much later along reactivated crustal boundaries around the Pliocene–Pleistocene boundary spanning 4.3–0.8 Ma ago (Rangin et al., 1995). The Cenozoic basalt magmatism changed from early tholeiitic flood basalts to scattered volcanic cones of alkaline composition (Hoang and Flower, 1998). Alkali basaltic rocks are considered to be the host of Ratanakiri zircon (Figure 2). During a number of eruptive events that were confined to intersections of strike-slip faults, zircon crystals were transported as xenocrysts in the alkaline magma from considerable depths to the earth's surface (Rangin et al., 1995; Balmer et al., 2009). Gem-bearing alluvial layers are presently scattered throughout the region, and they vary in thickness and depth below the surface.

Mining

Gem mining activities in Ratanakiri started in the mid-1930s (Saurin, 1957). At present, several zircon-bearing areas with numerous small workings are active (e.g. Figure 3). Their number, however, fluctuates depending on the economic situation. For instance, many mining sites closed during the past few years in favour of developing rubber plantations, which presently are more profitable than zircon mining. Productive areas for zircon are located near Ban Lung and Bae Srak (a settlement located just a few kilometres south of Ban Lung), and further east and northeast toward the Tonlé San River, especially around Bo Keo (the latter being 25 km east of Ban Lung and about 30 km from the border with Vietnam on the east). Here, gem zircon occurs in two different types of basalt-related deposits. The first consists of basaltic and pyroclastic material that is completely weathered into laterite soil, from which miners can easily extract zircon crystals by hand. The second type constitutes undecomposed basaltic gravels, requiring the use of water cannons to break up the material in search of zircon (cf. Smith

Figure 3: (a) A miner brings up a bucket filled with gravel-bearing soil at this zircon mine near Bo Keo, Ratanakiri, where shafts extend to 17 m depth. **(b)** Near Bo Loi, Ratanakiri, gravel panning is done in a small pool lined with a plastic tarp. **(c)** In addition to zircon, the washed material includes garnet, sapphire, quartz, ruby and spinel. **(d)** This reddish brown, euhedral zircon crystal is from Phnum Trom, Ratanakiri. Photos by Ralf Grunert (a, c) and L. Nasdala (b, d).

and Balmer, 2009; Balmer et al., 2009; Wanthanachaisaeng et al., 2014).

The mining methods are quite diverse because the zircon-bearing layers of various thicknesses occur at different depths. In the north (e.g. near Bo Loi, 25 km northeast of Ban Lung), gravel layers can be at fairly shallow depths; in some cases, they are even mineable in small open pits. Near Bo Keo and Phnum Trom (Bo Keo area), by contrast, miners must dig shafts up to 17 m deep into the red soil. These shafts typically are less than 1 m in diameter and have no reinforcement at all; just simple footsteps are dug into the side walls. At the bottom of the shaft, small horizontal tunnels are dug into the gravels. The miners face the constant danger of collapsing material. Buckets containing gravel and soil material are hoisted to the surface using manual winches (Figure 3a). Zircon and other heavy minerals are extracted by either dry hand-picking or pan-washing. In dry areas, washing may be done in small water-filled pits lined with plastic tarps (Figure 3b). Associated minerals found with the zircon include garnet, sapphire, quartz, ruby and spinel (Figure 3c).

Ratanakiri zircon is predominantly brown, often with a reddish or sometimes yellowish secondary hue; pale stones occur only occasionally. The shape of the zircon pieces varies considerably, ranging from completely rounded grains to perfectly euhedral crystals of predominantly short-prismatic habit (Figure 3d). Most, however, consist of moderately rounded, broken pieces that occasionally show crystal faces. Some of them have resorption features that might be due to transport in the basaltic magma (Balmer et al., 2009; Smith and Balmer, 2009).

Colour Enhancement

The brown zircon starting material is turned blue (Figure 4) by a simple heating process. The heat treatment takes place under reducing conditions at 900–1,000°C for one to a few hours (Smith and Balmer, 2009). The brown zircon (Figure 5a) is put into an alumina crucible (Figure 5b) that is sealed with a refractory clayey material (Figure 5c,d). The crucible is then enclosed in a larger crucible, which is sealed in the same manner. This assemblage is then placed in a charcoal furnace (Figure 5e) and covered with plenty of charcoal to achieve reducing conditions in an atmosphere of carbon monoxide and nitrogen. Obtaining the right temperature and atmosphere is a matter of experience; local gem treaters know the correct amount and type of charcoal to be used (for instance, charcoal made from mangrove wood works well). After two to three hours of heating, the crucible is opened and the still-hot zircon pieces initially appear colourless (Figure 5f). Only upon slow cooling do the zircon specimens develop the blue colour (Figure 5g,h).

The blue colouration of Ratanakiri zircon is long-term stable both in 'regular' daylight and in the dark; however, it shows a pronounced tenebrescence to both long- and short-wave UV radiation. Tenebrescence (i.e. reversible photochromism) is not a rare phenomenon in gems, and it has been occasionally observed for different colours and irradiations of zircon (McClure, 2011; Suthiyuth, 2014). The blue colour of Ratanakiri zircon changes to an unstable muddy greyish brown upon irradiation with long-wave UV radiation (including strong direct sunlight). The colour change appears to be fairly stable in the dark but reverses fairly soon after the sample is exposed to visible light without a UV component (Koivula and Misiorowski, 1986; Renfro, 2016).

Figure 4: These zircon samples from Ratanakiri (0.3–5.1 g) include two untreated brown crystals and three blue specimens that were heat treated at ~1,000°C under reducing conditions for a few hours. Photo by M. Zeug.

Figure 5: For the heat treatment of Ratanakiri zircon in a reducing environment, **(a)** the brown starting material is put into **(b)** an alumina crucible, and the lid is sealed with a refractory clayey material **(c, d)**. Heat treatment at ~900–1,000°C for 2–3 h is done in fairly simple ovens **(e)**, with plenty of charcoal to ensure reducing conditions. After opening the crucible lid, the still-hot zircon material appears rather colourless **(f)**, but becomes increasingly blue upon cooling **(g)**. A good fraction of the heated zircon **(h)** shows the typical vivid blue colour. Photos by L. Nasdala (a, d, e, h), Ralf Grunert (b, c, g) and Astrid Wittwer (f).

MATERIALS AND METHODS

Six gem-quality zircon specimens from Ratanakiri, Cambodia, ranging from 0.53 to 6.76 g, were sliced in half so that one part could be subjected to heating experiments while the other was retained for reference. Additional gem specimens from Ratanakiri also were heated without being sliced. The untreated samples were brown to reddish brown, some with light brown zones; the largest specimen showed fairly narrow primary growth zoning (Figure 6).

For comparison, we also analysed synthetic $ZrSiO_4$ crystals grown using Li-Mo flux techniques. These included (1) a batch of 0.5–0.8 mm 'sky'-blue V^{4+}-doped $ZrSiO_4$ (made available by Dr John M. Hanchar; for a description of the synthesis technique, see Hanchar et al., 2001); (2) one ~3 mm short-prismatic crystal of purplish blue U^{4+}-doped $ZrSiO_4$ (see Chase and

Osmer, 1966) provided by Dr George R. Rossman; and (3) various crystals of synthetic $ZrSiO_4$ individually doped with Pr, Sm, Nd, Tm or Dy, made available by Dr Dominik Talla (see Lenz et al., 2015). Optical absorption spectroscopy was performed on the first two sample sets, and photoluminescence (PL) spectroscopy was done on the third set, using the instrumentation described below.

The two largest Ratanakiri zircon specimens that were sliced—reportedly from Phnum Trom near Bo Keo—were bought from a local dealer in Ban Lung and were slabbed in his shop. Cutting was done parallel to the longest dimension of the nearly euhedral crystals to yield a pair of plates with matching faces. In both cases, the c-axis was oriented almost parallel to the cutting plane. One half of each specimen was then heat treated in Ban Lung by the same dealer (e.g. Figure 6). The other four zircon specimens that were sliced were first crystallographically oriented at the University of Vienna on a Nonius Kappa charge-coupled device (CCD) four-circle single-crystal X-ray diffraction system. Ten frames were obtained with a step width of 2° using Mo–K_α radiation. The samples were then cut in half along their c-axis using a diamond-coated tungsten wire. One half of each sample pair was subjected to heat treatment for two hours at 900°C in an electric oven, together with excess charcoal to ensure reducing conditions, whereas the other half was left in its original state. For all six samples, parallel-plane, doubly polished plates were prepared from both the heated slice and its untreated counterpart. After the completion of analyses, one blue zircon half was again heat treated, but this time under oxidising conditions at 1,000°C for three hours. Additional heating experiments were carried out on unsliced specimens under reducing conditions at 800°C, 900°C and 1,000°C, and under oxidising conditions at 300°C, 600°C, 800°C and 1,000°C. The samples were placed in a graphite crucible, which was heated at a rate of 10°C per minute to the designated temperature. After the three-hour annealing run, the furnace was switched off and the samples were allowed to cool down slowly. Those treated under reducing conditions were packed in charcoal, and those annealed under an oxidising atmosphere were simply heated in air.

Specific gravity values (here reported as mass density) were determined for the unheated halves of the two largest stones that were cut in Cambodia, as well as on the four other samples before they were sliced in half. All samples appeared more-or-less free of inclusions. The mass density values were determined by repeated weighing of the specimens in air and in distilled water (with a minute amount of detergent added to reduce surface tension).

Chemical analysis of major elements in the six samples, including both the untreated and annealed halves, was done by means of a Cameca SX 100 electron probe micro-analyser (EPMA) operated at 15 kV and 40 nA. The focal-spot diameter of the electron beam was 5 µm. The following synthetic and natural calibrant materials were used (lines analysed are shown in parentheses): $ZrSiO_4$ (Si–K_α; Zr–L_α), Hf metal (Hf–M_α), YPO_4 (Y–L_α), sanidine (Al–K_α), $ScVO_4$ (Sc–K_α), U

Figure 6: These two slices were cut from a gem-quality zircon crystal from Phnum Trom (largest dimension 17 mm). The samples were prepared as doubly polished plates (2.7 mm thick), and the half on the right was subjected to heat treatment whereas the one on the left remained in its initial state. The untreated specimen shows strong zoning, which disappeared after heat treatment. Photo by Astrid Wittwer.

metal (U–M_β), brabantite (Th–M_α), titanite (Ca–K_α), fluorapatite (P–K_α), almandine (Fe–K_α) and $YbPO_4$ (Yb–L_α). Peak/background counting times varied between 20/10 s and 80/40 s (the latter for the actinides). The modified φ(ρz) routine of Merlet (1994) was used for matrix correction and data reduction. Additional experimental details pertaining to EPMA analysis are described elsewhere (Breiter et al., 2010; Škoda et al., 2015).

Trace elements in the six samples, again including both untreated and annealed halves, were analysed with a Finnigan Element XR high-resolution laser ablation inductively coupled plasma mass spectrometer (LA-ICP-MS) system coupled to a GeoLas 193 nm excimer laser. The ablated material was transported to the ICP-MS using He carrier gas with a flow rate of 1.25 l/min, with additional Ar make-up gas added after the ablation cell. Elements in high abundance were analysed in analogue mode, whereas trace elements were analysed using a digital pulse counting mode. External independent calibration was done using NIST glasses 610 and 612 (Pearce et al., 1997) and USGS standard BCR-2G (Jochum et al., 2005). The laser spot size was varied between 40 µm (NIST glasses) and 59 µm (BCR-2G and zircon samples), resulting in an energy density of approximately 5 J/cm^2. The laser repetition rate was 8 Hz. Data reduction was done using the Iolite software package (Paton et al., 2011). For more analytical details, see Dorais and Tubrett (2012).

The U–Pb age of Ratanakiri zircon was determined for three fragments by means of solution isotope dilution thermal ionisation mass spectrometry (ID-TIMS) analysis (Krogh, 1973). The Pb and U isotope compositions were measured with a Finnigan MAT 262 mass spectrometer. After being cleaned with nitric acid, water and acetone, and weighed on a microbalance, the fragments were transferred to a Krogh-type FEP container and dissolved in hydrofluoric acid at 195°C after adding a ^{202}Pb–^{205}Pb–^{235}U spike. The spike composition was calibrated against synthetic ET100 solution (Condon et al., 2008) provided by the Earthtime initiative (www.earth-time.org). Further details of the analytical procedure are reported elsewhere (Corfu, 2004). All isotope ratios and ages were corrected for fractionation, spike and blank. The ^{204}Pb method was applied to correct for initial common Pb (based on Stacey and Kramers, 1975). The data were corrected for ^{230}Th disequilibrium according to Schärer (1984) and assuming a Th/U ratio of 4 in the magma.

Unit-cell dimensions were determined on five small chips (three brown and two blue) with a Huber 5042 four-circle single-crystal X-ray diffraction system. Analyses were done using non-monochromatised Mo radiation from a sealed-tube source at 50 kV and 30 mA. Fitting was done as implemented in the SINGLE software (Angel and Finger, 2010), and analytical settings of Hejny et al. (2012) were used.

Raman and PL spectroscopy of the six sliced samples, including untreated and annealed halves, was performed at room temperature using a dispersive Horiba LabRAM HR Evolution spectrometer equipped with an Olympus BX Series optical microscope and an Si-based, Peltier-cooled CCD detector. The analysed light was dispersed using a diffraction grating with 1,800 (Raman) or 600 (PL) grooves per millimetre. Raman spectra were excited with the 632.8 nm emission of an He-Ne laser, and PL spectra were obtained using the 473 nm emission of a diode-pumped solid-state laser. In both cases, the laser power was 10 mW at the sample. The system was calibrated using the Rayleigh line and emission lines of a Kr lamp, resulting in a wavenumber accuracy of better than 0.5 cm^{-1}. Band fitting was done after appropriate background correction, assuming Lorentzian–Gaussian band shapes. Calculated full widths at half-band maximum (FWHMs) were corrected for instrumental broadening using the empirical formula of Váczi (2014).

Optical absorption spectra in the visible to near-infrared range were obtained for all six samples in the two principal polarisations (i.e. E⊥c and E||c) in the spectral range 24,100–5,250 cm^{-1} (which roughly corresponds to 415–1,900 nm wavelength*). Analysis of the UV range was omitted because of the well-known tenebrescence

* In this article, optical absorption spectra and PL spectra are plotted and discussed on the wavenumber ($\tilde{\nu}$) scale. The wavenumber is defined as the reciprocal of the wavelength λ; it is quoted in reciprocal centimetres (conversion $\tilde{\nu}$ [cm^{-1}] = 10^7 / λ [nm]). The wavenumber scale is preferred when evaluating spectroscopic data because wavenumber values (but not the wavelengths) are proportional to the photon energy of the detected light. This makes possible reliable band fitting and direct comparison of important diagnostic features (e.g. FWHMs, band shapes and band asymmetries) across the entire spectral range. By contrast, spectra plotted on the wavelength scale are distorted in energy, with the blue and UV ranges being compressed and the red and NIR portions being stretched. This results in strongly distorted band shapes that will bias any band fitting. The authors understand that the wavelength scale is traditionally preferred among gemmologists for describing the UV, visible and NIR spectral ranges. For convenience, we therefore present all PL and optical absorption spectra with additional labels for the top abscissa axis showing the wavelength scale (in nm), and wavenumber values in the text and figures are accompanied by their respective wavelength values in parentheses.

of blue zircon (irradiation with UV light, as an analytical artefact, produces a colour change that would bias the spectra obtained). Spectra were recorded at room temperature using a Bruker IFS 66v/S Fourier-transform infrared spectrometer equipped with a mirror-optics IR-scope II microscope and a quartz beam splitter. A calcite Glan prism was used to polarise the light. Circular areas 200 µm in diameter were analysed in transmission geometry. The following combinations of light sources and detectors were used: Xe-lamp source and GaP detector for the spectral range 24,100–20,000 cm^{-1} (40 cm^{-1} spectral resolution; 1,024 scans), W-lamp source and Si detector for the range 20,000–10,000 cm^{-1} (20 cm^{-1} spectral resolution; 1,024 scans) and W-lamp source and Ge detector for the range 10,000–5,200 cm^{-1} (10 cm^{-1} spectral resolution; 512 scans). The final spectra therefore consisted of a combination of three sub-spectra that were aligned to match in absorbance if necessary.

RESULTS AND DISCUSSION

General Description and Heat Treatment

Many of the untreated brown Ratanakiri zircon specimens contained macroscopically visible dark impurities and/or large cavities. The latter were partially filled with baddeleyite (identified by Raman spectroscopy) and other secondary phases (Figure 7a,b). In addition, fluid inclusions showing various appearances were commonly observed. Some of them were transparent and colourless (Figure 7c), and others were dark brown and apparently opaque (Figure 7d) or consisted of two-phase inclusions filled with liquid and gas (Figure 7e). The fluid phase was predominantly composed of H_2O (broad, low-intensity Raman band in the 3,200–3,500 cm^{-1} range). Occasionally they contained CO_2 gas bubbles (Figure 7e; doublet of narrow Raman bands at 1,285 and 1,388 cm^{-1}). Many fluid inclusions were surrounded by a network of veinlets that appeared to be partially healed fissures (Figure 7c). Much more rarely, dark fluid inclusions sometimes were surrounded by a halo containing phases that obviously were derived from the inclusion itself (Figure 7d). The water-rich fluid phase in the halo occasionally contained hematite flakes (identified by Raman spectroscopy; see Figure 7d).

Mass density values of the six untreated samples averaged 4.674 ± 0.005 g/cm^3. This corresponds well to published density values in the range of 4.63–4.72 g/cm^3 for non- to mildly radiation-damaged zircon from Sri Lanka (Vaz and Senftle, 1971; Murakami et al., 1991).

Before heat treatment, the specimens showed brown to reddish brown colour, occasionally with an orangey hue, and some displayed distinct colour zoning (Figures 6 and 7f). Heating under reducing conditions at 800°C created a very pale blue colour. After heating at 900°C or 1,000°C under reducing conditions, the zircon samples showed a rather intense blue colouration, but with some variation in the depth of colour (see Figure 5h). The blue colour was rather uniform within single stones; primary growth zoning became invisible after the heating process (Figure 6). Our observation of a more-or-less equally intense blue colour after heating at 900°C and 1,000°C is in some contrast to the results of earlier studies. Thongcham et al. (2010) found maximum colouration after heating at 900°C, whereas at 1,000°C the colour was clearly paler. Laithummanoon and Wongkokua (2013), by contrast, produced a rather pale blue at 900°C, whereas the richest colour was reached at 1,100°C. Summarising all available data, we conclude that 900–1,000°C (Smith and Balmer, 2009) is the most promising temperature range for the creation of attractive blue colour in Ratanakiri zircon.

Heating of both the untreated brown and the heated blue zircon under oxidising conditions at 300°C resulted in significant but incomplete decolouration. This appears to be consistent with the results of Wanthanachaisaeng et al. (2014) and Siriaucharanon et al. (2017), who observed fading of the dark brown colour to nearly colourless at 400°C, although after initially heating their samples under reducing conditions. We found in our experiments that after oxidised heating at 600°C and above, the zircon samples became colourless to pale orange, without further significant changes at 800°C and 1,000°C.

We also did a series of 'alternative heating' experiments, in which the zircon specimens were subjected to multiple heat treatments at 1,000°C for three hours each: first in a reducing atmosphere, then under oxidising conditions, then again under a reducing atmosphere and so on. Heating in a reducing atmosphere resulted in blue, subsequent oxidised heating produced nearly colourless with an orange tinge, then the same shade of blue reappeared after heating under reducing conditions, etc. We were able to switch the blue colour on and off within the same specimen. In conclusion, the blue colouration can be restored, whereas there is no heat-treatment technique that recovers the initial brown to reddish brown colour. This indicates that the initial brown colour is likely caused by an irradiation-induced defect that anneals upon heat treatment.

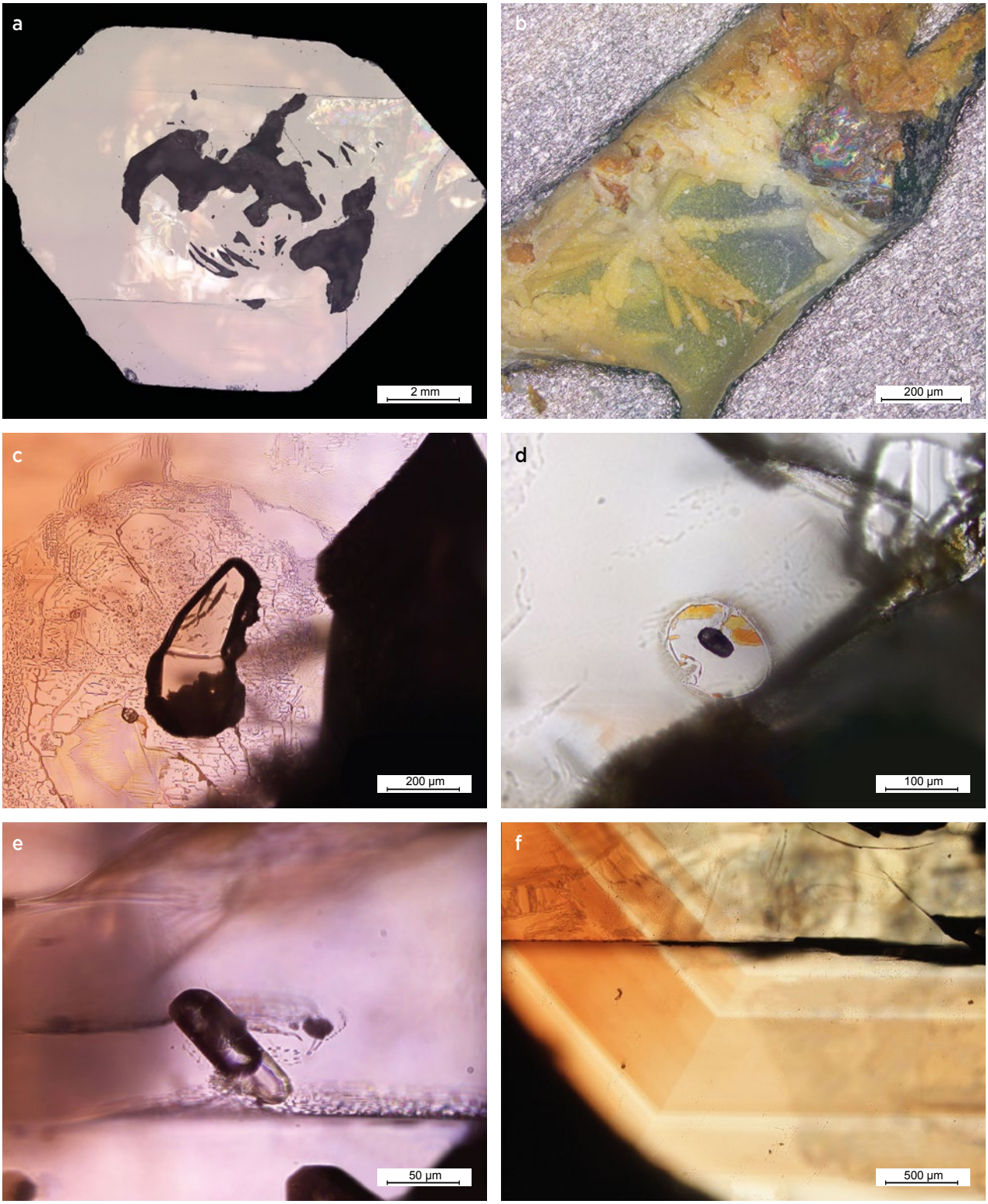

Figure 7: Various internal features are displayed by unheated Ratanakiri zircon. **(a)** Partially filled cavities are present inside a sliced zircon crystal. **(b)** The cavities are filled with yellowish baddeleyite and other unidentified alteration products. **(c)** This transparent fluid inclusion (mainly consisting of water) is surrounded by delicate patterns that trace fluid movement along fissures into the surrounding host. **(d)** An opaque inclusion of unknown composition is surrounded by a halo composed of water (clear area) and hematite (orange phase). **(e)** This fluid inclusion contains a large CO_2 bubble. **(f)** Typical primary colour zoning is shown in an unheated brown zircon specimen. Photomicrographs by M. Zeug, in reflected light (a, b) and plane-polarised transmitted light (c–f).

Chemical Composition

Chemical data for Ratanakiri zircon determined by EPMA and LA–ICP–MS analyses are summarised in Table I. The samples generally had low contents of non-formula elements, below the 0.1 wt.% level, with the only exception being Hf (~0.7 wt.% HfO_2). This value is well within the typical range for zircon and hence it does not provide any particular hint as to the formation milieu (e.g. Belousova et al., 2002). Actinide and REE concentrations were slightly higher in zones and areas of darker brown colour, compared to paler brown regions. The actinides U and Th had average concentrations of approximately 120 ppm and 95 ppm, respectively. As is common for zircon, heavy REEs were enriched relative to the middle and light REEs (Table I; cf. Hoskin and Schaltegger, 2003; Hanchar and Westrenen, 2007). This also was evident in laser-induced PL spectra, which were dominated by strong emissions of Dy^{3+}, along with lower-intensity emissions of Sm^{3+}, Pr^{3+}, Tm^{3+} and Nd^{3+} (Figure 8). The REE mass fractions of Ratanakiri zircon were slightly off the general trend for igneous zircon (Figure 9). We also observed a positive Ce anomaly (Ce/Ce* = 42) but virtually no Eu anomaly (Eu/Eu* = 1.07). By contrast, most igneous zircon samples display both a positive Ce anomaly and a negative Eu anomaly (Hoskin and Schaltegger, 2003). Our observations indicate formation of Ratanakiri zircon under oxidising conditions, where Eu is mainly trivalent and Ce is mainly tetravalent (Hanchar et al., 2001). The absence of a negative Eu anomaly is not unusual; it has been observed in zircon crystals derived from kimberlites (Hoskin and Ireland, 2000) and syenite xenoliths associated with corundum (Hinton and Upton, 1991; Sutherland et al., 2002).

Age Determination

Results of seven ID-TIMS analyses of Ratanakiri zircon are presented in Table II. The mean $^{206}Pb/^{238}U$ age was determined at 0.92 ± 0.07 Ma (error quoted at the 95% confidence level). This very young age appears consistent with the LA–ICP–MS results of Sutherland et al. (2015), who determined a mean $^{206}Pb/^{238}U$ age of 0.83 ± 0.15 Ma for three zircon inclusions in sapphires from Bo Loi, Ratanakiri. Those zircon inclusions, however, were genetically different from Ratanakiri gem zircon, as indicated by their much higher actinide concentrations of 299–1,114 ppm U and 150–1,270 ppm Th (Sutherland et al., 2015).

Table I: Average chemical composition of Ratanakiri zircon determined by EPMA and LA-ICP-MS.

EPMA results (n = 172)[a]		LA–ICP–MS results (n = 26)					
Oxide	Concentration (wt.%)[b]	Element	Isotope measured	Concentration (ppm)[c]	Element	Isotope measured	Concentration (ppm)[c]
SiO_2	32.6 ± 0.2	P	31	73.5 ± 15.6	Tb	159	4.37 ± 2.37
ZrO_2	66.8 ± 0.3	Ti	49	6.37 ± 2.46	Dy	163	48.5 ± 23.7
HfO_2	0.693 ± 0.035	V	51	nd[d]	Ho	165	16.3 ± 7.2
P_2O_5	0.042 ± 0.009	Y	89	440 ± 182	Er	166	63.6 ± 24.6
Total	100.2 ± 0.4	Nb	93	5.62 ± 3.97	Tm	169	12.1 ± 4.1
		La	139	nd	Yb	172	104 ± 31
		Ce	140	2.84 ± 1.89	Lu	175	16.6 ± 4.2
		Pr	141	0.07 ± 0.05	Hf	179	5,869 ± 266
		Nd	146	1.11 ± 0.83	Pb	208	nd
		Sm	147	2.30 ± 1.45	Th	232	94.2 ± 94.9
		Eu	153	1.84 ± 1.10	U	238	119 ± 68
		Gd	157	11.9 ± 6.7			

[a] Al_2O_3, Sc_2O_3, CaO, FeO, Yb_2O_3, UO_2 and ThO_2 were not detected or averages were below 0.005 wt.%.
[b] Quoted errors are 2σ. [c] Quoted errors are 1σ. [d] nd = not detected.

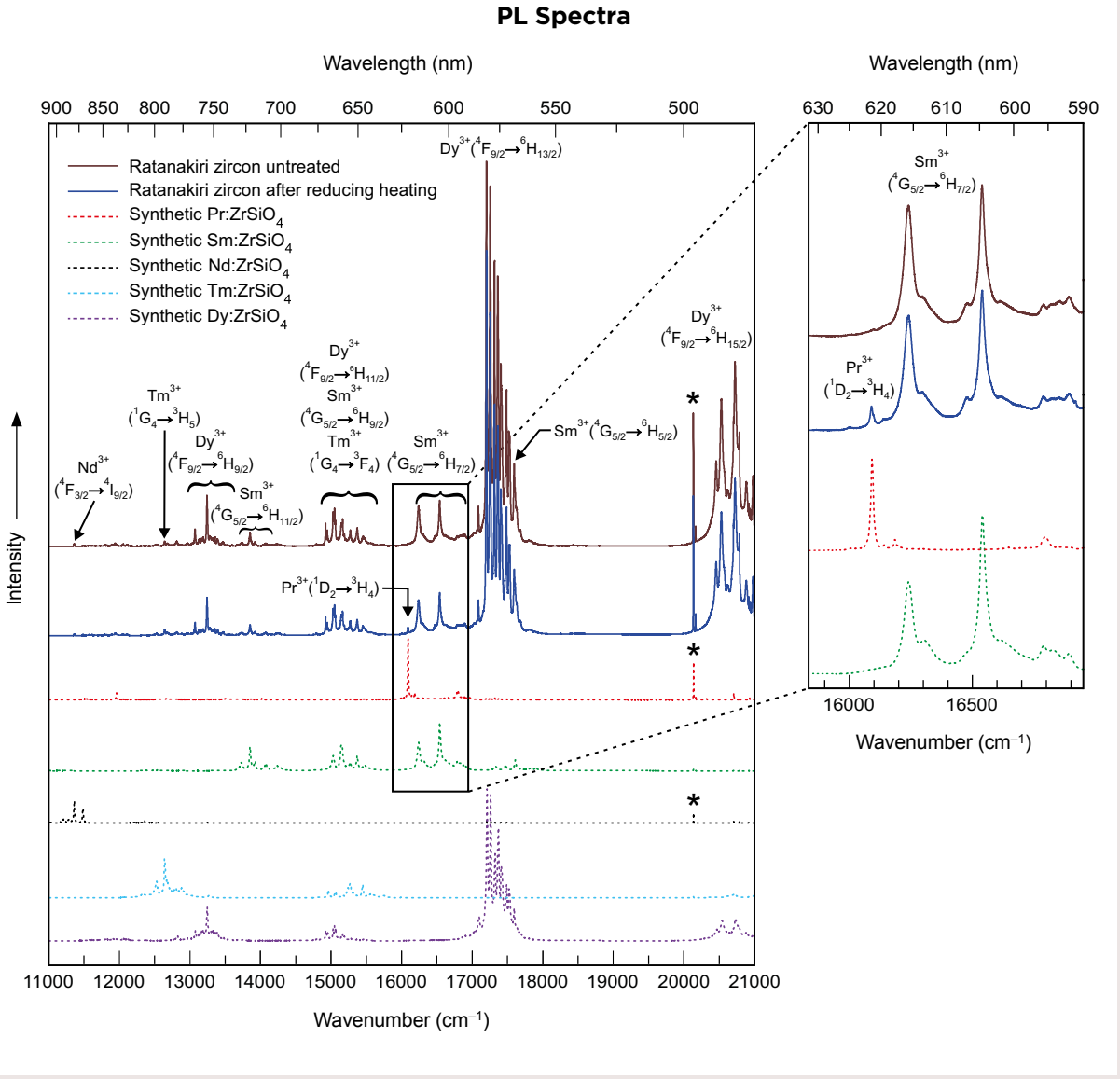

Figure 8: Representative PL spectra are shown for unheated and heat-treated Ratanakiri zircon, and compared to reference spectra of REE-doped synthetic $ZrSiO_4$. Note that the $^1D_2 \rightarrow {}^3H_4$ transition of Pr^{3+} is only observed in the PL spectrum of heat-treated blue Ratanakiri zircon. Raman bands in the PL spectra are marked by asterisks. For assignment of PL lines see Gaft et al. (2000) and Lenz et al. (2015); for assignment of Raman bands see Nasdala et al. (1995; and references therein).

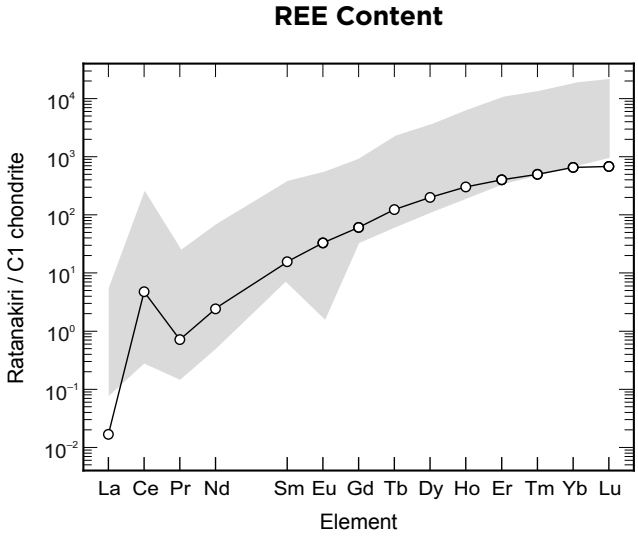

Figure 9: The average C1 chondrite-normalised REE concentrations in Ratanakiri zircon determined by LA-ICP-MS are plotted together with a shaded grey area, which shows the REE ranges of typical unaltered igneous zircon (graphically extracted from Figure 4 of Hoskin and Schaltegger, 2003).

Table II: U-Pb geochronology data (ID-TIMS results) for Ratanakiri zircon.

Analysis no.	Weight (µg)	Pb (ppm)	U (ppm)	Th (ppm)	Pb_{com}[a] (pg)	$^{206}Pb/^{204}Pb$[b]	$^{206}Pb/^{238}U$)	$^{206}Pb/^{238}U$ age (Ma)	$^{207}Pb/^{235}U$	$^{207}Pb/^{206}Pb$
389/10	529	0.020	39.4	6.9	9.8	37.8	0.000160 ± 0.000003	**1.03 ± 0.02**	0.00124 ± 0.00021	0.0563 ± 0.0100
389/10[c]	–	0.008	39.5	11.6	3.6	64.9	0.000143 ± 0.000001	**0.92 ± 0.01**	0.00093 ± 0.00010	0.0472 ± 0.0051
391/1	1166	0.004	31.9	11.6	1.8	191.1	0.000145 ± 0.000000	**0.93 ± 0.00**	0.00108 ± 0.00004	0.0539 ± 0.0020
394/1	585	0.031	39.3	54.3	16.4	29.0	0.000128 ± 0.000004	**0.83 ± 0.03**	0.00080 ± 0.00025	0.0451 ± 0.0155
391/2	840	0.014	46.4	20.5	8.5	56.6	0.000148 ± 0.000001	**0.95 ± 0.01**	0.00136 ± 0.00008	0.0668 ± 0.0044
394/2	948	0.022	58.1	24.1	14.9	47.9	0.000142 ± 0.000002	**0.91 ± 0.01**	0.00132 ± 0.00010	0.0676 ± 0.0054
394/3	833	0.038	40.0	1.1	29.1	27.1	0.000134 ± 0.000005	**0.86 ± 0.03**	0.00094 ± 0.00030	0.0510 ± 0.0187

[a] Pb_{com} = total common Pb in sample (initial plus blank).
[b] Raw data, corrected for fractionation and spike.
[c] The solution for sample 389/10 was separated after dissolution and before chemical separation, for aliquot analysis.

Structural State

The dimensions of the tetragonal unit cell were determined as a_0 = 6.604 ± 0.001 Å and c_0 = 5.979 ± 0.001 Å, resulting in a unit cell volume of 260.73 Å^3. These values coincide (within errors) with the unit cell parameters of synthetic pure $ZrSiO_4$ (Nasdala et al., 2002; Van Westrenen et al., 2004). The unit cell dimensions convert to an 'X-ray mass density' of 4.6699 g/cm^3, comparable to the average measured density of 4.674 ± 0.005 g/cm^3. The FWHM of the $\nu_3(SiO_4)$ Raman band, which is used to estimate the degree of self-irradiation damage in zircon (Nasdala et al., 1995), averaged 1.8 ± 0.2 cm^{-1} (Figure 10a), indicative of a very high degree of crystallinity. The Raman spectrum of Ratanakiri zircon is, therefore, indistinguishable from that of synthetic pure $ZrSiO_4$ (Nasdala et al., 2002).

Both X-ray and Raman results were identical within errors for unheated samples and their heat-treated analogues. This, and the conformity to synthetic pure $ZrSiO_4$, indicates first that the generally low amounts of trace elements do not cause detectable deviation from the ideal zircon structure. Second, the absence of any detectable structural change upon annealing indicates that Ratanakiri zircon has not accumulated noticeable amounts of radiation damage. The alpha dose, calculated from the U–Pb age and average U and Th concentrations, is 4 × 10^{14} α/g, which is well below the self-irradiation level of ~5 × 10^{16} α/g that is known to cause initial spectroscopically detectable changes to zircon (Figure 10b; cf. Zhang et al., 2000; Nasdala et al., 2001).

Hence, it is not possible to unravel the heat treatment of Ratanakiri zircon by means of structural analysis. By contrast, there was a minor but interesting difference in the PL spectra: We found that the emission of treated Ratanakiri zircon always contained a low-intensity, narrow line at 16,090 cm^{-1} (621.5 nm wavelength; strong E⊥c polarisation), whereas untreated specimens did not show this feature. It is assigned to the $^1D_2 \rightarrow {}^3H_4$ electronic transition of Pr^{3+} (Figure 8; cf. Gaft et al., 2000). Its presence, however, cannot be used as a general indicator for the heat treatment of zircon, as the Pr^{3+} line has also been observed in untreated zircon specimens (e.g. the Sri Lankan reference zircon GZ7; Nasdala et al., research in progress).

Optical Absorption Spectroscopy

Optical absorption spectra are shown in Figure 11. Note again that the UV spectral region was not analysed in the present study because of the material's strong photochromism—that is, the fairly fast blue-to-brown colour change upon irradiation with, and hence analysis in, UV light.

The optical absorption spectrum of untreated Ratanakiri zircon was dominated by the following features: an intense absorption edge that extended from the UV into the blue range and down towards the NIR region; an intense broad absorption band near 19,800 cm^{-1} (505 nm wavelength); a rather weak, broad absorption band near 12,500 cm^{-1} (800 nm wavelength); and two groups of narrow absorption bands near 9,025 cm^{-1} (1,108.0 nm wavelength, with a shoulder at ~9,190 cm^{-1} or 1,088.1 nm) and 6,665 cm^{-1} (1,500.4 nm wavelength) that are polarised with E⊥c (Figure 11a). The reddish brown colour of the unheated zircon is due to the combination of the first two features listed above, which cause enhanced absorption in the blue-to-green range. The

~19,800 cm^{-1} (~505 nm) band appears to be an analogue of the 510–515 nm absorption band described by Klinger et al. (2012). Those authors assigned reddish brown zircon colouration to a paramagnetic oxygen-hole centre nearest-neighbouring to an uncompensated Y^{3+} that substitutes for Zr^{4+}. This assignment is supported by the disappearance of the 505–515 nm band upon heating: It has been known for a long time that electron- or hole-related colour centres are irreversibly destroyed at fairly low temperatures of a few hundred degrees Celsius (Gastil et al., 1967; Fielding, 1970). Such hole centres may be generated slowly in zircon by radioactive self-irradiation (Rossman, 1981). If this is confirmed true, the very low self-irradiation dose experienced by Ratanakiri zircon might suggest that both the development of Y^{3+}-related brown colouration and its saturation require fairly low irradiation levels. The two narrow absorptions in the spectral range below 10,000 cm^{-1} (i.e. above 1,000 nm wavelength) are due to U^{5+} (Vance and Mackey, 1974; Zhang et al., 2003). However, they do not contribute to the colouration, as these absorptions are in the NIR range.

After heating at 1,000°C in reducing conditions, the absorption edge and the bands at ~19,800 cm^{-1} (~505 nm) and ~12,500 cm^{-1} (~800 nm) were reduced significantly in intensity (Figure 11b). The spectra showed a new, strongly pleochroic (E⊥c) absorption band centred at ~15,600 cm^{-1} (~640 nm wavelength) with an FWHM of >3,000 cm^{-1} (≥125 nm wavelength; Figure 11b). The absorption in the 18,200–13,000 cm^{-1} (~550–770 nm wavelength) range results in a 'window' of reduced absorption in the blue to greenish blue region. Only a minor fraction of the uranium was reduced to U^{4+}, whereas the majority remained in the pentavalent state. The appearance of tetravalent U is seen in particular with E⊥c polarisation by two narrow, low-intensity bands at 15,290 cm^{-1} (654.0 nm wavelength) and 14,480 cm^{-1} (690.6 nm wavelength). Due to their very small area integral compared to that of the broad ~15,600 cm^{-1} (~640 nm) band, the contribution of U^{4+} absorption is considered insignificant for blue zircon colouration.

After heating at 1,000°C in oxidising conditions, the ~15,600 cm^{-1} (~640 nm) band disappeared completely (Figure 11c). It is worth noting that oxidised heating was

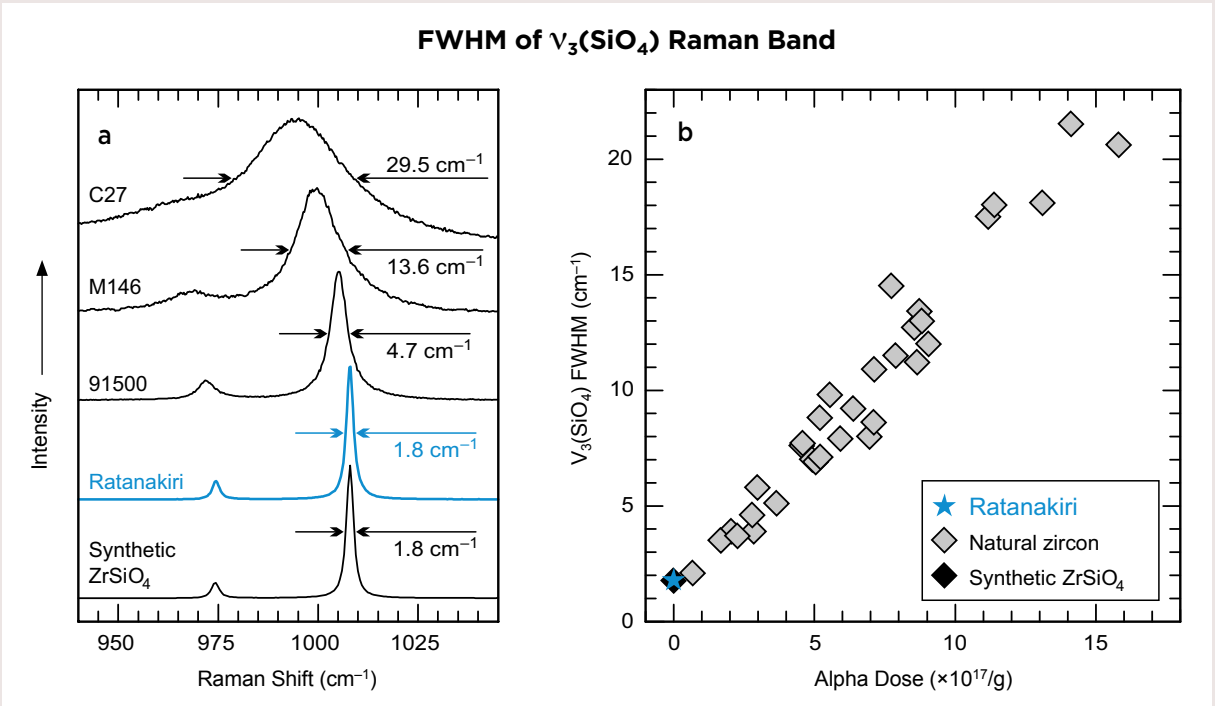

Figure 10: (a) The Raman spectrum (SiO_4 stretching region) of Ratanakiri zircon is shown in comparison with spectra of synthetic $ZrSiO_4$ and three natural zircons with different degrees of radiation damage: sample 91500 from Kuehl Lake, Ontario, Canada (mildly damaged; see Wiedenbeck et al., 2004); and samples M146 (moderately damaged) and C27 (severely damaged), both from gem gravels in Ratnapura, Sri Lanka (for both, see Nasdala et al., 2004). **(b)** A plot of the FWHM of the $\nu_3(SiO_4)$ Raman band near 1,000 cm^{-1} against the alpha dose includes data for Ratanakiri zircon, various samples of natural zircon (from Nasdala et al., 2001) and synthetic $ZrSiO_4$. Both plots reveal that Ratanakiri zircon is spectroscopically indistinguishable from (perfectly crystalline) synthetic $ZrSiO_4$, indicating that Ratanakiri zircon has accumulated extremely low amounts of radiation damage.

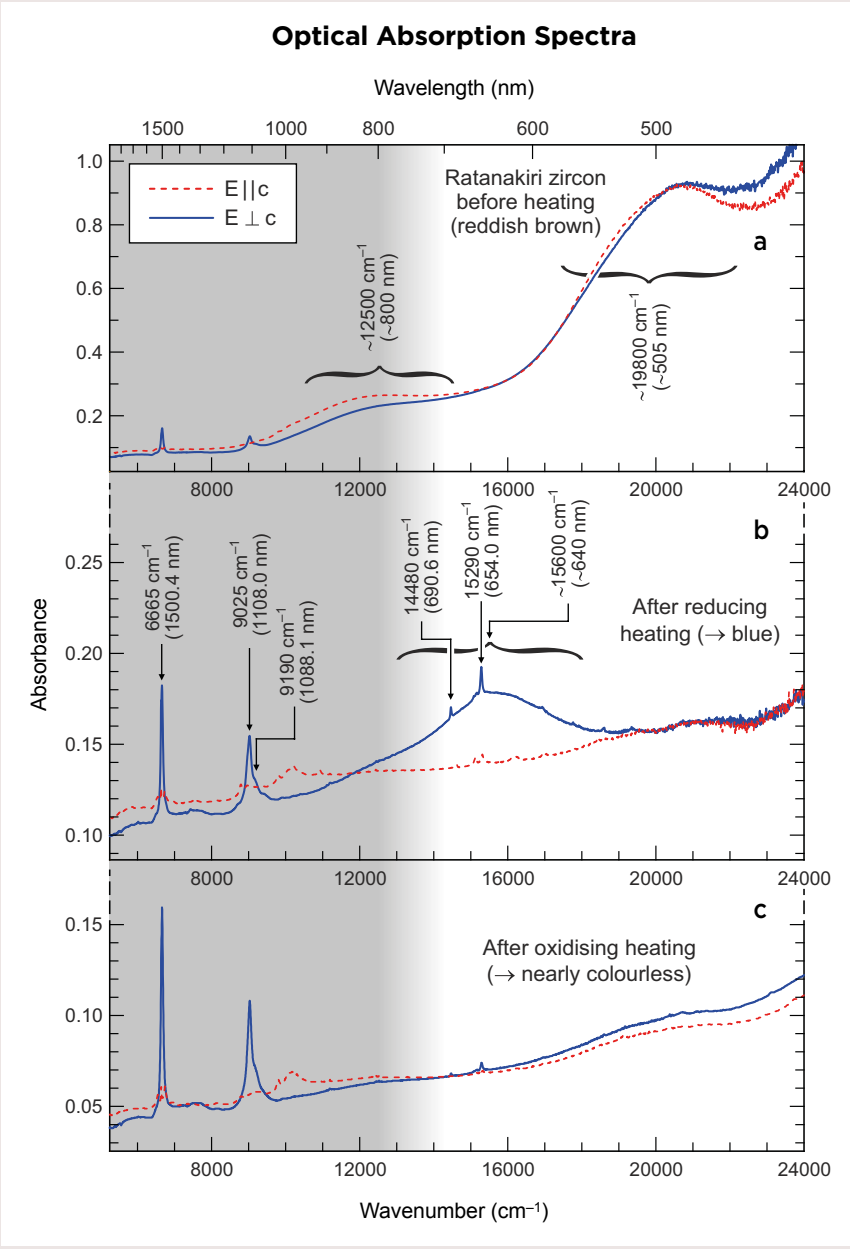

Figure 11: Polarised optical absorption spectra of Ratanakiri zircon (sample thickness 2.7 mm) were obtained from the same specimen **(a)** before heating, and then after heat treatment at 1,000°C under **(b)** reducing and **(c)** oxidising conditions. The near-infrared range, invisible to the human eye, is shaded grey. After heating under reducing conditions, a broad absorption band in the 18,200–13,000 cm^{-1} (~550–770 nm) region is observed with E⊥c. This band, of unknown attribution, results in a 'window' of reduced absorption in the blue to greenish blue range. Intense, sharp bands in the NIR region, especially at 6,665 cm^{-1} (1,500.4 nm) and 9,025 cm^{-1} (1,108.0 nm) are assigned to U^{5+}-related centres; these bands, however, do not contribute to the colouration.

found to produce the same colouration (near-colourless) and absorption spectrum, independent of whether the starting material was unheated reddish brown or heat-treated blue. Similar to the results obtained for blue samples, the absorption edge and the ~19,800 cm^{-1} (~505 nm) and ~12,500 cm^{-1} (~800 nm) bands were reduced significantly, with the absorption in the entire visible range being even slightly lower than in samples heated under reducing conditions. Compared to the spectrum of the blue zircon, the U^{4+} absorption features at 15,290 cm^{-1} (654.0 nm) and 14,480 cm^{-1} (690.6 nm) were appreciably lessened, in favour of a slight re-increase of the U^{5+} features at 9,025 cm^{-1} (1,108.0 nm) and 6,665 cm^{-1} (1,500.4 nm).

Cause of the Blue Colouration

The interpretation of the ~15,600 cm^{-1} (~640 nm) band that causes blue colouration is problematic. This band appears quite similar in spectral position, width and polarisation to the ~15,650 cm^{-1} (~639 nm) absorption band of V^{4+} in synthetic $ZrSiO_4$ (Figure 12a; cf. Niesert et al., 2002). Nevertheless, the blue colour of Ratanakiri zircon cannot be assigned to V^{4+}. First, the ~6,900 cm^{-1} (~1,450 nm wavelength) absorption of V^{4+} with E||c is missing from the optical absorption spectra of blue Ratanakiri zircon. Second, the concentration of V in Ratanakiri zircon is below the LA-ICP-MS detection limit (< 0.04 ppm), whereas blue V^{4+}-doped $ZrSiO_4$ has vanadium concentrations in the weight percent range (e.g. Niesert

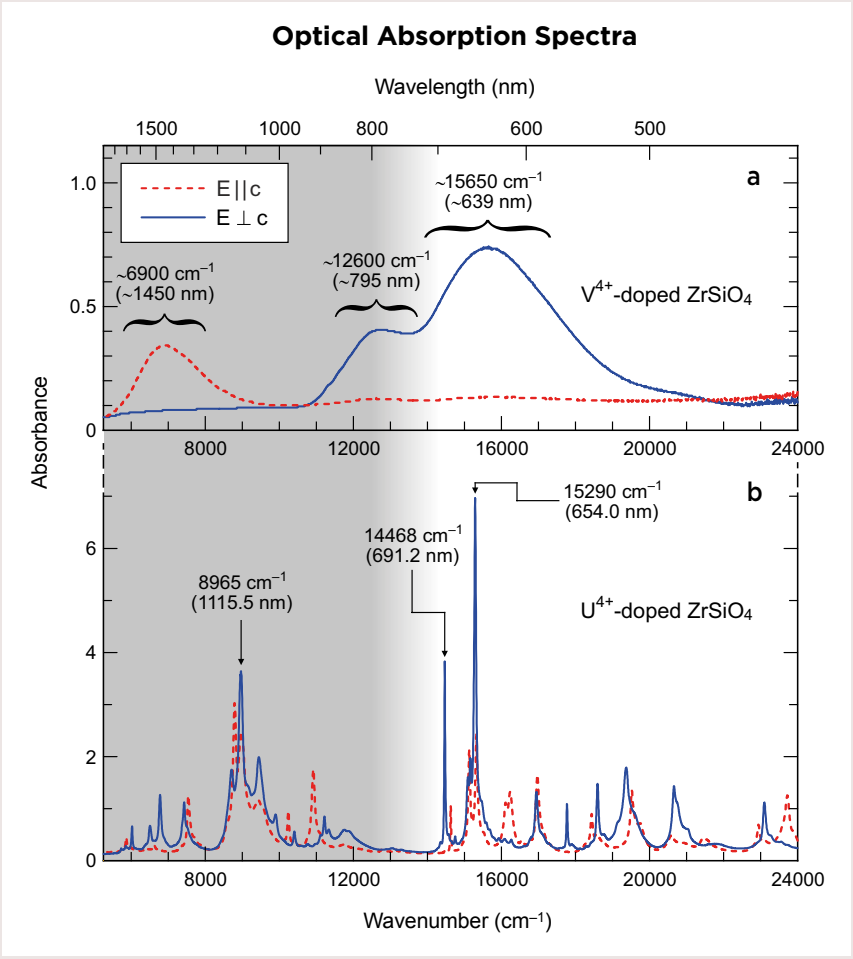

Figure 12: These polarised optical absorption spectra of two blue synthetic $ZrSiO_4$ samples doped with **(a)** V^{4+} (sample thickness ~0.3 mm) and **(b)** U^{4+} (~1.5 mm thick) are shown for comparison with the Ratanakiri zircon in Figure 11.

et al., 2002 reported 1.28 wt.% V for their blue pigment). Third, if V^{4+} caused the colour of Ratanakiri zircon, a valence change of the V needs to be assumed to explain the colour change upon oxidised heating. This is in contrast to the fact that blue V^{4+}-doped $ZrSiO_4$ is grown under oxidising conditions (Niesert et al., 2002). Also, we performed heat-treatment experiments on V^{4+}-doped $ZrSiO_4$ crystals, and neither reduced nor oxidised heating seemed to affect their blue colouration.

Another possible cause of the blue colour of zircon is the elevated presence of U^{4+}. The absorption of this ion in the $ZrSiO_4$ structure is characterised by numerous, strongly polarised lines (Richman et al., 1967), with the strongest absorptions in the red range. Together with the commonly present absorption edge that extends from the UV into the blue range, U^{4+} absorption might cause green zircon colouration (Kempe et al., 2016, and references therein), whereas U^{4+} alone causes blue. We had the opportunity to verify this by studying one of the historic synthetic U^{4+}-doped $ZrSiO_4$ crystals grown by Judith A. Osmer, now in the sample collection of Dr George R. Rossman. Whereas Chase and Osmer (1966) described green U-doped zircon, the specimen loaned to us displayed blue colour with a weak purplish hue. The optical absorption spectra are shown in Figure 12b.

Previous authors (Wanthanachaisaeng et al., 2010; Satitkune et al., 2013) have assumed that the blue colour of Ratanakiri zircon might be assigned to a change in the oxidation state of uranium. This was questioned by Thongcham et al. (2010), who found that upon heating above 900°C, the blue colour decreased whereas the narrow U^{4+} absorption still increased. Our optical absorption spectra of blue Ratanakiri zircon (Figure 11) show U^{4+} absorption lines of very low intensity. Despite the reducing conditions during heating, most of the U remained in the pentavalent state. There was minor $U^{5+} \rightarrow U^{4+}$ transformation; this, however, was negligible compared to the observed change in colour. Another consideration questioning U as the colour cause is that, of all zircons, the low-U Ratanakiri material is particularly susceptible to develop blue colour. One would expect that if U caused blue colour, zircon containing

Figure 13: This yellow gold ring contains a 4.84 ct heat-treated Ratanakiri zircon. Courtesy of Beau Soleil (Scottsdale, Arizona, USA); photo by Jeff Scovil.

more U should show an even more intense blue. That, however, is not the case.

Another attempted assignment of the blue colour was published by Laithummanoon and Wongkokua (2013). They speculated that the blue colouration is due to a change in the oxidation state of Tb (i.e. $Tb^{4+} \rightarrow Tb^{3+}$) upon heating under reducing conditions. This was based on the two observations that the colour change was accompanied (1) by the disappearance of Tb^{4+} signals in electron paramagnetic resonance spectra and (2) by the concurrent appearance of a small absorption feature near 650 nm. However, the ~650 nm feature also was present in optical absorption spectra obtained by Laithummanoon and Wongkokua (2013) after oxidised heating at 600°C and 700°C, which produced nearly colourless samples and questions the contribution of the ~650 nm feature to zircon colouration. We assign the broad ~650 nm band observed by Laithummanoon and Wongkokua (2013) to U^{4+} (cf. 15,290 cm^{-1} or 654.0 nm band in Figure 12b). Also, one should note that the electronic structure of Tb^{3+} shows a huge gap between ~20,000 and 6,000 cm^{-1} (~500–1,667 nm wavelength; Dieke and Crosswhite, 1963; Couwenberg et al., 1998), which suggests that absorption of visible light is only possible in the blue range.

CONCLUSIONS

Zircon from Ratanakiri Province in north-eastern Cambodia is mined from secondary deposits associated with the weathering of alkali basaltic rocks. We determined a mean $^{206}Pb/^{238}U$ age of 0.92 ± 0.07 Ma for the zircon. The unit cell dimensions and Raman data indicated a very high degree of crystallinity, which is consistent with the young age and the low concentration of actinides. Our samples also had consistently low contents of other non-formula elements (i.e. below the 0.1 wt.% level), with the only exception being Hf (~0.7 wt.% HfO_2, which falls within the typical range for zircon).

Ratanakiri zircon turns vivid blue (e.g. Figure 13) upon heat treatment under reducing conditions at 900–1,000°C. Based on the new data presented here, the authors exclude several of the potential colour causes that have been proposed in the literature thus far. However, we are still unable to provide convincing explanations (1) for the blue colour of Ratanakiri zircon and (2) for why zircon from other localities is much less, or even not at all, susceptible to an analogous colour change. Even though we have demonstrated that the blue colour is due to a broad, strongly polarised absorption band (E⊥c) in the red-to-yellow range (centred at ~15,600 cm^{-1}, or ~640 nm wavelength), a definitive assignment of this band remains enigmatic.

REFERENCES

Anderson B.W. and Payne C.J., 1998. Absorption spectra of zircon. In R.K. Mitchell, Ed., *The Spectroscope and Gemmology*, GemStone Press, Woodstock, Vermont, USA, 194–202.

Angel R.J. and Finger L.W., 2010. SINGLE: A program to control single-crystal diffractometers. *Journal of Applied Crystallography*, **44**(1), 247–251, http://dx.doi.org/10.1107/s0021889810042305.

Balmer W.A., Smith M.H., Sriprasert B. and Wanthanachaisaeng B., 2009. Ratanakiri, the legendary zircon province of Cambodia. *European Gemmological Symposium*, Berne, Switzerland, 5–7 June, 51–53.

Belousova E., Griffin W., O'Reilly S.Y. and Fisher N., 2002. Igneous zircon: Trace element composition as an indicator of source rock type. *Contributions to Mineralogy and Petrology*, **143**(5), 602–622, http://dx.doi.org/10.1007/s00410-002-0364-7.

Breiter K., Copjakova R. and Skoda R., 2010. The involvement of F, CO_2, and As in the alteration of Zr-Th-REE-bearing accessory minerals in the Hora Svate Kateriny A-type granite, Czech Republic. *Canadian Mineralogist*, **47**(6), 1375–1398, http://dx.doi.org/10.3749/canmin.47.6.1375.

Burns R.G., 1993. *Mineralogical Applications of Crystal Field Theory*, 2nd edn. Cambridge University Press, Cambridge, 576 pp.

Cappelletti G., Ardizzone S., Fermo P. and Gilardoni S., 2005. The influence of iron content on the promotion of the zircon structure and the optical properties of pink coral pigments. *Journal of the European Ceramic Society*, **25**(6), 911–917, http://dx.doi.org/10.1016/j.jeurceramsoc.2004.04.023.

Chase A.B. and Osmer J.A., 1966. Growth and preferential doping of zircon and thorite. *Journal of the Electrochemical Society*, **113**(2), 198–199, http://dx.doi.org/10.1149/1.2423904.

Chen T., Ai H., Yang M., Zheng S. and Liu Y., 2011. Brownish red zircon from Muling, China. *Gems & Gemology*, **47**(1), 36–41, http://dx.doi.org/10.5741/gems.47.1.36.

Condon D., McLean N., Schoene B., Bowring S., Parrish R. and Noble S., 2008. Synthetic U-Pb 'standard' solutions for ID-TIMS geochronology. *Geochimica et Cosmochimica Acta*, **72**(12S), Goldschmidt Abstracts 2008-C, A175, http://dx.doi.org/10.1016/j.gca.2008.05.006.

Corfu F., 2004. U-Pb age, setting and tectonic significance of the anorthosite-mangerite-charnockite-granite suite, Lofoten-Vesteralen, Norway. *Journal of Petrology*, **45**(9), 1799–1819, http://dx.doi.org/10.1093/petrology/egh034.

Couwenberg I., Binnemans K., De Leebeeck H. and Görller-Walrand C., 1998. Spectroscopic properties of the trivalent terbium ion in the huntite matrix $TbAl_3(BO_3)_4$. *Journal of Alloys and Compounds*, **274**(1–2), 157–163, http://dx.doi.org/10.1016/s0925-8388(98)00549-0.

Del Nero G., Cappelletti G., Ardizzone S., Fermo P. and Gilardoni S., 2004. Yellow Pr-zircon pigments: The role of praseodymium and of the mineralizer. *Journal of the European Ceramic Society*, **24**(14), 3603–3611, http://dx.doi.org/10.1016/j.jeurceramsoc.2004.01.003.

Demiray T., Nath D.K. and Hummel F.A., 1970. Zircon-vanadium blue pigment. *Journal of the American Ceramic Society*, **53**(1), 1–4, http://dx.doi.org/10.1111/j.1151-2916.1970.tb11987.x.

Dieke G.H. and Crosswhite H.M., 1963. The spectra of the doubly and triply ionized rare earths. *Applied Optics*, **2**(7), 675–686, http://dx.doi.org/10.1364/ao.2.000675.

Dorais M.J. and Tubrett M., 2012. Detecting peritectic garnet in the peraluminous Cardigan pluton, New Hampshire. *Journal of Petrology*, **53**(2), 299–324, http://dx.doi.org/10.1093/petrology/egr063.

Douglas J.G., Carò F. and Fischer C., 2008. Evidence of sandstone usage for sculpture during the Khmer Empire in Cambodia through petrographic analysis. *Udaya, Journal of Khmer Studies*, **9**, 1–17.

Ewing R.C., 1994. The metamict state: 1993 — The centennial. *Nuclear Instruments and Methods in Physics Research Section B: Beam Interactions with Materials and Atoms*, **91**(1–4), 22–29, http://dx.doi.org/10.1016/0168-583x(94)96186-7.

Ewing R.C., Meldrum A., Wang L., Weber W.J. and Corrales L.R., 2003. Radiation effects in zircon. *Reviews in Mineralogy and Geochemistry*, **53**(1), 387–425, http://dx.doi.org/10.2113/0530387.

Faulkner M.J. and Shigley J.E., 1989. Zircon from the Harts Range, Northern Territory, Australia. *Gems & Gemology*, **25**(4), 207–215, http://dx.doi.org/10.5741/gems.25.4.207.

Fielding P.E., 1970. The distribution of uranium, rare earths, and color centers in a crystal of natural zircon. *American Mineralogist*, **55**(3–4), 428–440.

Gaft M., Panczer G., Reisfeld R. and Shinno I., 2000. Laser-induced luminescence of rare-earth elements in natural zircon. *Journal of Alloys and Compounds*, **300–301**, 267–274, http://dx.doi.org/10.1016/s0925-8388(99)00781-1.

Gastil R.G., DeLisle M. and Morgan J.R., 1967. Some effects of progressive metamorphism on zircons. *Geological Society of America Bulletin*, **78**(7), 879–906, http://dx.doi.org/10.1130/0016-7606(1967)78%5B879:seopmo%5D2.0.co;2.

Gibbons A.D., Zahirovic S., Müller R.D., Whittaker J.M. and Yatheesh V., 2015. A tectonic model reconciling evidence for the collisions between India, Eurasia and intra-oceanic arcs of the central-eastern Tethys. *Gondwana Research*, **28**(2), 451–492, http://dx.doi.org/10.1016/j.gr.2015.01.001.

Hanchar J.M. and van Westrenen W., 2007. Rare earth element behavior in zircon-melt systems. *Elements*, **3**(1), 37–42, http://dx.doi.org/10.2113/gselements.3.1.37.

Hanchar J.M., Finch R.J., Hoskin P.W.O., Watson E.B., Cherniak D.J. and Mariano A.N., 2001. Rare earth elements in synthetic zircon: Part 1. Synthesis, and rare earth element and phosphorus doping. *American Mineralogist*, **86**(5–6), 667–680, http://dx.doi.org/10.2138/am-2001-5-607.

Hay D.C. and Dempster T.J., 2009. Zircon behaviour during low-temperature metamorphism. *Journal of Petrology*, **50**(4), 571–589, http://dx.doi.org/10.1093/petrology/egp011.

Hejny C., Miletich R., Jasser A., Schouwink P., Crichton W. and Kahlenberg V., 2012. Second-order $P\bar{6}c2$-$P31c$ transition and structural crystallography of the cyclosilicate benitoite, $BaTiSi_3O_9$, at high pressure. *American Mineralogist*, **97**(10), 1749–1763, http://dx.doi.org/10.2138/am.2012.4175.

Hinton R.W. and Upton B.G.J., 1991. The chemistry of zircon: Variations within and between large crystals from syenite and alkali basalt xenoliths. *Geochimica et Cosmochimica Acta*, **55**(11), 3287–3302, http://dx.doi.org/10.1016/0016-7037(91)90489-r.

Hoang N. and Flower M., 1998. Petrogenesis of Cenozoic basalts from Vietnam: Implication for origins of a 'diffuse igneous province'. *Journal of Petrology*, **39**(3), 369–395, http://dx.doi.org/10.1093/petroj/39.3.369.

Holland H.D. and Gottfried D., 1955. The effect of nuclear radiation on the structure of zircon. *Acta Crystallographica*, **8**(6), 291–300, http://dx.doi.org/10.1107/s0365110x55000947.

Hoskin P.W.O. and Ireland T.R., 2000. Rare earth element chemistry of zircon and its use as a provenance indicator. *Geology*, **28**(7), 627–630, http://dx.doi.org/10.1130/0091-7613(2000)28%3C627:reecoz%3E2.0.co;2.

Hoskin P.W.O. and Schaltegger U., 2003. The composition of zircon and igneous and metamorphic petrogenesis. *Reviews in Mineralogy and Geochemistry*, **53**(1), 27–62, http://dx.doi.org/10.2113/0530027.

Hoskin P.W.O., Kinny P.D., Wyborn D. and Chappell B.W., 2000. Identifying accessory mineral saturation during differentiation in granitoid magmas: An integrated approach. *Journal of Petrology*, **41**(9), 1365–1396, http://dx.doi.org/10.1093/petrology/41.9.1365.

Huong L.T.-T., Vuong B.S., Thuyet N.T.M., Khoi N.N., Satitkune S., Wanthanachaisaeng B., Hofmeister W., Häger T. and Hauzenberger C., 2016. Geology, gemmological properties and preliminary heat treatment of gem-quality zircon from the Central Highlands of Vietnam. *Journal of Gemmology*, **35**(4), 308–318, http://dx.doi.org/10.15506/JoG.2016.35.4.308.

Jochum K.P., Nohl U., Herwig K., Lammel E., Stoll B. and Hofmann A.W., 2005. GeoReM: A new geochemical database for reference materials and isotopic standards. *Geostandards and Geoanalytical Research*, **29**(3), 333–338, http://dx.doi.org/10.1111/j.1751-908X.2005.tb00904.x.

Kar J.K., Stevens R. and Bowen C.R., 2004. Novel terbium-zircon yellow pigment. *Journal of Materials Science*, **39**(18), 5755–5763, http://dx.doi.org/10.1023/b:jmsc.0000040086.92465.50.

Kempe U., Trinkler M., Pöppl A. and Himcinschi C., 2016. Coloration of natural zircon. *Canadian Mineralogist*, **54**(3), 635–660, http://dx.doi.org/10.3749/canmin.1500093.

Klinger M., Kempe U., Pöpl A., Böttcher R. and Trinkler M., 2012. Paramagnetic hole centres in natural zircon and zircon coloration. *European Journal of Mineralogy*, **24**(6), 1005–1016, http://dx.doi.org/10.1127/0935-1221/2012/0024-2236.

Koivula J.I. and Misiorowski E., Eds. 1986. Gem News: Undesirable color change in blue zircon. *Gems & Gemology*, **22**(3), 188–189.

Krogh T.E., 1973. A low-contamination method for hydrothermal decomposition of zircon and extraction of U and Pb for isotopic age determinations. *Geochimica et Cosmochimica Acta*, **37**(3), 485–494, http://dx.doi.org/10.1016/0016-7037(73)90213-5.

Laithummanoon T. and Wongkokua W., 2013. Effect of heat treatment on color of natural zircon. *Journal of King Mongkut's University of Technology North Bangkok*, **23**(2), 261–269.

Lenz C., Nasdala L., Talla D., Hauzenberger C., Seitz R. and Kolitsch U., 2015. Laser-induced REE^{3+} photoluminescence of selected accessory minerals — An "advantageous artefact" in Raman spectroscopy. *Chemical Geology*, **415**, 1–16, http://dx.doi.org/10.1016/j.chemgeo.2015.09.001.

Ma C. and Rossman G.R., 2005. Microanalysis of hafnian zircon. *Microscopy and Microanalysis*, **11**(S02), 1304–1305, http://dx.doi.org/10.1017/s1431927605510730.

Malusà M.G., Carter A., Limoncelli M., Villa I.M. and Garzanti E., 2013. Bias in detrital zircon geochronology and thermochronometry. *Chemical Geology*, **359**, 90–107, http://dx.doi.org/10.1016/j.chemgeo.2013.09.016.

McClure S.F., 2011. Lab Notes: Tenebrescent zircon. *Gems & Gemology*, **47**(4), 314–315.

Merlet C., 1994. An accurate computer correction program for quantitative electron probe microanalysis. *Microchimica Acta*, **114**(1), 363–376, http://dx.doi.org/10.1007/bf01244563.

Murakami T., Chakoumakos B.C., Ewing R.C., Lumpkin G.R. and Weber W.J., 1991. Alpha-decay event damage in zircon. *American Mineralogist*, **76**, 1510–1532.

Nasdala L., Irmer G. and Wolf D., 1995. The degree of metamictization in zircon: A Raman spectroscopic study. *European Journal of Mineralogy*, **7**(3), 471–478, http://dx.doi.org/10.1127/ejm/7/3/0471.

Nasdala L., Wenzel M., Vavra G., Irmer G., Wenzel T. and Kober B., 2001. Metamictisation of natural zircon: Accumulation versus thermal annealing of radioactivity-induced damage. *Contributions to Mineralogy and Petrology*, **141**(2), 125–144, http://dx.doi.org/10.1007/s004100000235.

Nasdala L., Lengauer C.L., Hanchar J.M., Kronz A., Wirth R., Blanc P., Kennedy A.K. and Seydoux-Guillaume A.-M., 2002. Annealing radiation damage and the recovery of cathodoluminescence. *Chemical Geology*, **191**(1–3), 121–140, http://dx.doi.org/10.1016/s0009-2541(02)00152-3.

Nasdala L., Zhang M., Kempe U., Panczer G., Gaft M., Andrut M. and Plötze M., 2003. Spectroscopic methods applied to zircon. *Reviews in Mineralogy and Geochemistry*, **53**(1), 427–467, http://dx.doi.org/10.2113/0530427.

Nasdala L., Reiners P.W., Garver J.I., Kennedy A.K., Stern R.A., Balan E. and Wirth R., 2004. Incomplete retention of radiation damage in zircon from Sri Lanka. *American Mineralogist*, **89**(1), 219–231, http://dx.doi.org/10.2138/am-2004-0126.

Niesert A., Hanrath M., Siggel A., Jansen M. and Langer K., 2002. Theoretical study of the polarized electronic absorption spectra of vanadium-doped zircon. *Journal of Solid State Chemistry*, **169**(1), 6–12, http://dx.doi.org/10.1016/s0022-4596(02)00010-5.

Paton C., Hellstrom J., Paul B., Woodhead J. and Hergt J., 2011. Iolite: Freeware for the visualisation and processing of mass spectrometric data. *Journal of Analytical Atomic Spectrometry*, **26**(12), 2508–2518, http://dx.doi.org/10.1039/c1ja10172b.

Pearce N.J.G., Perkins W.T., Westgate J.A., Gorton M.P., Jackson S.E., Neal C.R. and Chenery S.P., 1997. A compilation of new and published major and trace element data for NIST SRM 610 and NIST SRM 612 glass reference materials. *Geostandards and Geoanalytical Research*, **21**(1), 115–144, http://dx.doi.org/10.1111/j.1751-908X.1997.tb00538.x.

Pérez-Soba C., Villaseca C., Del Tanago J.G. and Nasdala L., 2007. The composition of zircon in the peraluminous Hercynian granites of the Spanish Central System batholith. *Canadian Mineralogist*, **45**(3), 509–527, http://dx.doi.org/10.2113/gscanmin.45.3.509.

Pyon K.-R., Han K.-S. and Lee B.-H., 2011. Formation and color properties of vanadium doped $ZrSiO_4$ ceramic pigments. *Journal of Ceramic Processing Research*, **12**(3), 279–288.

Rangin C., Huchon P., Le Pichon X., Bellon H., Lepvrier C., Roques D., Hoe N.D. and Quynh P.V., 1995. Cenozoic deformation of central and south Vietnam. *Tectonophysics*, **251**(1–4), 179–196, http://dx.doi.org/10.1016/0040-1951(95)00006-2.

Renfro N.D., 2016. Reversible color modification of blue zircon by long-wave ultraviolet radiation. *Gems & Gemology*, **52**(3), 246–251, http://dx.doi.org/10.5741/gems.52.3.246.

Richman I., Kisliuk P. and Wong E.Y., 1967. Absorption spectrum of U^{4+} in zircon ($ZrSiO_4$). *Physical Review*, **155**(2), 262–267, http://dx.doi.org/10.1103/PhysRev.155.262.

Roskin G., 2003. Cambodian blue zircon. www.jckonline.com/magazine-article/cambodian-blue-zircon, 1 November, accessed 14 April 2018.

Rossman G.R., 1981. Color in gems: The new technologies. *Gems & Gemology*, **17**(2), 60–71, http://dx.doi.org/10.5741/gems.17.2.60.

Russo d.M. and Punzo I., 2004. *I minerali del Somma-Vesuvio*. Associazione Micro-mineralogica Italiana, Cremona, Italy, 320 pp.

Sahama T.G., 1981. Growth structure in Ceylon zircon. *Bulletin de Minéralogie*, **104**, 89–94.

Satitkune S., Wanthanachaisaeng B., Won-in K., Wongkokau W., Chantararat P., Leelawattanasuk T. and Wathanakul P., 2013. Heat treatment of zircon samples from Kanchanaburi, Thailand and Ratanakiri, Cambodia. *33rd International Gemmological Conference*, Hanoi, Vietnam, 12–16 October, 158–160.

Saurin E., 1957. Some gem occurrences in Cambodia. *Rocks & Minerals*, **32**(7–8), 397–398, http://dx.doi.org/10.1080/00357529.1957.11766953.

Schärer U., 1984. The effect of initial ^{230}Th disequilibrium on young U–Pb ages: The Makalu case, Himalaya. *Earth and Planetary Science Letters*, **67**(2), 191–204, http://dx.doi.org/10.1016/0012-821x(84)90114-6.

Shigley J.E., Laurs B.M., Janse A.J.A., Elen S. and Dirlam D.M., 2010. Gem localities of the 2000s. *Gems & Gemology*, **46**(3), 188–216, http://dx.doi.org/10.5741/gems.46.3.188.

Siriaucharanon W., Lomthong P. and Wanthanachaisaeng B., 2017. Heat treatment of zircon from Tanzania and Cambodia. *GIT Gems & Jewelry*, No. 20, 29.

Škoda R., Plášil J., Jonsson E., Čopjaková R., Langhof J. and Galiová M.V., 2015. Redefinition of thalénite-(Y) and discreditation of fluorthalénite-(Y): A re-investigation of type material from the Österby pegmatite, Dalarna, Sweden, and from additional localities. *Mineralogical Magazine*, **79**(4), 965–983, http://dx.doi.org/10.1180/minmag.2015.079.4.07.

Smith M.H. and Balmer W.A., 2009. Gem News International: Zircon mining in Cambodia. *Gems & Gemology*, **45**(2), 152–153.

Stacey J.S. and Kramers J.D., 1975. Approximation of terrestrial lead isotope evolution by a two-stage model. *Earth and Planetary Science Letters*, **26**(2), 207–221, http://dx.doi.org/10.1016/0012-821x(75)90088-6.

Stiebler M., Steudtner C. and Kemmler-Sack S., 1992. Praseodymium zircon yellow. *Physica Status Solidi (a)*, **132**(2), 495–500, http://dx.doi.org/10.1002/pssa.2211320225.

Sutherland F.L., Bosshart G., Fanning C.M., Hoskin P.W.O. and Coenraads R.R., 2002. Sapphire crystallization, age and origin, Ban Huai Sai, Laos: Age based on zircon inclusions. *Journal of Asian Earth Sciences*, **20**(7), 841–849, http://dx.doi.org/10.1016/s1367-9120(01)00067-0.

Sutherland F., Piilonen P.C., Zaw K., Meffre S. and Thompson J., 2015. Sapphire within zircon-rich gem deposits, Bo Loei, Ratanakiri Province, Cambodia: Trace elements, inclusions, U–Pb dating and genesis. *Australian Journal of Earth Sciences*, **62**(6), 761–773.

Sutherland L., Graham I., Yaxley G., Armstrong R., Giuliani G., Hoskin P., Nechaev V. and Woodhead J., 2016. Major zircon megacryst suites of the Indo-Pacific lithospheric margin (ZIP) and their petrogenetic and regional implications. *Mineralogy and Petrology*, **110**(2–3), 399–420, http://dx.doi.org/10.1007/s00710-015-0421-3.

Suthiyuth R., 2014. Lab Notes: Tenebrescent zircon. *Gems & Gemology*, **50**(2), 156–157.

Thongcham K., Sahavat S. and Wongkokua W., 2010. Effects of annealing to colour of zircon. *Pro-Gem-Geo-Mat 2010: 5th International Workshop on Provenance and Properties of Gems and Geo-Materials*, Hanoi, Vietnam, 17–24 October, 111–113.

United Nations, 1993. *Atlas of Mineral Resources of the ESCAP Region. Vol. 10, Cambodia*. United Nations Economic and Social Commission for Asia and the Pacific, New York, New York, USA, 87 pp.

Váczi T., 2014. A new, simple approximation for the deconvolution of instrumental broadening in spectroscopic band profiles. *Applied Spectroscopy*, **68**(11), 1274–1278, http://dx.doi.org/10.1366/13-07275.

Van Lichtervelde M., Melcher F. and Wirth R., 2009. Magmatic vs. hydrothermal origins for zircon associated with tantalum mineralization in the Tanco pegmatite, Manitoba, Canada. *American Mineralogist*, **94**(4), 439–450, http://dx.doi.org/10.2138/am.2009.2952.

Van Westrenen W., Frank M.R., Hanchar J.M., Fei Y., Finch R.J. and Zha C.-S., 2004. In situ determination of the compressibility of synthetic pure zircon ($ZrSiO_4$) and the onset of the zircon-reidite phase transition. *American Mineralogist*, **89**(1), 197–203, http://dx.doi.org/10.2138/am-2004-0123.

Vance E.R. and Mackey D.J., 1974. Optical study of U^{5+} in zircon. *Journal of Physics C: Solid State Physics*, **7**(10), 1898–1908, http://dx.doi.org/10.1088/0022-3719/7/10/017.

Vaz J.E. and Senftle F.E., 1971. Thermoluminescence study of the natural radiation damage in zircon. *Journal of Geophysical Research*, **76**, 2038–2050, http://dx.doi.org/10.1029/JB076i008p02038.

Wanthanachaisaeng B., Bunnag N., Sutthirat C., Ounorn P., Phattarawarin P. and Pisutha-Arnond V., 2010. Determination of heat treated zircon by FTIR spectrophotometer. *Pro-Gem-Geo-Mat 2010: 5th International Workshop on Provenance and Properties of Gems and Geo-Materials*, Hanoi, Vietnam, 17–20 October, 97–99.

Wanthanachaisaeng B., Bunnag N., Satitkune S., Ounorn P., Sutthirat C. and Pisutha-Arnond V., 2014. Influence of irradiation and heating on the Ratanakiri zircon structure. *4th International Gem and Jewelry Conference (GIT 2014)*, Chiang Mai, Thailand, 8–12 December, 101–103.

Watson E.B., 2007. Zircon in technology and everyday life. *Elements*, **3**(1), 52.

Wiedenbeck M., Hanchar J.M., Peck W.H., Sylvester P., Valley J., Whitehouse M., Kronz A., Morishita Y., Nasdala L., Fiebig J., Franchi I., Girard J.P., Greenwood R.C., Hinton R., Kita N., Mason P.R.D., Norman M., Ogasawara M., Piccoli P.M., Rhede D., Satoh H., Schulz-Dobrick B., Skår O., Spicuzza M.J., Terada K., Tindle A., Togashi S., Vennemann T., Xie Q. and Zheng Y.F., 2004. Further characterisation of the 91500 zircon crystal. *Geostandards and Geoanalytical Research*, **28**(1), 9–39, http://dx.doi.org/10.1111/j.1751-908X.2004.tb01041.x.

Xu X.-S., Zhang M., Zhu K.-Y., Chen X.-M. and He Z.-Y., 2012. Reverse age zonation of zircon formed by metamictisation and hydrothermal fluid leaching. *Lithos*, **150**, 256–267, http://dx.doi.org/10.1016/j.lithos.2011.12.014.

Zamyatin D.A., Shchapova Y.V., Votyakov S.L., Nasdala L. and Lenz C., 2017. Alteration and chemical U-Th-total Pb dating of heterogeneous high-uranium zircon from a pegmatite from the Aduiskii Massif, Middle Urals, Russia. *Mineralogy and Petrology*, **111**(4), 475–497, http://dx.doi.org/10.1007/s00710-017-0513-3.

Zhang M., Salje E.K.H., Farnan I., Graeme-Barber A., Daniel P., Ewing R.C., Clark A.M. and Leroux H., 2000. Metamictization of zircon: Raman spectroscopic study. *Journal of Physics: Condensed Matter*, **12**(8), 1915–1925, http://dx.doi.org/10.1088/0953-8984/12/8/333.

Zhang M., Salje E.K.H. and Ewing R.C., 2003. Oxidation state of uranium in metamict and annealed zircon: Near-infrared spectroscopic quantitative analysis. *Journal of Physics: Condensed Matter*, **15**(20), 3445–3470, http://dx.doi.org/10.1088/0953-8984/15/20/307.

The Authors

Manuela Zeug, Prof. Dr Lutz Nasdala and Prof. Dr Manfred Wildner
Institut für Mineralogie und Kristallographie, University of Vienna, Althanstraße 14, 1090 Vienna, Austria. Email: manuela.zeug@univie.ac.at

Dr Walter A. Balmer
SSEF Swiss Gemmological Institute, Aeschengraben 26, 4051 Basel, Switzerland; and Department of Geology, Faculty of Science, Chulalongkorn University, Bangkok 10330, Thailand

Dr Fernando Corfu
Department of Geosciences and CEED (Centre for Earth Evolution and Dynamics), University of Oslo, P.O. Box 1047, Blindern, 0316 Oslo, Norway

Dr Bhuwadol Wanthanachaisaeng
Faculty of Science, Srinakharinwirot University, 114 Sukhumvit 23, Bangkok 10110, Thailand; and Faculty of Gems, Burapha University, Chanthaburi 22170, Thailand

Acknowledgements

Authors WAB, LN and BW are deeply indebted to Mr Votha Un (deceased) of Pailin, Cambodia, who in 2008 and 2012 guided field trips to several zircon deposits in Ratanakiri Province. Ralf Grunert, Mark H. Smith and Astrid Wittwer kindly provided photographs. We thank Dr George R. Rossman and Dr John M. Hanchar for the loan of synthetic blue $ZrSiO_4$ crystals, and Dr Dominik Talla for providing REE-doped $ZrSiO_4$ crystals. Thanks also are due to Andreas Wagner for sample preparation. We are indebted to Dr Radek Škoda, Wilfredo G. Diegor, Christian Petautschnig, Dr Martin Ende and Dr Gerald Giester for experimental help, and to Wolfgang Zirbs for technical assistance. We thank Dr Klaus Krambrock for helpful discussions and constructive comments. Author LN acknowledges support of the 2012 field trip to Ratanakiri by ASEA-Uninet. Author BW acknowledges support by the Gem and Jewelry Institute of Thailand (Public Organisation).

An innovator in gemstone reporting

• Identification of colored gemstones • Country of origin determination • Full quality and color grading analysis

AMERICAN GEMOLOGICAL LABORATORIES AGL

580 5th Ave • Suite 706 • New York, NY 10036, USA
www.aglgemlab.com • +1 (212) 704 - 0727

A Thick Overgrowth of CVD Synthetic Diamond on a Natural Diamond

Shi Tang, Jun Su, Taijin Lu, Yongwang Ma, Jie Ke, Zhonghua Song, Jun Zhang and Houxiang Liu

ABSTRACT: In October 2017, a natural diamond overgrown by a thick layer of CVD synthetic diamond was identified at the Beijing laboratory of the National Gemstone Testing Center (NGTC). The round-brilliant-cut sample was near-colourless and weighed 0.11 ct. No sign of the overgrowth was observed with magnification. However, DiamondView images showed a distinct boundary in the pavilion separating layers of different luminescence: The upper layer displayed red fluorescence with greenish blue phosphorescence, while the lower portion showed deep blue fluorescence and no phosphorescence. Infrared spectroscopy revealed that the upper layer was type IIa and the lower portion was type Ia. Ultraviolet-visible-near infrared (UV-Vis-NIR) spectroscopy recorded an unusual co-existence of the N3 centre at 415 nm together with absorption due to $[Si\text{-}V]^-$ defects at 737 nm. The photoluminescence (PL) spectrum confirmed a high level of $[Si\text{-}V]^-$ defects. The approximate thickness of the CVD synthetic layer was ~740 µm, which is much thicker than previously reported for such overgrowths. The presence of the N3 centre in the natural diamond layer caused this sample to be passed as natural by various screening instruments. Luminescence imaging is key to identifying such overgrowths, and should be relied upon more heavily in the screening procedures used by gemmological laboratories in the future.

The Journal of Gemmology, **36**(2), 2018, pp. 134–141, http://dx.doi.org/10.15506/JoG.2018.36.2.134

The deposition of single-crystal synthetic diamond thin films on natural diamond by the chemical vapour deposition (CVD) method has been known for many years. One case reported in 1993 involved a greyish blue type IIb CVD synthetic diamond thin film grown on nonconductive natural diamond, resulting in a product very similar to high-quality natural type IIb blue diamond (Fritsch and Phelps, 1993). The same year, another study reported on the preferential incorporation of defects in CVD synthetic diamond films grown on different crystal faces of diamond substrates (Yacobi et al., 1993). More recently, additional types of coatings have been documented, such as Au- or Ag-doped SiO_2/Fe_2O_3 films on natural diamond to induce fancy colours (Shen et al., 2007), and nanocrystalline diamond-like films to improve the appearance and/or durability of colourless cubic zirconia (i.e. 'Diamantine'; Shigley et al., 2012). Subsequently, Eaton-Magaña (2014) reported on a boron-doped CVD synthetic diamond film deposited on the pavilion of a natural diamond to create a bluish colour; that particular sample showed significant degradation in colour appearance due to years of daily wear. In all of these studies, the thickness of the coating layer was no more than 10 µm, which is negligible compared to the thickness of the substrates, so the existence of the films did not significantly influence the size or weight of the substrates (although in some cases they were sufficient to change the overall colour appearance).

Not until 2017 was the first example of synthetic CVD overgrowth on natural diamond reported by a laboratory on a client stone (Moe et al., 2017). The 0.33 ct Fancy blue sample was composed of a layer of type IIb blue CVD synthetic diamond on a natural colourless type

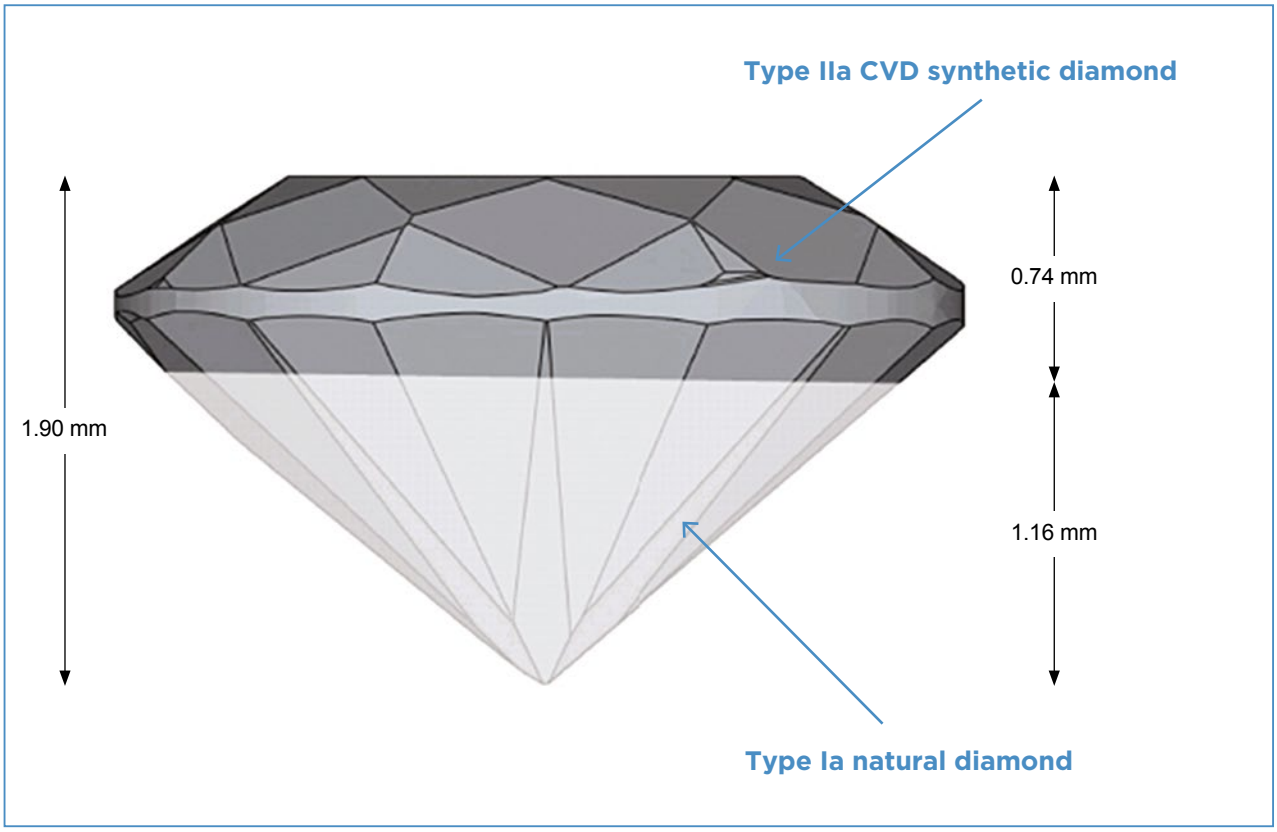

Figure 1: This drawing shows the distribution of the CVD synthetic diamond overgrowth on natural diamond that constitutes the 0.11 ct sample described in this article.

Ia diamond. The CVD layer was confined to the top of the crown and was approximately 80 µm thick, much greater than typical CVD coatings or films. The infrared spectrum revealed very unusual mixed-type Ia and IIb features. DiamondView imaging showed yellowish green fluorescence and phosphorescence when examined face-up, and deep blue fluorescence and no phosphorescence in the face-down view. PL spectra showed emissions from $[Si\text{-}V]^-$ defects at 736.6 and 736.9 nm. A distinct interface was visible under magnification, with cloud-like inclusions trapped at the boundary with the overgrowth, as well as dark needles located at or near this interface. Furthermore, Serov et al. (2017) described five 'hybrid' diamonds produced by a company in Russia. These 0.08–0.29 ct faceted samples consisted of natural diamond with a thick layer (~400 µm) of CVD synthetic diamond deposited on their crowns.

The growth of type IIa CVD synthetic diamond on the surface of natural type Ia diamond is strictly limited by many technical factors, such as crystal lattice matching, growth conditions and surface preparation. As a result, the technique's progress has been relatively slow, and few such samples are known so far. Nevertheless, on 26 October 2017, NGTC's Beijing laboratory identified such an overgrowth on a 0.11 ct near-colourless round brilliant. The lower pavilion of the sample was colourless natural diamond and the top part consisted of a thick layer (~740 µm) of colourless CVD synthetic diamond (Figure 1).

The sample was submitted by a client for an identification report. According to the client, the gem was bought at a jewellery fair in Hong Kong. The customer was told that the diamond was treated but received no further information. NGTC subsequently learned that the sample was manufactured in China by a company that keeps a low profile. According to the company, the main purpose of the overgrowth is to increase the weight of diamond gemstones. As of late 2017, the technique was still undergoing development and had not yet been applied on a large scale.

This is the first time that such an overgrowth-bearing diamond has been encountered in a gemmological laboratory in China, and it is also the thickest CVD overgrowth reported so far on a natural diamond. A brief announcement about this sample was made in December 2017 (Rapaport News, 2017), and this article describes its gemmological characteristics and the results of testing with various screening instruments.

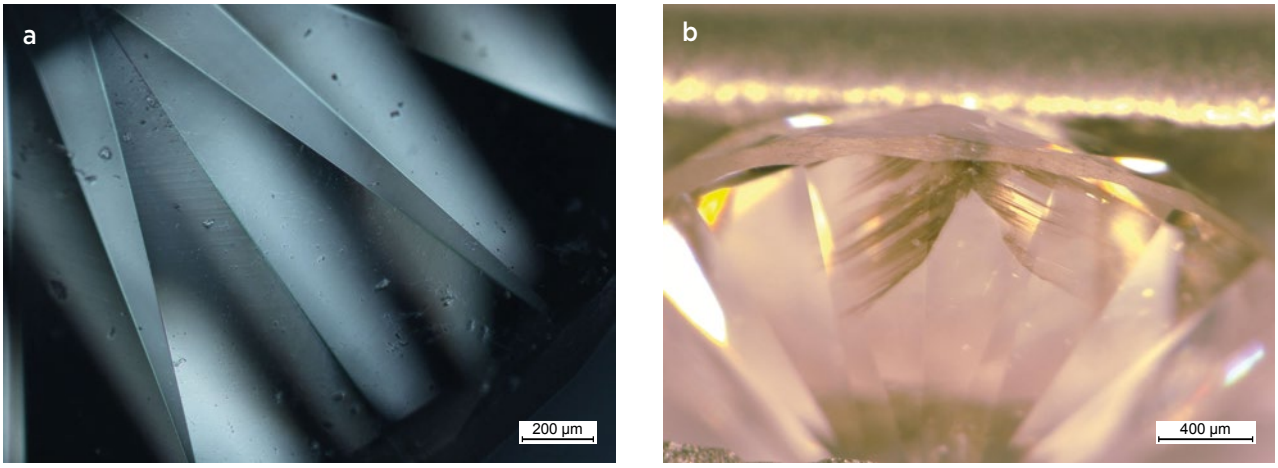

Figure 2: (a) The sample showed no visible signs of overgrowth with microscopic observation, as shown here on the pavilion with reflected light. **(b)** Near the girdle of the specimen, a large fracture ran through the crown and pavilion, including both the CVD synthetic and natural diamond layers. Photomicrographs by S. Tang.

MATERIALS AND METHODS

A thorough characterisation of the 0.11 ct sample was done at the NGTC laboratory in Beijing. Inclusions and anomalous birefringence were observed with a standard gemmological microscope and a high-powered microscope (up to 100×). A DiamondView instrument was used to observe the fluorescence and phosphorescence, as well as growth structures in multiple orientations. Fourier-transform infrared (FTIR) spectra were obtained separately through the upper and lower layers of the sample using a Thermo Nicolet 6700 spectrometer (6000–400 cm^{-1} range, 1,280 scans and 2 cm^{-1} resolution). A Gem-3000 UV-Vis-NIR spectrometer was used to obtain absorption spectra at room temperature. PL spectra were collected with four laser excitations (325, 473, 532 and 785 nm), at liquid-nitrogen temperature, using a Renishaw InVia Raman microspectrometer. The sample also was tested with two commonly used screening instruments, a DiamondSure and a DS2000 Natural Diamond Selector.

RESULTS AND DISCUSSION

Basic Properties

Weighing 0.11 ct, the round-brilliant-cut sample was near-colourless with a slight brown hue and low clarity (equivalent to L colour and I_1 clarity, respectively, in GIA's diamond grading system).

The total depth of the specimen was 1.90 mm. Based on the ratio of the two layers revealed by the DiamondView (described below), the approximate thickness of the CVD synthetic diamond layer was 0.74 mm, while the natural diamond substrate was 1.16 mm thick. A rough calculation of the volumes of the two parts showed that the natural diamond portion weighed ~0.0078 g (0.039 ct), which means the CVD synthetic diamond layer constituted two-thirds of the sample's total weight.

Microscopic Characteristics

Observations using both a standard gemmological microscope and a high-powered microscope showed no internal or external characteristics that related to, or indicated the existence of, a synthetic overgrowth (Figure 2a). There was no visible boundary marking the interface of the two layers, and the sample displayed uniformity in every aspect such as colour distribution, clarity characteristics, and cutting and polishing condition. On one side of the girdle there was a large fracture that ran through the crown and pavilion, through both the natural and synthetic layers, reinforcing the appearance of a homogeneous diamond (Figure 2b). High-power microscopic observation with crossed polarisers revealed no obvious differences in anomalous birefringence (as expected, given the small size of the sample).

Luminescence Features

When observed with a standard UV lamp, the specimen displayed no noticeable luminescence. However, in the DiamondView instrument the sample emitted distinctly different colours of luminescence and showed a sharp fluorescence boundary in particular directions. Viewed table-up, red fluorescence and bluish green phosphorescence were seen (Figure 3a,b). In the table-down view, a large area of the pavilion showed deep blue fluorescence and no phosphorescence, but the area toward the girdle displayed a ring of red fluorescence

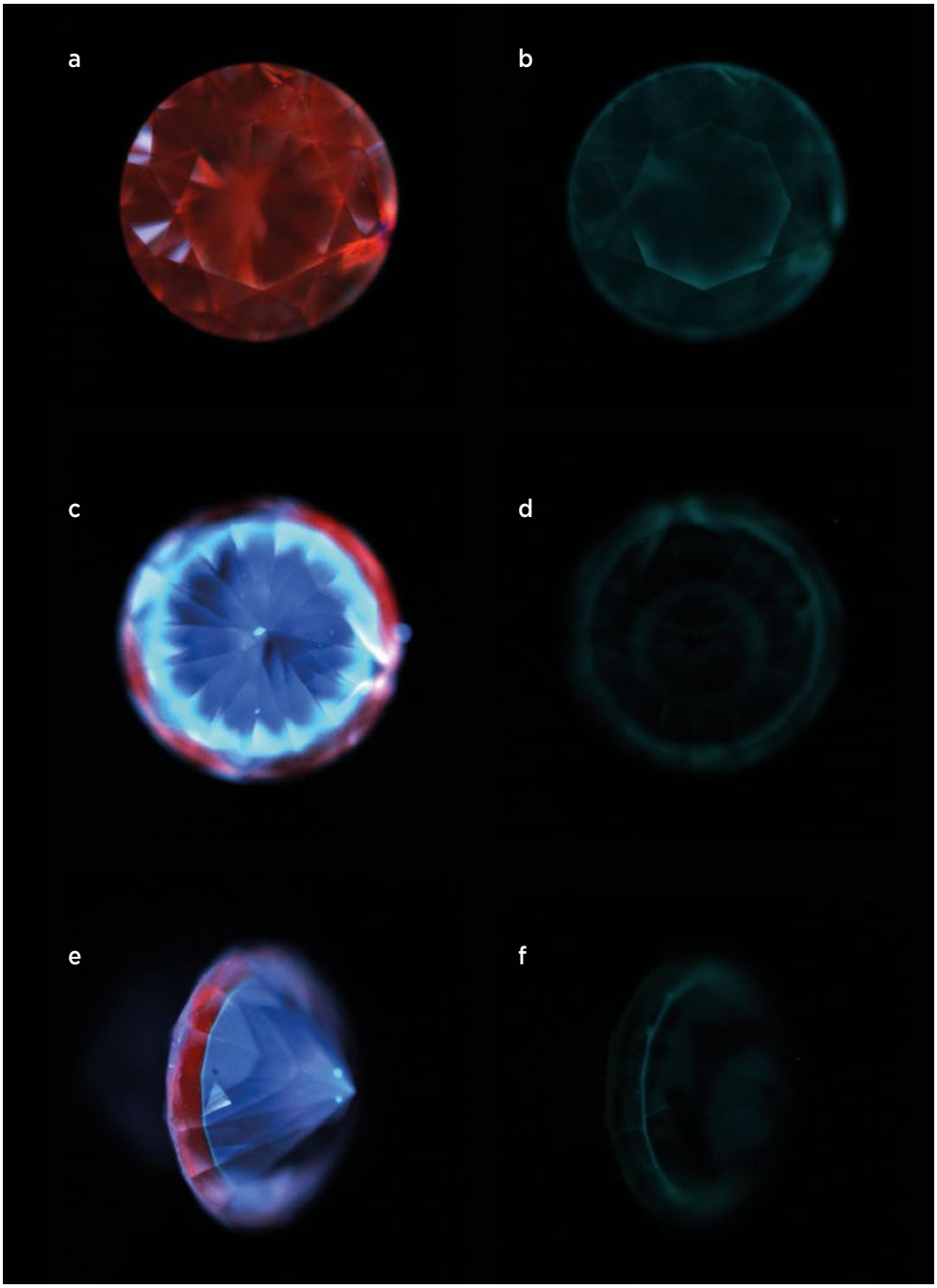

Figure 3: Fluorescence (left) and phosphorescence (right) images of the 0.11 ct sample are shown with the DiamondView instrument, as viewed table-up, table-down and obliquely through the pavilion. The CVD layer displays red fluorescence and greenish blue phosphorescence, while the natural diamond substrate emits deep blue fluorescence and no phosphorescence. Images by S. Tang.

and bluish green phosphorescence (Figure 3c,d). Viewed obliquely through the pavilion, a distinct boundary was clearly seen between the two layers of luminescence, and significantly stronger phosphorescence was visible along the interface (Figure 3e,f). The red fluorescence resulted from NV centres associated with trace single-nitrogen impurities in the CVD synthetic diamond layer, while the deep blue fluorescence dominating the natural diamond substrate was generated by large-scale lattice dislocations as well as abundant N3 centres (cf. Luo and Breeding, 2013).

UV-Vis-NIR Absorption Spectrum

The sample's UV-Vis-NIR absorption spectrum showed an unusual coexistence of the N3 centre at 415 nm and the $[Si\text{-}V]^-$ defect at 737 nm (Figure 4). The N3 centre, which is formed by three nitrogen atoms surrounding a vacancy, is the most commonly seen colour centre in type Ia natural diamond and is seldom found in synthetic diamond. The $[Si\text{-}V]^-$ defect is generated by a silicon impurity combined with a vacancy and is negatively charged; it is quite common in CVD synthetic diamonds and has become a main identification criterion for them.

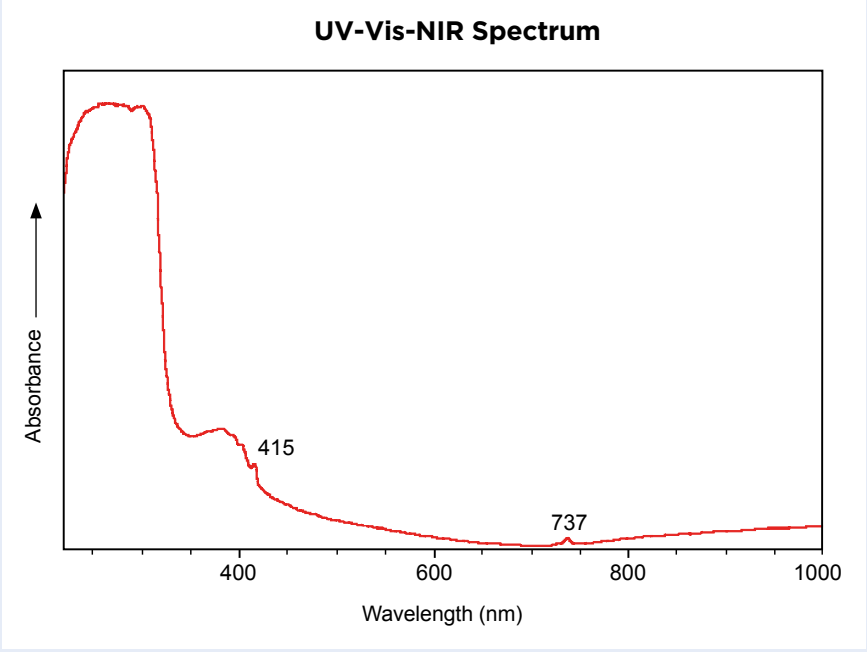

Figure 4: The UV-Vis-NIR spectrum of the hybrid diamond displays a very unusual combination of absorptions from the N3 centre at 415 nm and the $[Si\text{-}V]^-$ defect at 737 nm.

Occasionally the $[Si\text{-}V]^-$ defect does appear in natural diamond, but the content is so low that it cannot be detected by UV-Vis-NIR spectroscopy (Breeding and Wang, 2008). Only with PL spectroscopy can this defect be detected in natural diamond. The phenomenon of coexisting absorptions from the N3 centre and $[Si\text{-}V]^-$ defect in the same spectrum is extremely unusual and should arouse suspicion about a sample's origin.

FTIR Spectra

FTIR transmission spectra were obtained separately through the pavilion (near the culet) and through the crown of the sample (Figure 5). To avoid collecting mixed signals, for each measurement the infrared beam passed through the sample in a direction parallel to the table facet. The resulting spectra showed that the lower portion of the pavilion was type Ia, with absorptions from aggregated nitrogen impurities at 1368 and 1282 cm^{-1}. However, the crown of the sample turned out to be type IIa, since no absorption related to nitrogen impurities appeared between 1400 and 1100 cm^{-1}, and no boron-related absorptions were detected at 2800 or 1290 cm^{-1}. Natural diamonds are nearly all (98%) type Ia and contain nitrogen impurities detectable with the FTIR spectrometer. Most of these impurities exist in the form of aggregated nitrogen, characteristic of type Ia diamond (Breeding and Shigley, 2009). Colourless and near-colourless CVD synthetic diamonds normally contain no detectable nitrogen (or extremely low amounts of single-nitrogen defects), defining them as type IIa by their FTIR spectra. CVD synthetic diamonds doped with boron during their growth are type IIb and show blue colouration.

The two distinct FTIR spectra obtained from the sample show that it is composed of two different types of diamond material. It should be noted that a bulk FTIR scan of the sample would result in a mixed-type spectrum consisting of features from both layers, and the specimen would thus appear to be type Ia.

Photoluminescence Spectra

The PL spectra of the sample collected at liquid-nitrogen temperature using various laser excitations revealed more detailed information about the subtle impurities and defects it contained. The 532 nm laser excited a strong $[Si\text{-}V]^-$ defect emission at 737 nm, along with a weak doublet at 596/597 nm (Figure 6a). Both of these features are regarded as diagnostic for CVD synthetic diamonds (Wang et al., 2003). The 596/597 nm doublet emission is unstable in a high-temperature environment and would be eliminated during post-growth high-pressure, high-temperature (HPHT) treatment (Eaton-Magaña and D'Haenens-Johansson, 2012). The brownish hue of near-colourless CVD synthetic diamond is commonly reduced or even removed by HPHT treatment, which also transforms NV centres into H3 defects. As a result, the dominant fluorescence colour changes from red to green or bluish green, depending on the treatment temperature (Eaton-Magaña and Shigley, 2016). Thus, we deduce that the

present sample had not undergone high-temperature colour treatment, based on the existence of the 596/597 nm doublet and the red fluorescence colour of the CVD layer, as well as the slightly brownish hue of the sample.

PL spectra collected with both the 473 and 532 nm lasers exhibited strong emissions due to the NV^- centre at 637 nm and the NV^0 defect at 575 nm, consistent with the red fluorescence of the CVD layer.

PL spectra obtained with 325 nm excitation caused an emission at 415 nm from the N3 centre in the natural diamond layer, even when the beam was focused on the surface of the table facet (Figure 6b). Ni-related emissions at 883/885 nm were generated by the 785 nm laser (Figure 6c), and were far more intense when the culet was analysed with the 830 nm laser, together with multiple peaks of unknown attribution at 829–831 nm. Although Ni-related features are often attributed to an HPHT synthetic origin, they also can appear rarely in natural diamond (Tang et al., 2017).

Although PL spectra were recorded from both the crown and pavilion sides of this small sample, overall they showed few differences except for the strengths of some emissions. Even when focused on the natural diamond near the culet, excitation with the 532 nm laser still produced the 737 nm emission. In addition, when analysed on the table facet (CVD side) with the 325 nm laser, the 415 nm emission was shown as well.

Testing with Screening Devices

Over the past decades—especially during the last few years, after colourless HPHT synthetic diamonds became more common—various types of diamond screening devices have been developed and effectively applied. Most of these devices are based on the same detection principle: testing a sample for absorption at 415 nm due to the N3 centre. As mentioned above, the vast majority of natural colourless to near-colourless diamonds are type Ia, which contain nitrogen impurities, and the N3 centre is the most commonly seen defect in these stones. Conversely, colourless to near-colourless synthetic diamonds are normally type IIa, with no N3 centre. As a result, by detecting only the existence of the N3 centre, a diamond can be quickly diagnosed as natural or suspect. The small percentage of suspect samples then can be tested further with FTIR spectroscopy to determine their diamond type, and type Ia diamonds are passed as natural (leaving only type IIa specimens in need of further testing). However, natural diamonds with an overgrowth layer of CVD synthetic diamond might not be properly detected with such screening devices.

Testing of the 0.11 ct sample in multiple orientations with both the DiamondSure and the DS2000 instruments gave 'pass' results, since the N3 absorption was detectable regardless of how the specimen was oriented.

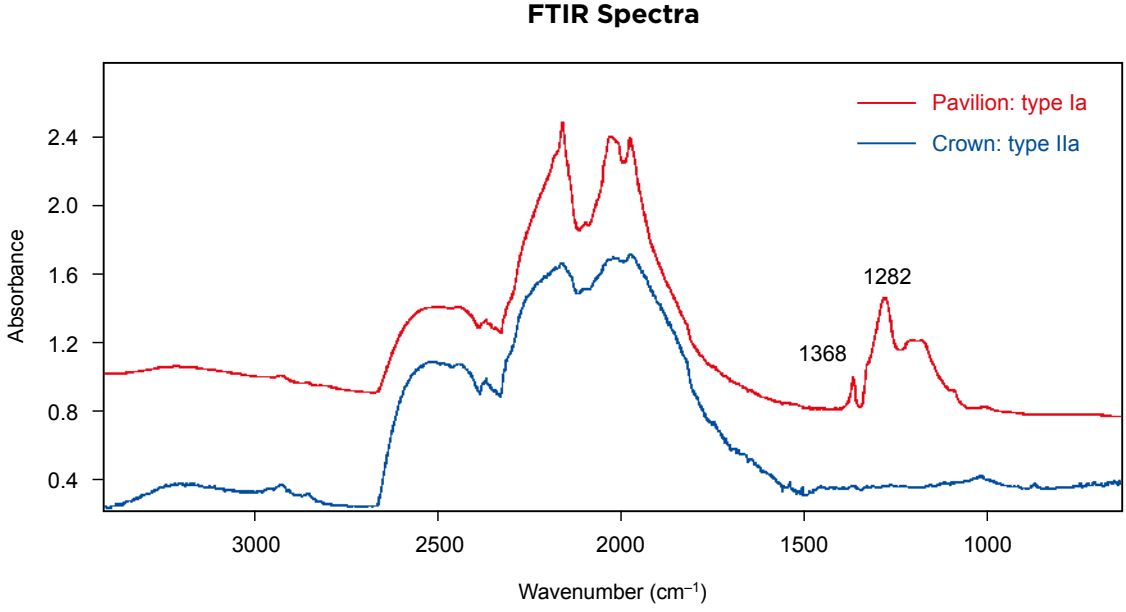

Figure 5: FTIR spectra of the two different layers of the sample show features indicative of type Ia diamond in the lower pavilion and type IIa diamond in the crown. The absorptions in the 3000–2800 cm^{-1} region are artefacts due to surface oils. The spectra are stacked vertically for clarity.

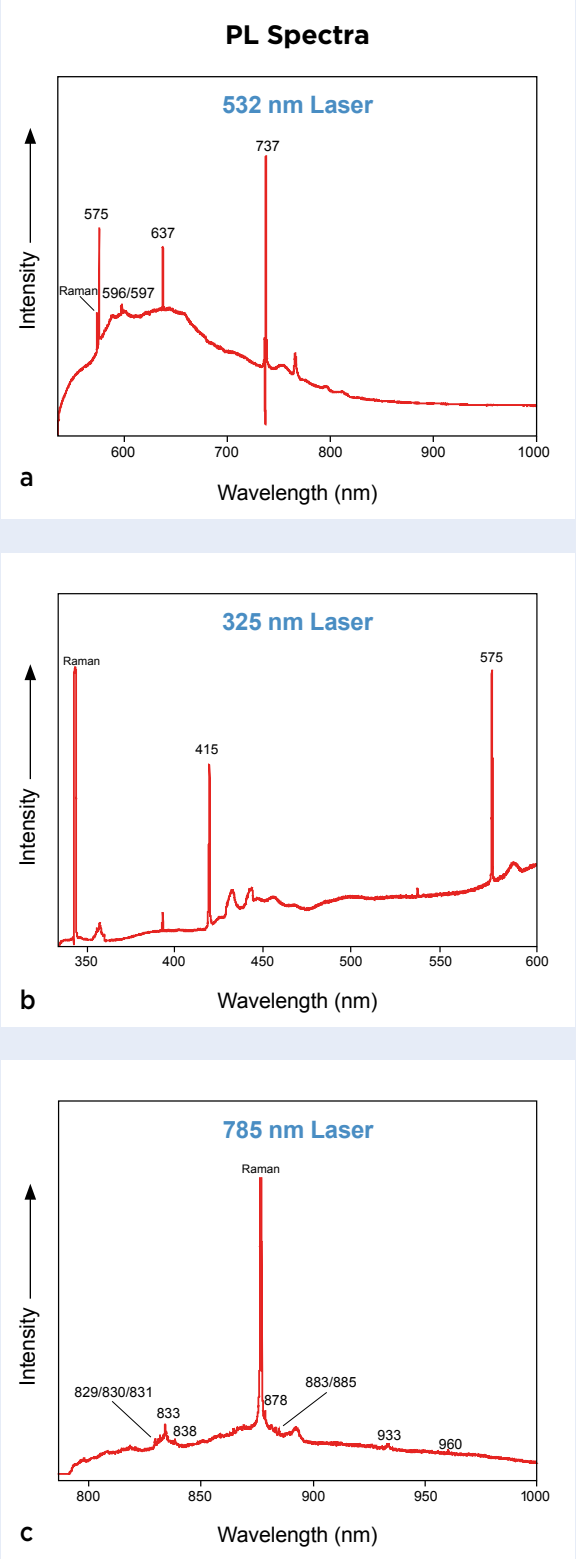

Figure 6: The PL spectra of the sample collected with **(a)** 532 nm, **(b)** 325 nm and **(c)** 785 nm laser excitation at liquid-nitrogen temperature reveal features representative of two different diamond types and raise questions as to the nature of this hybrid specimen.

It is clear that a single absorption criterion (such as the N3) or a single feature (such as diamond type classification) is not enough to correctly identify such a hybrid diamond.

DISCUSSION AND CONCLUSIONS

This is the first time that CVD synthetic diamond overgrown on natural diamond has been encountered in a Chinese gemmological laboratory. The thickness of the synthetic layer (~740 µm) was much greater than previously reported for such overgrowth-bearing diamonds, and it significantly influenced the weight and size of the sample. Although we initially suspected that the sample might have resulted from simply not removing the natural diamond substrate material after prolonged CVD growth, our further investigations into the producer showed that the synthetic overgrowth was done deliberately to increase the weight of the natural diamond.

The visual appearance of the synthetic overgrowth layer was indistinguishable from that of the natural diamond. Unlike a type IIb CVD synthetic layer, which has a blue colour different from the colourless natural diamond substrate, the type IIa CVD layer on the near-colourless type Ia natural diamond showed no visible colour difference or boundary. In addition, we observed no inclusions located at or near the interface, such as dark needles that were described previously (Moe et al., 2017). The major inclusion in the 0.11 ct sample was a large fracture extending across the crown and pavilion. The evenly distributed colour and lack of distinguishing features increased the difficulty of properly identifying the sample.

Screening instruments that rely on detecting N3 absorption in a bulk infrared spectrum would likely pass such a sample as type Ia natural diamond due to the presence of nitrogen defects in the natural layer. However, the 737 nm feature due to $[Si\text{-}V]^-$ defects in the CVD synthetic layer was easy to detect in a UV-Vis-NIR absorption spectrum taken at room temperature. In addition, DiamondView images illustrated the overgrowth very clearly as a separate layer. The PL spectrum provided further confirmation of the hybrid origin of the specimen. In the laboratory report for this sample, we used the wording 'natural diamond with synthetic diamond overgrowth'.

To conclude, the identification of a thick CVD synthetic overgrowth is not difficult for a well-equipped gemmological laboratory, as long as thorough testing and comprehensive judgements are performed. Of concern, however, is the challenge to screening methods and

equipment that are based on specific spectral characteristics or diamond type classification. Traditional screening procedures for colourless to near-colourless diamonds that rely on single features are not sufficient and need to be improved. While it is unknown how rapidly this overgrowth technique might progress, for now the impact seems more academic than practical, since currently there is no indication that such products are becoming more common in the market (e.g. no additional samples of this type have been identified by the authors, even after initiating a full-range screening process in our Beijing laboratory to test not only for the N3 centre but also for the $[Si\text{-}V]^-$ defect). However, this sample does illustrate the need for future development of procedures and instrumentation to deal with such hybrid diamonds.

REFERENCES

Breeding C.M. and Wang W., 2008. Occurrence of the Si-V defect centre in natural colourless diamonds. *Diamond and Related Materials*, **17**(7–10), 1335–1344, http://dx.doi.org/10.1016/j.diamond.2008.01.075.

Breeding C.M. and Shigley J.E., 2009. The "type" classification system of diamonds and its importance in gemology. *Gems & Gemology*, **45**(2), 96–111, http://dx.doi.org/10.5741/gems.45.2.96.

Eaton-Magaña S., 2014. Lab Notes: Long-term durability of CVD synthetic film on diamond. *Gems & Gemology*, **50**(2), 152.

Eaton-Magaña S. and D'Haenens-Johansson U.F.S., 2012. Recent advances in CVD synthetic diamond quality. *Gems & Gemology*, **48**(2), 124–127, http://dx.doi.org/10.5741/gems.48.2.124.

Eaton-Magaña S. and Shigley J.E., 2016. Observations on CVD-grown synthetic diamonds: A review. *Gems & Gemology*, **52**(3), 222–246, http://dx.doi.org/10.5741/gems.52.3.222.

Fritsch E. and Phelps A.W., 1993. Type IIb diamond thin films deposited onto near-colorless natural gem diamonds. *Diamond and Related Materials*, **2**(2–4), 70–74, http://dx.doi.org/10.1016/0925-9635(93)90033-x.

Luo Y. and Breeding C., 2013. Fluorescence produced by optical defects in diamond: Measurement, characterization, and challenges. *Gems & Gemology*, **49**(2), 82–97, http://dx.doi.org/10.5741/gems.49.2.82.

Moe K.S., Johnson P., D'Haenens-Johansson U. and Wang W., 2017. Lab Notes: A synthetic diamond overgrowth on a natural diamond. *Gems & Gemology*, **53**(2), 237–239.

Rapaport News, 2017. Lab spots stone with CVD coating, 7 December, www.diamonds.net/News/NewsItem.aspx?ArticleID=59646, date accessed 7 December 2017.

Serov R., Shelementiev Y. and Serova A., 2017. Hybrid diamonds: Natural diamonds overgrown with CVD synthetic. *35th International Gemmological Conference*, Windhoek, Namibia, 11–15 October, 51–53.

Shen A.H., Wang W., Hall M.S., Novak S., McClure S.F., Shigley J.E. and Moses T.M., 2007. Serenity coated colored diamonds: Detection and durability. *Gems & Gemology*, **43**(1), 16–33, http://dx.doi.org/10.5741/gems.43.1.16.

Shigley J.E., Gilbertson A. and Eaton-Magaña S., 2012. Characterization of colorless coated cubic zirconia (Diamantine). *Gems & Gemology*, **48**(1), 18–30, http://dx.doi.org/10.5741/gems.48.1.18.

Tang S., Song Z., Lu T., Su J. and Ma Y., 2017. Gem News International: Two natural type IIa diamonds with strong phosphorescence and Ni-related defects. *Gems & Gemology*, **53**(4), 476–478.

Wang W., Moses T., Linares R.C., Shigley J.E., Hall M. and Butler J.E., 2003. Gem-quality synthetic diamonds grown by a chemical vapor deposition (CVD) method. *Gems & Gemology*, **39**(4), 268–283, http://dx.doi.org/10.5741/gems.39.4.268.

Yacobi B.G., Lebens J., Vahala K.J., Badzian A.R. and Badzian T., 1993. Preferential incorporation of defects in monocrystalline diamond films. *Diamond and Related Materials*, **2**(2–4), 92–99, http://dx.doi.org/10.1016/0925-9635(93)90037-3.

The Authors

Shi Tang, Jun Su, Yongwang Ma, Jie Ke and Jun Zhang
National Gemstone Testing Center, 22 F Building C, Global Trade Center, 36 North Third Ring East Road, Beijing 100013, China. Email: tangs@ngtc.com.cn

Dr Taijin Lu
Beijing Gems & Jewelry Research Institute, National Gems & Jewelry Technology Administrative Center, 22 F Building C, Global Trade Center, 36 North Third Ring East Road, Beijing 100013, China

Zhonghua Song
National Gemstone Testing Center, Room 501, 72 Xishuncheng Street, Shenyang 110013, China

Dr Houxiang Liu
National Gemstone Testing Center, 11 F Shanghai Diamond Exchange, 1701 Century Avenue, Shanghai 200122, China

Acknowledgement

This study was partially supported by the National Natural Science Foundation of China (grants nos. 41473030 and 41272086).

Figure 1: The 25.85 ct chameleon diamond studied by the authors is shown with its slightly greyish green 'stable' colour at room temperature (left) and its greyish yellow 'heated' colour (right). Photos by A. Delaunay.

What Truly Characterises a Chameleon Diamond? An Example of an Atypical 25.85 ct Stone

Emmanuel Fritsch and Aurélien Delaunay

ABSTRACT: We document an exceptionally large, 25.85 ct diamond that shows a slight colour change but exhibits some atypical properties for chameleon diamonds, including white luminescence to long- and short-wave UV radiation, as well as a network-like pattern seen in most orientations with the DiamondView. In considering whether to call this a chameleon diamond, we undertook a review of available data to compile the properties that are commonly exhibited by these gems. We found that, in addition to their defining photochromic and thermochromic behaviour, nine characteristics all must be present: long-lasting yellow phosphorescence, a zoned DiamondView growth pattern showing yellow-green/blue/inert areas, the presence of dominant A aggregates and also some hydrogen in the infrared spectrum, a continuum of absorption in the visible range related to a very weak type Ib character, a 480 nm absorption band that is possibly related to trace amounts of oxygen, a 425 nm absorption band, a weaker absorption band in the red to near-infrared region consistent with hydrogen-related defects, and traces of nickel detected with photoluminescence spectroscopy.

The Journal of Gemmology, **36**(2), 2018, pp. 142–151, http://dx.doi.org/10.15506/JoG.2018.36.2.142

Chameleon diamonds change colour when heated or left in the dark. Such gems are thus thermochromic and photochromic, respectively. Obviously, the term *chameleon* refers to the reptile known to change colour according to its environment. The 'heated' colour of such diamonds is at best an attractive orangey yellow, while the other ('stable') colour is much less saturated and darker, often tending toward greyish green. This unusual colour behaviour, combined with the attraction for coloured diamonds in general, makes chameleon diamonds much-valued collectibles, and gemmological laboratories occasionally issue reports on them. Here, we detail an unusual example, which poses the questions: What is the definition of a chameleon diamond? What properties must a diamond have to be properly named *chameleon*?

In addition to their collectable and gemmological aspects, chameleon diamonds are of interest to science in general. The so-called 'X-chrome' materials (X- being *thermo*, *photo*, *tribo*, *electro* or some other prefix related to an excitation that results in a change in colour) have a great interest in physics (e.g. for optical storage; Irie, 2000). Hence chemists have produced a number of X-chromes, and physicists attempt to understand the physical phenomena behind the colour change. From this perspective, chameleon diamonds represent a superlative as they combine two X-chrome behaviours with a super-material, diamond, also often used by theoreticians because of its simple chemistry and structure. Thus, several studies have attempted to understand the electronic structure and atomic defects responsible for this colour behaviour, so far unsuccessfully. If one could duplicate such behaviour in diamond, this would be an outstanding X-chrome material as diamond is already an exceptional substance—even without the chameleon effect. This would be a good example of what we call mineralo-mimetism: Nature is capable of producing minerals with interesting properties that humans try to duplicate for their own benefit. (This notion parallels bio-mimetism, but outside the biological world.) Amusingly, while humans do not entirely understand the mechanism involved in chameleon diamond, the colour behaviour of the eponymous reptile has only recently been elucidated (Teyssier et al., 2015).

The French Gemmological Laboratory (Laboratoire Français de Gemmologie, LFG) recently documented a 25.85 ct chameleon diamond submitted for a grading report (Figures 1 and 2). This is the largest such diamond seen at LFG, and it was analysed in detail. Its properties are somewhat surprising, such that it was not readily recognised as a chameleon when submitted. Its remarkable phosphorescence is what prompted the laboratory to test its change of colour, which was present but subtle.

Many chameleon diamonds have been documented in the gemmological literature. The largest one is the 31.31 ct oval-cut Chopard diamond acquired by the Swiss jeweller in 2007 (Fritsch et al., 2004; Chopard, 2014). Until now, the second largest was a 22.28 ct heart-shaped stone named 'the 22 ct Green Chameleon Diamond' (Moses, 1992; Fritsch et al., 1995). The stone documented in the present article represents a new second-largest documented chameleon diamond, which further explains our interest in scrutinising its characteristics.

METHODS

The diamond was graded using standard procedures, and its colouration was documented in a Macbeth Judge II viewing booth using a D65-like illuminator. Luminescence was observed with a Vilber Lourmat VL-6 UV lamp equipped with 6 W tubes (long-wave 365 nm and short-wave 254 nm) in a standard cabinet, with the diamond placed about 7 cm from the lamp. Luminescence images excited with ultra-short-wave UV radiation (~220–230 nm) were acquired with a DiamondView instrument. A Fourier-transform infrared (FTIR) absorption spectrum was obtained with a Bruker Tensor 27 infrared spectrometer with 2 cm^{-1} resolution, accumulating 2,000 scans to improve the signal-to-noise ratio. An ultraviolet-visible (UV-Vis) absorption spectrum was collected with a

Figure 2: Viewed here table-down, the 25.85 ct chameleon diamond displays a progressive change in colour when heated from ambient conditions (left) to 160°C (right). Photos by A. Delaunay.

Figure 3: The 25.85 ct diamond luminesces intense chalky white to long-wave UV radiation (left) and weaker white to short-wave UV (centre). The unusual yellow phosphorescence (right) is characteristic of chameleon diamonds. Photos by A. Delaunay.

Jasco V-670 spectrophotometer, with a sampling interval and spectral bandwidth of 1 nm. Photoluminescence (PL) spectra were obtained at liquid-nitrogen temperature with a Renishaw inVia Raman spectrometer using two laser excitations (325 and 514 nm), with a sampling interval of 0.043 nm in a single scan.

RESULTS

The diamond weighed 25.85 ct and measured approximately 19.22 × 19.71 × 11.31 mm. Its clarity grade was VS_1 due to small feathers on the crown and little chips on the crown and girdle. The colour changed from Fancy slightly greyish green to Fancy greyish yellow when heated to 160°C on a chemistry heating plate (again, see Figure 2). The diamond reverted to its 'stable' colour very rapidly (in less than one minute) when left at room temperature. In addition to this thermochromic behaviour, the diamond became yellower after being stored overnight in a dark safe, demonstrating its photochromism.

Under long-wave UV radiation, the diamond emitted an intense chalky white luminescence with some vaguely yellowish and bluish zones (Figure 3). White fluorescence is not common in diamond, and often is forgotten as a possible colour of luminescence. It results from concurrent blue and yellow emissions which, taken separately, are the most common colours of fluorescence in diamond. When the UV lamp was turned off, a strong yellow phosphorescence was observed that decayed slowly (approximately 5 minutes). Weaker white luminescence and shorter yellow phosphorescence were also observed with the short-wave UV lamp.

Luminescence images acquired with the DiamondView revealed the surprising presence of what appeared to be a dislocation network superimposed on the diamond's overall blue emission (Figure 4). The dislocation network was inert on the surrounding blue matrix, which is exactly the reverse of what has been observed in many natural type IIa diamonds. The network appeared somewhat layered or banded. The pavilion of the stone contained a distinct zone of yellow-green emission (with inert and blue areas) along graining in the diamond (Figure 5). This yellow-green luminescence is somewhat different from the green emission produced by the H3 centre. Yellow-green/blue/inert zoned luminescence is characteristic of 'classic' chameleon diamonds in the DiamondView.

The FTIR absorption spectrum was typical of type Ia diamond with high nitrogen content (Figure 6). The relative proportion of A to B aggregates can be seen by comparing the bands at 482 cm^{-1} (A aggregates) and 1010 cm^{-1} (B aggregates). A comparison of the size of these two bands indicates that the diamond is type IaA>>B, like other chameleons described in the past (see, e.g., Hainschwang et al., 2005). In addition, some hydrogen-related absorptions at 3107 and 1405 cm^{-1} were recorded, indicating a moderate H content. Hydrogen is always present in chameleon diamonds, but often at relatively high concentrations (approaching 'H-rich' amounts; Hainschwang et al., 2005), which is not the case here.

The UV-Vis absorption spectrum consisted of a combination of several features. An underlying continuum gradually increased from the red towards the violet region. On it was superimposed a complex, broad band located in the red to near-infrared region starting at ~580 nm. This feature is postulated to be related, at least in part, to the thermochromic behaviour (Fritsch et al., 1995). Considering its spectral range, as well as its complex multi-component nature, it is similar to absorption features related to hydrogen (Fritsch et al., 2007a). In addition, there was a weak feature at 425 nm and a broad

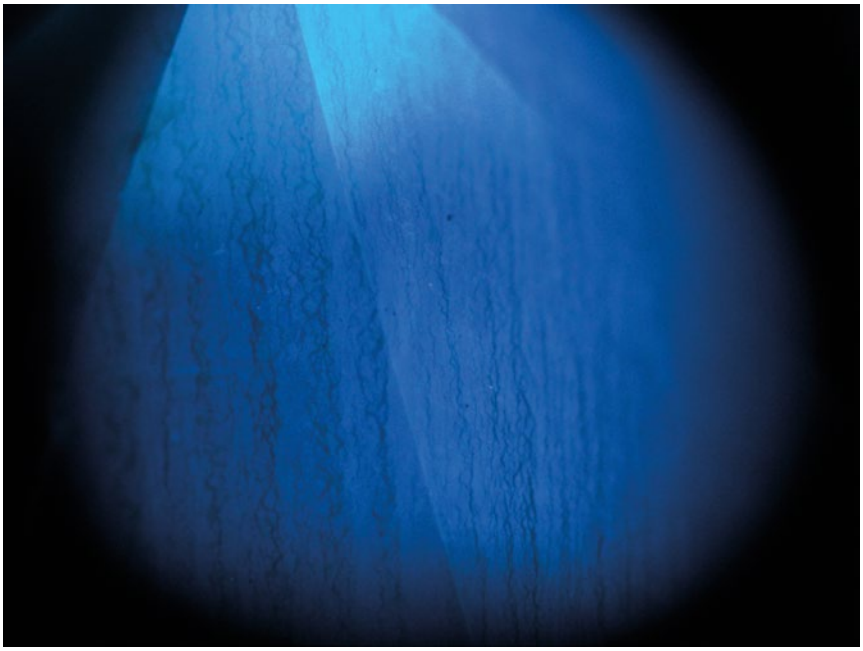

Figure 4: In the DiamondView, the 25.85 ct diamond shows an atypical dislocation network. Photomicrograph by A. Delaunay; image width 9 mm.

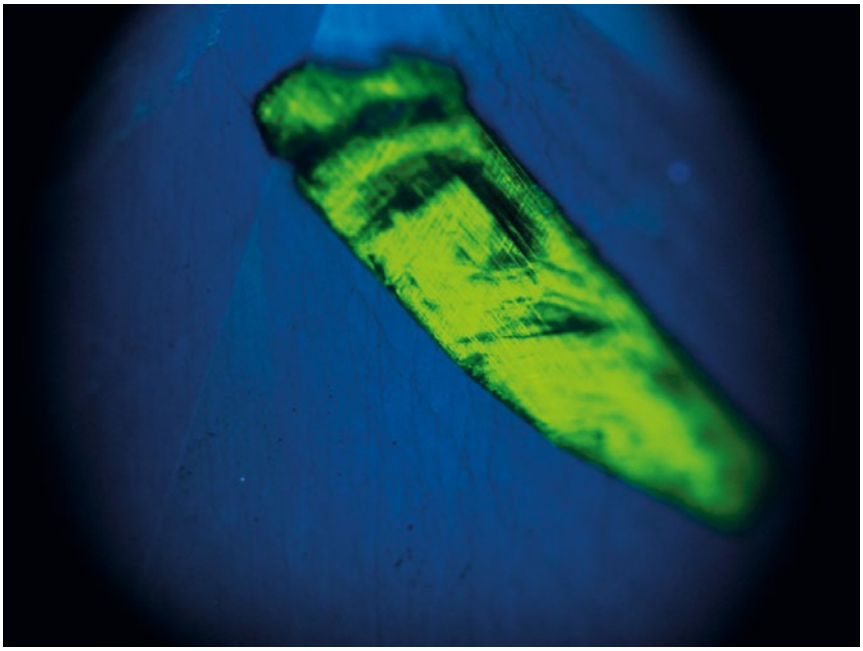

Figure 5: A yellow-green-luminescing zone with graining is seen on the pavilion of the chameleon diamond with the DiamondView, together with black (inert) and blue zones. Photomicrograph by A. Delaunay; image width 9 mm.

band at 480 nm (Figure 7; Hainschwang et al., 2005). The 480 nm band is known to occur in yellow-orange diamonds and is always present in chameleons, along with its 425 nm companion (Chabert and Reinitz, 2000). The 480 nm band is possibly due to traces of oxygen (Hainschwang et al., 2008). The N3 centre at 415 nm was also observed, and has been documented previously in chameleon diamonds (Chabert and Reinitz, 2000).

Photoluminescence spectra obtained with 514 nm excitation revealed Ni-related emissions at 700.5, 793.6 and 881.3 nm (Figure 8), which have been documented previously in typical chameleon diamonds (Hainschwang et al., 2005). In addition, there was a weak peak at 884.7 nm, which might be part of the well-known Ni-related doublet in the 883 nm region. A broad band at 630 nm was seen in the 514 nm PL spectrum, as well as other weaker underlying broad bands. The 630 nm band was previously documented in type IaA/Ib orange to

orange-yellow diamonds that exhibit the 480 nm absorption (Hainschwang et al., 2005). Other broad bands were present as well, roughly at ~700 and 800 nm. No GR1 (741 nm) feature was observed for this stone, whereas all previous chameleon diamonds studied by the authors displayed a weak GR1. In the PL spectrum obtained with 325 nm excitation, the main broad band was at ~560 nm. Emission peaks of the N3 centre at 415 nm and the H3 centre at 503 nm were otherwise the most prominent features of this spectrum (Figure 9), and there also appeared to be an underlying broad, intense feature, possibly centred in the red region.

DISCUSSION: WHAT IS COMMON TO ALL CHAMELEON DIAMONDS?

The fact that this diamond, as well as some others before it, at first eluded proper identification as chameleons (see, e.g., Fryer, 1981) proves that such diamonds cover a range of possible properties. This begs the question: What combination of properties are always present in chameleon diamonds that might be considered unique to this variety? We will exclude the 'reverse chameleon' variety defined by Hainschwang et al. (2005), which has not been documented again since. The following

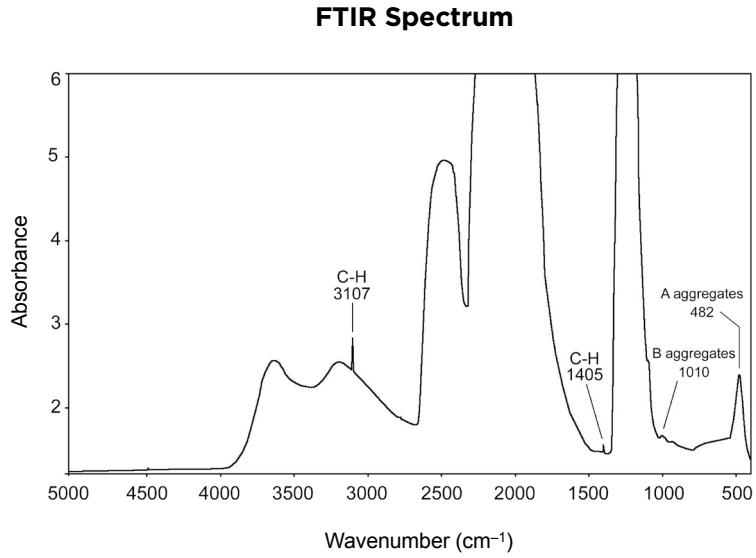

Figure 6: The FTIR spectrum of the chameleon diamond reveals a high concentration of nitrogen in A-aggregate form (482 cm^{-1}), a small amount of B aggregates (1010 cm^{-1}) and a low content of hydrogen (3107 and 1405 cm^{-1}).

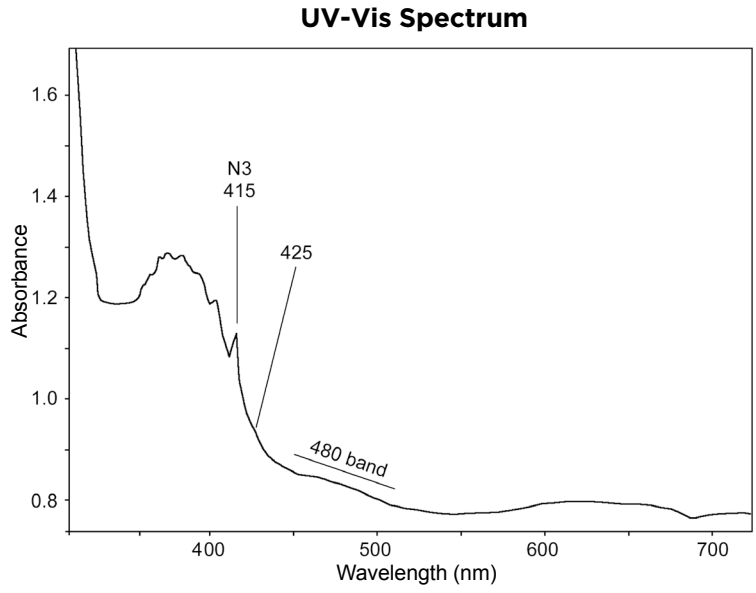

Figure 7: The UV-Vis spectrum of the chameleon diamond taken at room temperature displays the N3 centre at 415 nm, a weak band at 425 nm, a broad band at 480 nm and another broad band in the red to near-infrared region. These features are all superimposed on a slight absorption continuum that rises towards the ultraviolet. The spectrum was obtained through the girdle, for an approximate optical path length of 19.5 mm.

discussion is based on the authors' documentation of approximately 100 chameleon diamonds, often during short loans. Thus, not all properties could be documented for all of them, depending on the time and instrumentation available. However, a consistent pattern appears from this intermittent study over almost 30 years.

Again, the defining property of classic chameleon diamonds is their combined thermochromic and photochromic behaviour. They must change colour when left in the dark for several hours or after being moderately heated (160–200°C). The return to the original colour is generally within a minute after being brought from darkness to normal lighting conditions, or after being left at room temperature in normal lighting after heating. There is a range of possibilities for the two hues observed. Overall, the diamond changes from a tint containing some green to another containing yellow (see, e.g., Koivula and Kammerling, 1991; Fritsch; 1998; Hofer, 1998). Figure 10 illustrates a diamond showing a distinct colour change, in contrast to the subtle change in the ~25 ct gem reported here. Brown and grey also are common colour components of chameleon diamonds (Breeding et al., 2018). Hofer (1998) described some chameleon colours as 'olive', an imprecise term, which consists of a mixture of colours

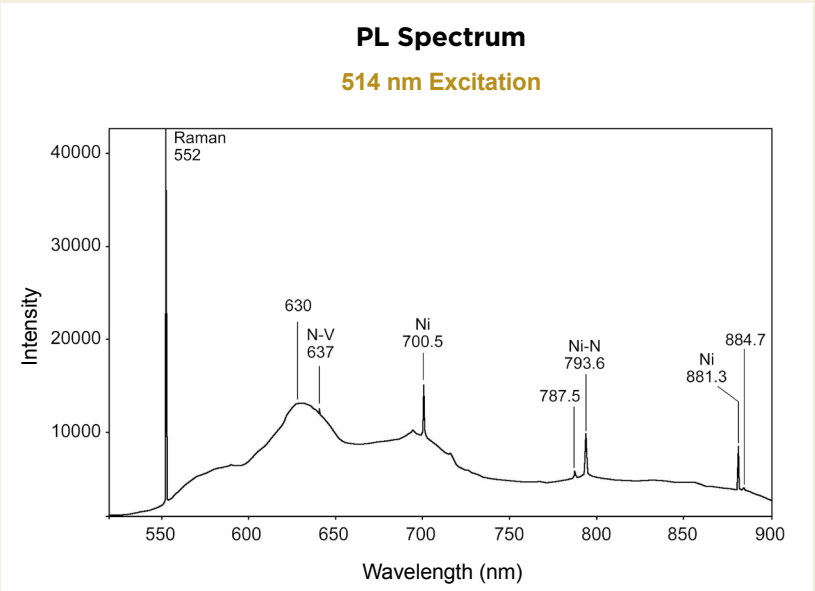

Figure 8: Photoluminescence spectroscopy of the chameleon diamond with 514 nm laser excitation at liquid-nitrogen temperature reveals numerous emissions related to Ni.

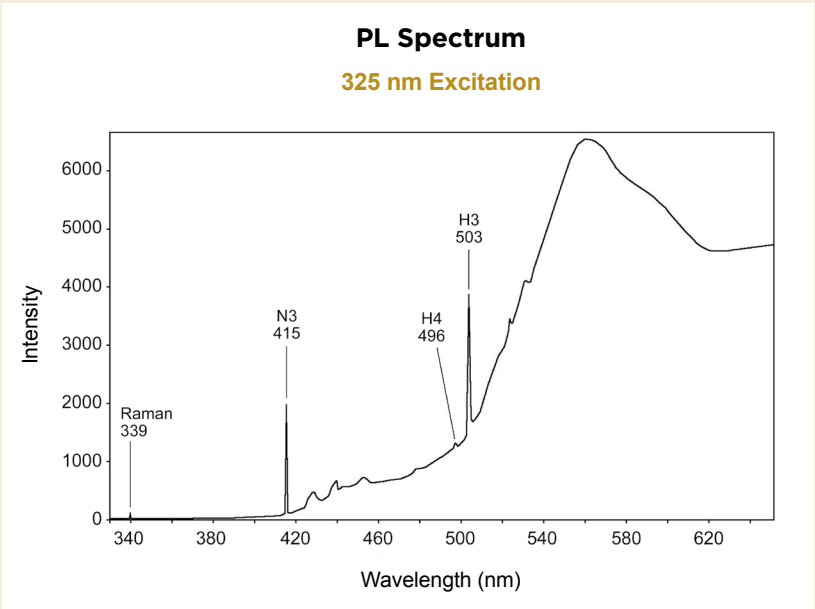

Figure 9: Distinct emissions from N3 and H3 centres are seen in the PL spectrum of the chameleon diamond obtained with 325 nm laser excitation at liquid-nitrogen temperature.

Figure 10: This 4.85 ct chameleon diamond shows a pronounced colour change (here, with heating) from greyish green to orangey yellow. Photo courtesy of SanaDiam, Antwerp, Belgium.

including green, with the addition of brown, yellow and grey (Hofer, 1998; Gaillou and Rossman, 2017).

Thermochromic behaviour has been associated with 'chameleon' diamonds since at least 1867 (Figuier, 1867). At that time, however, it was described as a reversible change from near-colourless to pink. This curious property was subsequently mentioned in one of the least-known books by Jules Verne, *The Star of the South* (*L'Etoile du Sud*), published in 1884 (Fritsch, 2016). In the book, the 'chameleon' diamond changed from black to pink. The first modern definition of a chameleon diamond that we could find is in the first edition of *The Diamond Dictionary* (Copeland et al., 1960).

The characteristic that often alerts a gemmologist that a diamond might be a chameleon is yellow phosphorescence excited by a typical short-wave UV lamp. The phosphorescence may be of varying intensity, but it is characteristically quite prolonged (i.e. over several minutes if observed in total darkness). However, this property alone does not correlate to the chameleon character (Moe et al., 2017). It is just a convenient method to highlight diamonds that might be chameleons, as this yellow phosphorescence is otherwise rare in diamond. It is generally accompanied by a strong yellow emission (which was present in the 25.85 ct stone together with blue N3 emission) when excited with long-wave UV radiation (Breeding et al., 2018). This yellow emission, as mentioned above, is indirectly related to the 480 nm band in chameleon diamonds (explained below). It has been described as a broad band of 'moderate' intensity centred at ~560 nm (i.e. using fluorescence spectroscopy; Eaton-Magaña et al., 2007). Sometimes a sharper feature at about 507 nm accompanies this broad emission band (Byrne et al., 2015).

In the small number of cases (about a dozen) when chameleon diamonds were observed by the authors in the DiamondView, they all showed a patchy yellow-green and blue emission with some inert areas (Figure 11). Characteristics of the colour distribution are consistent with the blue zones resulting from octahedral growth, whereas the yellow-green zones (often with curved boundaries) correspond to cuboid growth. Although these two growth habits are often associated in diamond, this specific pattern seems unique to chameleons. In addition, we have never seen such an appearance in the DiamondView for non-chameleon diamonds, for which we have carefully documented hundreds, and possibly thousands, of patterns. Furthermore, we were able to identify two chameleon diamonds through their DiamondView pattern that had not been recognised previously as such.

The zoning described above is a curious aspect of chameleon diamonds. Despite this rather obvious and distinct growth zoning, both the body colour distribution and the colour change appear homogeneous when observed with the unaided eye.

Regarding their infrared spectra, chameleon diamonds are consistently type Ia, with low-to-moderate concentrations of nitrogen. In all cases, A aggregates largely dominate, even in some rare diamonds that also contain B aggregates; absorption from the latter is never as strong as that of the A aggregates (e.g. Panjikar and Panjikar, 2015). In the infrared region, they always show low-to-moderate absorption of the 3107 cm^{-1} system (Fritsch et al., 2007a), some even reaching the 'H-rich' level (Fritsch, 1998).

In the UV-Vis region, chameleon diamonds all show a combination of: (1) a continuum of absorption rising

towards the UV, starting at ~550 nm; (2) an often weak but distinct 480 nm broad band and its companion band at ~425 nm; and (3) a broad band in the red to near-infrared region. Of course, the individual components are easier to identify if the spectrum is obtained at liquid-nitrogen temperature. The N3 absorption is common but sometimes absent, so its presence does not seem mandatory for chameleon diamonds. The change of colour with heat corresponds in our experience to a slight shift of the continuum towards higher wavelength, combined with a decrease of the red to near-infrared feature. This makes the green transmission window disappear, together with the green colour component. The resulting spectrum is typical of some orangey yellow diamonds, with both the shifted continuum and the 480 nm feature contributing to the yellow component. In our view, the slight decrease of the 425 and 480 nm bands plays almost no role in the change of colour. By contrast, Khan et al. (2010) as well as Gaillou and Rossman (2017) attributed the change in colour to variations in 480 and 800 nm absorptions, not taking into account the underlying continuum.

The absorption continuum, starting at ~560 nm and increasing towards the ultraviolet, might be attributed to a very weak type Ib component, which can be resolved in the infrared spectrum of many chameleon diamonds (Hainschwang et al., 2005), but not all. A type Ib visible-range absorption continuum can be found even in the absence of the 1344 cm^{-1} infrared absorption typical of type Ib diamond (Hainschwang, 2014). As those infrared features are slight, they might easily be missed or not looked for in some stones. The temperature behaviour of the continuum, which is slightly thermochromic, is consistent with that of type Ib diamonds. A band at 425 nm is found in type Ia diamonds known to contain hydrogen (Fritsch et al., 2007b), but this band in chameleon diamonds might be due to a different defect, given that it appears to be a 'companion' of the 480 nm band (Collins, 1982). The 480 nm band typically found in all chameleons (Chan et al., 2015) is believed to be related to the presence of oxygen (Hainschwang et al., 2008, and references therein). In addition, three non-chameleon yellow diamonds displaying the 480 nm absorption contained ESR-active defects linked to oxygen (unpublished data of Solveig Felton at the University of Warwick in 2009). The red to near-infrared feature seems to vary in shape from chameleon to chameleon, probably because it is a combination of several features, possibly involving other broad bands in the near-infrared (Fritsch et al., 2007a). This pattern might be related to the presence of hydrogen-related defects, possibly linked to A aggregates (Goss et al., 2011).

In laser-excited photoluminescence spectra, no single peak seems absolutely characteristic, but the ~701 nm system appears very common. As with some other emissions documented in chameleon diamonds, this one is related to traces of nickel. Thus Ni traces might be necessary to obtain the chameleon effect. Nickel was detected by energy-dispersive X-ray fluorescence spectroscopy in some chameleon diamonds (as well as 'canary' diamonds) exhibiting the 480 nm absorption (De Weerdt and Van Royen, 2001). In essence, when Ni is looked for in a chameleon diamond, it is found. Nickel is actually not so rare an impurity in natural diamond, particularly in natural type Ib diamonds

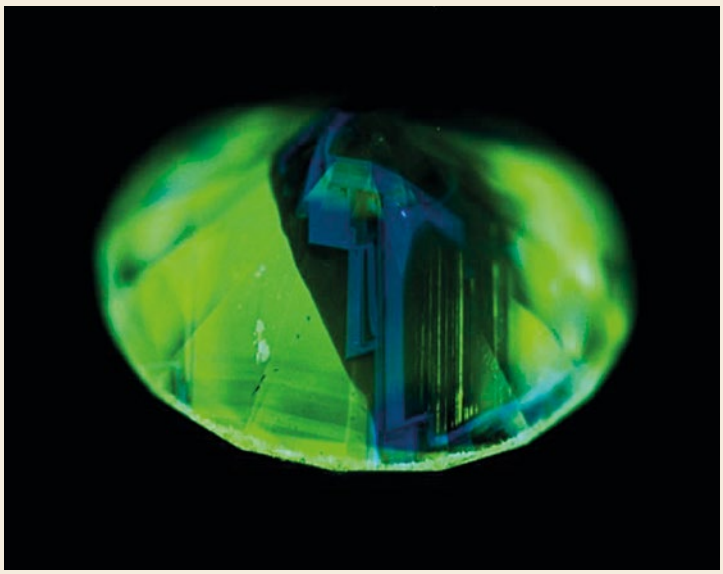

Figure 11: This 0.27 ct chameleon diamond shows a DiamondView pattern typical for chameleons, with a combination of yellow-green, blue and inert zones. The straight blue-luminescing growth zones represent octahedral growth. The curved boundary between the inert and yellow-green zones is reminiscent of a cuboid sector. Photomicrograph by A. Delaunay; image width 6.4 mm.

(Hainschwang et al., 2013), even outside the chameleon variety. However, it was not always detected in the past in chameleon diamonds (Fritsch et al., 2007b), simply because the necessary instrumentation was not available or, alternatively, it was not looked for.

The list below summarises the features documented in all the chameleon diamonds that we have examined, in addition to their defining photochromic and thermochromic behaviour: They change from a greener to a yellower colour when left in the dark for several hours, or after being moderately heated (160–200°C) for about a minute.

- Long-lasting (several minutes) yellow phosphorescence to short-wave UV radiation
- Zoned growth pattern, with a combination of blue octahedral and yellow-green cuboid growth, seen in the DiamondView
- Type IaA dominant, plus a type Ib component
- Some hydrogen, as indicated by the 3107 cm^{-1} system
- Absorption continuum in the UV-Vis range, related to the type Ib character
- 480 nm band, possibly related to an oxygen impurity
- 425 nm band, possibly related to hydrogen
- Broad feature in red to near-infrared region, likely H-related
- Traces of Ni

We thus believe that all of these features must be taken into account to explain the thermochromism and photochromism shown by chameleon diamonds. This list, which is quite long, is difficult to reconcile with a simple electronic structure relating to the defects responsible for chameleon behaviour. Various authors have suggested different explanations (Massi et al., 2006; Fritsch et al., 2007b; Butler et al., 2017; Byrne et al., 2018), but the complex nature of chameleon diamonds, combined with the nine characteristics listed above, makes their optical behaviour difficult to model. Numerous defects are present, associated with several impurities (nitrogen, in particular N-N or A aggregates, as well as hydrogen, nickel and oxygen), and it is difficult to assess if all necessarily play a role. However, the consistency of our observations on chameleon diamonds for almost 30 years leads us to believe that all these factors are significant. The list of nine characteristics should thus be taken into account in any forthcoming model for the chameleon-inducing electronic structure in diamond.

CONCLUSION

The study of an exceptionally large, 25.85 ct diamond with some unusual properties for chameleon diamonds prompted the question of what actually defines this unusual variety. By compiling the data provided by the available literature and combining it with the authors' own experience, it appears that the specifications are more numerous than expected. Indeed, the nine characteristics identified in this article appear to be necessary in combination. This likely explains why the origin of the chameleon behaviour in diamond remains a mystery.

Even though the 25.85 ct stone documented in this article had some unusual properties, it did have all of the characteristics required for a chameleon diamond.

REFERENCES

Breeding C.M., Eaton-Magaña S. and Shigley J.E., 2018. Natural-color green diamonds: A beautiful conundrum. *Gems & Gemology*, **54**(1), 2–27, http://dx.doi.org/10.5741/GEMS.54.1.2.

Butler J.E., Byrne K.S., Wang W. and Post J.E., 2017. A proposed mechanism for the color change in chameleon diamonds. *68th Diamond Conference*, University of Warwick, abstract O10 (unpublished).

Byrne K.S., Post J.E. and Butler J.E., 2015. Dynamics of luminescence processes in chameleon diamonds. *66th Diamond Conference*, University of Warwick, abstract P31 (unpublished).

Byrne K.S., Butler J.E., Wang W. and Post J.E., 2018. Chameleon diamonds: Thermal processes governing luminescence and a model for the color change. *Diamond and Related Materials*, **81**, 45–53, http://dx.doi.org/10.1016/j.diamond.2017.10.014.

Chabert V. and Reinitz I., 2000. Gem Trade Lab Notes: Diamonds—Chameleon, with blue-to-violet "transmission" luminescence. *Gems & Gemology*, **36**(1), 60–61.

Chan S., Zhou J.Y. and Johnson P., 2015. Lab Notes: Artificially irradiated color-change diamonds. *Gems & Gemology*, **51**(1), 60.

Chopard, 2014. The mystery of the chameleon diamond, www.chopard.com/intl/diary/the-mystery-of-the-chameleon-diamond, accessed 9 December 2017.

Collins A.T., 1982. Colour centres in diamond. *Journal of Gemmology*, **18**(1), 37–75, http://dx.doi.org/10.15506/JoG.1982.18.1.37.

Copeland L.L., Liddicoat R.T., Benson L.B., Martin J.G.M. and Crowningshield G.R., 1960. *The Diamond Dictionary*. Gemological Institute of America, Los Angeles, California, USA, 317 pp.

De Weerdt F. and Van Royen J., 2001. Defects in coloured natural diamonds. *Diamond and Related Materials*, **10**(3–7), 474–479, http://dx.doi.org/10.1016/s0925-9635(00)00521-5.

Eaton-Magaña S., Post J.E., Heaney P.J., Walters R.A., Breeding C.M. and Butler J.E., 2007. Fluorescence spectra of colored diamonds using a rapid, mobile spectrometer. *Gems & Gemology*, **43**(4), 332–351, http://dx.doi.org/10.5741/gems.43.4.332.

Figuier L., 1867. Le diamant caméléon. *L'Année Scientifique et Industrielle*, **2**, 144.

Fritsch E., 1998. The nature of color in diamonds. In G.E. Harlow, Ed., *The Nature of Diamonds*, American Museum of Natural History & Cambridge University Press, Cambridge, 23–47.

Fritsch E., 2016. Propheties étonnantes et fallacies délirantes: Le point de vue d'un gemmologue (Astonishing prophecies and delirious fallacies: The point of view of a gemmologist). *Planète Jules Verne*, No. 4, 51–57 (in French).

Fritsch E., Shigley J.E., Moses T., Rossman G.R., Zucker B. and Balfour I., 1995. Examination of the twenty-two carat green chameleon diamond. In D.J. Content, Ed., *A Green Diamond: A Study of Chameleonism*, W. S. Maney & Son, Leeds, 42 pp.

Fritsch E., Notari F., Respinger A. and Grobon C., 2004. Part II: The chameleon diamond, an exceptional stone. In H. Bari, Ed., *In the Kingdom of Diamonds*, National Natural History Museum, Doha, Qatar, 29–34.

Fritsch E., Hainschwang T., Massi L. and Rondeau B., 2007a. Hydrogen-related optical centers in natural diamond: An update. *New Diamond and Frontier Carbon Technology*, **17**(2), 63–89.

Fritsch E., Massi L., Rossman G.R., Hainschwang T., Jobic S. and Dessapt R., 2007b. Thermochromic and photochromic behaviour of "chameleon" diamonds. *Diamond and Related Materials*, **16**(2), 401–408, http://dx.doi.org/10.1016/j.diamond.2006.08.014.

Fryer C.W., 1981. Gem Trade Lab Notes: "Chameleon" diamond. *Gems & Gemology*, **27**(4), 227.

Gaillou E. and Rossman G.R., 2017. On the beauty of defects. In J.W. Harris and G.A. Staebler, Eds., *Diamond—The Ultimate Gemstone*, MINERAL Monograph No. 19, Lithographie LLC, Arvada, Colorado, USA, 40–53.

Goss J.P., Ewels C.P., Briddon P.R. and Fritsch E., 2011. Bistable N_2–H complexes: The first proposed structure of a H-related colour-causing defect in diamond. *Diamond and Related Materials*, **20**(7), 896–901, http://dx.doi.org/10.1016/j.diamond.2011.05.004.

Hainschwang T., 2014. Type Ib Diamonds: Relations Between the Physical and Gemological Properties of Single Nitrogen Containing Diamonds. PhD thesis, University of Nantes, France, 411 pp. (in French).

Hainschwang T., Simic D., Fritsch E., Deljanin B., Woodring S. and DelRe N., 2005. A gemological study of a collection of chameleon diamonds. *Gems & Gemology*, **41**(1), 20–34, http://dx.doi.org/10.5741/gems.41.1.20.

Hainschwang T., Notari F., Fritsch E., Massi L., Rondeau B., Breeding C.M. and Vollstaedt H., 2008. HPHT treatment of CO_2 containing and CO_2-related brown diamonds. *Diamond and Related Materials*, **17**(3), 340–351, http://dx.doi.org/10.1016/j.diamond.2008.01.022.

Hainschwang T., Fritsch E., Notari F., Rondeau B. and Katrusha A., 2013. The origin of color in natural C center bearing diamonds. *Diamond and Related Materials*, **39**, 27–40, http://dx.doi.org/10.1016/j.diamond.2013.07.007.

Hofer S.C., 1998. *Collecting and Classifying Coloured Diamonds: An Illustrated Study of the Aurora Collection*. Ashland Press, New York, New York, USA, 742 pp.

Irie M., 2000. Photochromism: Memories and switches—Introduction. *Chemical Reviews*, **100**(5), 1683–1684, http://dx.doi.org/10.1021/cr980068l.

Khan R.U.A., Martineau P.M., Cann B.L., Newton M.E., Dhillon H.K. and Twitchen D.J., 2010. Color alterations in CVD synthetic diamond with heat and UV exposure: Implications for color grading and identification. *Gems & Gemology*, **46**(1), 18–26, http://dx.doi.org/10.5741/gems.46.1.18.

Koivula J.I. and Kammerling R.C., Eds., 1991. Gem News: Large "chameleon" diamond. *Gems & Gemology*, **27**(2), 116.

Massi L., Fritsch E., Rossman G.R., Hainschwang T., Jobic S. and Dessapt R., 2006. Chameleon diamonds: A proposed model to explain thermochromic and photochromic behaviors. *Gems & Gemology*, **42**(3), 101–102.

Moe K.S., Neal J. and Johnson P., 2017. Lab Notes: Cape diamond with yellow phosphorescence. *Gems & Gemology*, **53**(1), 92–93.

Moses T., 1992. Gem Trade Lab Notes: Large chameleon-type diamond. *Gems & Gemology*, **28**(2), 124.

Panjikar J. and Panjikar A., 2015. An investigation in the color changing effects of diamond. *66th Diamond Conference*, University of Warwick, abstract P21 (unpublished).

Teyssier J., Saenko S.V., van der Marel D. and Milinkovitch M.C., 2015. Photonic crystals cause active colour change in chameleons. *Nature Communications*, **6**(1), article 6368, 7 pp., http://dx.doi.org/10.1038/ncomms7368.

The Authors

Dr Emmanuel Fritsch FGA
Institut des Matériaux Jean Rouxel, University of Nantes, CNRS, 2 rue de la Houssinière, BP 32229, 44322 Nantes Cedex 3, France.
Email: emmanuel.fritsch@cnrs-imn.fr

Aurélien Delaunay
Laboratoire Français de Gemmologie, 30 rue Notre Dame des Victoires, 75002 Paris, France

DNA Fingerprinting of Pearls, Corals and Ivory: A Brief Review of Applications in Gemmology

Laurent E. Cartier, Michael S. Krzemnicki, Bertalan Lendvay and Joana B. Meyer

ABSTRACT: This article reviews the extraction of DNA (deoxyribonucleic acid) from biogenic gem materials (pearls, corals and ivory) for determining species identification and geographic/genetic origin. We describe recent developments in the methodology adapted for gem samples that is minimally destructive, as well as the successful DNA fingerprinting of cultured pearls from various *Pinctada* molluscs to identify their species. The DNA analysis methods presented here can also potentially be used for fingerprinting corals and ivory.

The Journal of Gemmology, **36**(2), 2018, pp. 152–160 http://dx.doi.org/10.15506/JoG.2018.36.2.152

Biogenic gems—often called 'organic gems' (see Galopim de Carvalho, 2018, for a recent discussion of terminology)—are some of the oldest-used gem materials and have been cherished since pre-history (Hayward, 1990; Tsounis et al., 2010; Charpentier et al., 2012). Rather than having a geological origin, these gem materials—such as pearls, precious corals and ivory (e.g. Figure 1)—are products of biomineralisation processes in which living animals produce mineral substances (e.g. calcium carbonate or calcium phosphate) in terrestrial and marine environments (Mann, 2001). Due to their importance in jewellery and decorative arts, the study of biogenic gem materials constitutes an important part of gemmological research.

Natural pearls form in wild molluscs without any assistance, whereas cultured pearls are the result of human intervention on cultivated pearl-producing molluscs (Strack, 2006; Hänni, 2012). Pearls and their shells consist of secretions of different polymorphs of calcium carbonate ($CaCO_3$) such as aragonite, calcite and vaterite. Pearls are sometimes coloured by organic pigments.

Precious corals have not been cultivated commercially so far, and those used in jewellery and *objets d'art* represent the coral skeleton (secreted by living polyps), which consists of $CaCO_3$ as well as protein, glycosaminoglycans and proteoglycans (Debreuil et al., 2012). They can be coloured by carotenoids and other types of pigments.

Finally, elephant ivory from African (*Loxodonta spp.*) and Asian (*Elephas spp.*) elephant tusks is comprised of collagen and carbonate-rich hydroxyapatite (dahllite, $Ca_{10}[PO4]_6[CO_3] \cdot H_2O$; Edwards et al., 2006). Ivory can be found in a large number of animal species, of which elephant ivory is the most studied due to its value, recognition and cultural importance. In recent years, fossilised mammoth ivory has appeared more widely on the market, as elephant ivory trade restrictions have taken force (e.g. under the Convention on International Trade in Endangered Species of Wild Fauna and Flora, or CITES; www.cites.org/eng/niaps). CITES regulates the trade in biogenic gem materials that are produced by species included in its Appendices I, II or III. Among these are various species of precious coral, queen conch (pearls) and giant clam (pearls).

The ability to trace biogenic gem materials back to their species-related and geographic origins can provide greater transparency and help curb trade in illegal materials (and thus restrict poaching and smuggling). Furthermore, such research can yield important information

on the sources and trade routes of biogenic gems in historic items. The aim of this article is to provide an overview of DNA fingerprinting techniques to a gemmological audience, with particular emphasis on a previous detailed publication by some of the authors (Meyer et al., 2013) that focused on technical aspects concerning pearl genetics for species identification.

GEMMOLOGICAL RESEARCH

Traditional gemmological testing of pearls, corals and ivory in past decades was carried out mainly to separate these biogenic gem materials from imitations and, in the case of pearls, to separate natural from cultured (i.e. since the appearance of the latter on the market in the early 20th century: Anderson, 1932; Farn, 1986). This testing mostly has been visual, focusing both on the surface of examined materials and their internal structures. In addition, pigment analysis to help detect pearl treatments and gather more information for the possible determination of pearl species has also been carried out (Li and Chen, 2001; Elen, 2002; Karampelas et al., 2011). In recent years, research has focused on three-dimensional visualisation techniques of pearls and their internal structures (Krzemnicki et al., 2010; Revol et al., 2016; Mannes et al., 2017). Radiocarbon age dating of pearls has also been reported (Krzemnicki et al., 2017).

Research on corals in gemmology is much sparser than for pearls, and has focused on spectroscopic approaches (Rolandi et al., 2005; Henn, 2006; Smith et al., 2007; Karampelas et al., 2009). Elephant ivory has also been studied using techniques such as Raman and Fourier-transform infrared spectroscopy (Edwards and Farwell, 1995; Edwards et al., 2006), along with detailed visual analysis and preliminary trace-element studies (Yin et al., 2013). In addition, geochemical research on isotopes present in ivory has been conducted (van der Merwe et al., 1990; Ziegler et al., 2016).

BIOLOGICAL RESEARCH

A large amount of research has been carried out on the biological formation and characteristics of pearl-producing molluscs and also corals. This research is rarely linked to, and used in, gemmology. Much of this work focuses on detailed genetic aspects of pearl-producing molluscs, including various *Pinctada* species used for pearl farming. Among these are *P. maxima* (Kono et al., 2000; Lind et al., 2012), *P. margaritifera* (Arnaud-Haond et al., 2003a), *P. mazatlanica* (Arnaud-Haond et al., 2003b) and the *Pinctada* genealogy (Cunha et al., 2010), as well as the Akoya pearl oyster complex

Figure 1: Biogenic gem materials suitable for DNA testing include items such as these from the SSEF and H. A. Hänni collections: cultured pearls and associated shell material (*P. maxima* and *P. margaritifera*, ~15 cm tall), corals (including *Corallium rubrum* branches up to ~10 cm tall) and ivory (warthog and mammoth). Photo by Vito Lanzafame, SSEF.

(Wada and Tëmkin, 2008; Al-Saadi, 2013) and Pteriidae-family species such as *Pteria sterna* (Arnaud-Haond et al., 2005). The above-mentioned Akoya complex includes *Pinctada* species such as *P. fucata*, *P. imbricata*, *P. martensii* and *P. radiata*, which are closely related in genetic terms (Cunha et al., 2010). In addition, the genetics of freshwater mussel species used in cultured pearl production have been intensively studied (Peng et al., 2012; Shi et al., 2015). Most of this research was done with the goal of reducing mortality during pearl cultivation and improving the quality of cultured pearls.

Precious coral species such as *Corallium rubrum* (Mediterranean or Sardinian coral) have been studied extensively to understand their formation mechanisms (Grillo et al., 1993; Allemand and Bénazet-Tambutté, 1996), genetic diversity (Ledoux et al., 2010) and populations (Santangelo et al., 2003). Again, little of this biological research has crossed over to the gemmological community.

In elephant research, the link between declining populations and demand for ivory has been widely researched (Maisels et al., 2013, Wittemyer et al., 2014). Much of the scholarly work has focused on declining elephant populations and how to address poaching.

Figure 3: Vigorous vortexing of the nacre sample material in EDTA solution is necessary to detach the DNA molecules from the $CaCO_3$ framework. Photo by L. Cartier, SSEF.

DNA FINGERPRINTING FOR SPECIES (AND ORIGIN) DETERMINATION

Pearls

Pearls and pearl oyster shells contain small amounts of organic matter interspersed within a nacreous mineral matrix (Cuif and Dauphin, 1996; Comps et al., 2000; see Figure 2). In particular, they consist of approximately 92% $CaCO_3$, 4% organic matter (mainly conchiolin and porphyrins), 4% water and minute amounts of other substances (Taylor and Strack, 2008). The organic material has been studied in detail and contains different types of proteins, but previously it had not been reported to contain DNA (Levi-Kalisman et al., 2001; Nudelman et al., 2006; Dauphin et al., 2009). Nevertheless, negatively charged DNA molecules are known to have a high affinity for the Ca^{2+} ions of $CaCO_3$ (Barton et al., 2006), which might enhance the conservation of DNA in biogenic gems such as pearls.

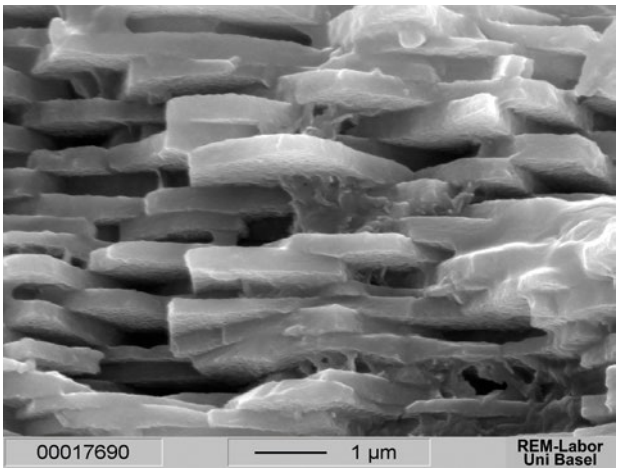

Figure 2: Scanning electron microscopy reveals the individual aragonite tablets in a cross-section through pearl nacre. DNA is thought to be found in organic matter between the individual tablets. Image by Henry A. Hänni and Marcel Düggelin, Zentrum für Mikroscopie, University of Basel, Switzerland.

Research by some of the present authors (Meyer et al., 2013) found DNA in organic matter within nacre from *P. margaritifera* (Tahitian black-lip pearl oyster), *P. maxima* (South Sea pearl oyster) and *P. radiata* (from the Arabian/Persian Gulf, part of the Akoya complex), thus allowing the separation of pearls (and mother-of-pearl) from different *Pinctada* species. A destructive technique for DNA identification was recently published by Saruwatari et al. (2018) focusing on *P. fucata* cultured pearls from Japan. For minimally destructive DNA extraction, the present authors developed a method that uses only a minute sample quantity and thus is applicable to jewellery-quality pearls (Meyer et al., 2013, and subsequent unpublished research by the authors).

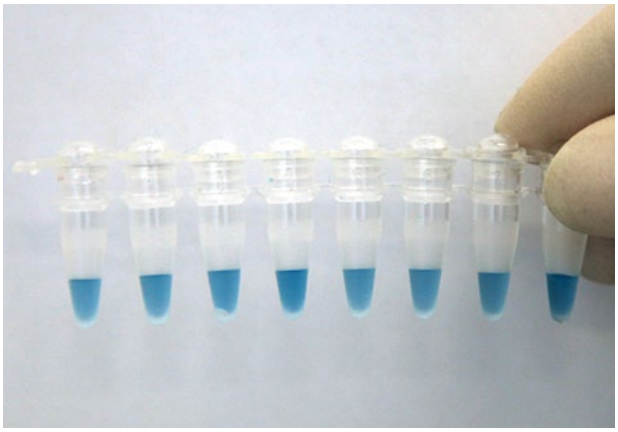

Figure 4: These tubes contain the amplified PCR product (internal transcribed spacer, ITS2) obtained for eight cultured pearls. Photo by L. Cartier, SSEF.

A Dremel workstation with a fixed 1 mm drill head was used to make a small hole in the nacre, and then a second non-fixed 0.9 mm drill bit was used to slightly enlarge the interior part of the hole without damaging the surface around it. The sample material was collected in a Petri dish. Given that most pearls are already drilled for jewellery use, the extraction of 10–20 mg (0.05–0.10 ct) of nacre material from within a pre-existing drill hole is considered quasi-non-destructive. However, this is not the case for pearls that cannot be drilled. The drill powder was then suspended in 1,000–2,000 µl of ethylenediaminetetraacetic acid solution (0.5 M EDTA solution at pH 8.0), vigorously vortexed for two minutes (Figure 3) and incubated overnight at 56°C in a water bath. EDTA dissolves the calcium carbonate structure of the mother-of-pearl. Oyster DNA was extracted from the sample material using a DNA extraction kit according to specific protocols (see Meyer et al., 2013). To genetically discriminate between *Pinctada* species, PCR-RFLP analysis (see Glossary) was performed on a PCR-amplified DNA fragment (internal transcribed spacer, ITS2; see Figure 4), and compared to equivalent RFLP profiles obtained from reference-positive controls (i.e. fresh mollusc tissue from these species; see Figure 5). Alternatively, PCR amplification only of specific ITS2 regions that discriminate between the oyster species was performed.

The research by Meyer et al. (2013) showed that in most cases it was possible to separate pearl oyster species based on their DNA profile extracted from only a minute amount of nacre material. Interestingly, amplification was also successful from samples composed of white nacre powder (i.e. no organic matter evidently visible), indicating that DNA can be obtained through demineralisation from the $CaCO_3$ structure of the nacre and/or from small samples (e.g. 10–20 mg). As technology costs come down and these methods are further refined, the authors foresee DNA fingerprinting being carried out on even smaller amounts of nacre material.

Current research by the authors shows that DNA fingerprinting can be adapted to other species of pearl-bearing molluscs and their pearls. This includes a range of freshwater mussels such as Chinese *Hyriopsis schlegelii* and *Hyriopsis cumingii schlegelii* mussel hybrids or the American washboard mussel (*Megalonaias nervosa*) that is frequently used as bead nucleus material in Akoya,

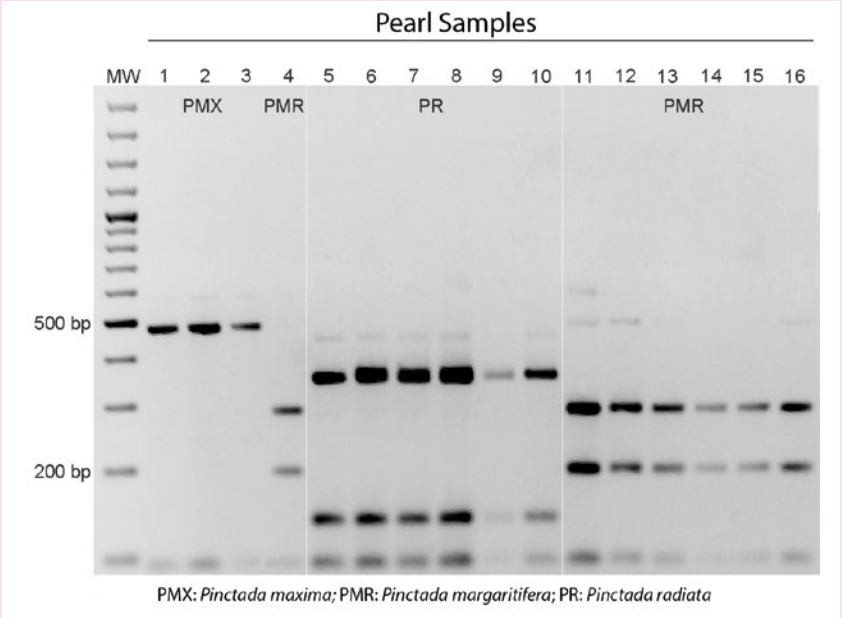

Figure 5: A PCR-RFLP assay of the ITS2 DNA fragment was used to differentiate the species associated with 16 cultured pearls. Lanes 1–3 correspond to *Pinctada maxima*, lanes 4 and 11–16 are for *P. margaritifera* and lanes 5–10 are for *P. radiata*. 'MW' corresponds to molecular weight and 'bp' to base pairs. Image by J. B. Meyer; modified from Meyer et al. (2013).

Figure 6: This five-row necklace contains 377 natural pearls ranging from 3.90 to 9.45 mm, likely from *P. radiata* of the Arabian Gulf. DNA fingerprinting could provide further documentation of the provenance for such exceptional pearls. Photo by Luc Phan, SSEF.

South Sea, Tahitian and Fijian pearl cultivation. We also are adapting this analytical approach to conch pearls (*Lobatus gigas*, formerly commonly known as *Strombus gigas*) and pearls from the giant clam (*Tridacna gigas*), in anticipation that DNA fingerprinting could contribute to more transparency in these CITES-regulated pearls.

Other Biogenic Gem Materials

The methodology used by Meyer et al. (2013) has been recently piloted by the authors on samples from various precious coral species commonly used in jewellery (including those from the Mediterranean, Asian and Midway Islands regions). This ongoing research should allow the separation of different species of precious corals and conclusively identify and distinguish non-CITES-regulated species (e.g. *Corallium rubrum*, or Mediterranean coral) from CITES-regulated species (e.g. *Corallium elatius*, known in the trade as Momo, Cerasuolo or Satsuma coral).

There have also been developments in techniques to determine geographic/genetic origin and species identification of seized elephant ivory using DNA and microsatellite methods (i.e. analysis of repeated DNA sequences in the genome that enable the distinction between different elephant population groups). However, so far this has been performed in a destructive way, requiring relatively large amounts of material (Comstock et al., 2003; Wasser et al., 2004, 2015). A less destructive method, like that used by Meyer et al. (2013), might be adapted to ivory too, thereby requiring much smaller amounts of material for testing such samples.

RESEARCH OUTLOOK AND CONCLUSIONS

DNA fingerprinting offers various advantages for the research and trade in biogenic gem materials. It provides a new option to increase transparency (through origin and species determination) and to help address fraud or illegal trading by separating protected from non-protected species.

The state-of-the-art minimally destructive extraction methodology outlined in this article can offer conclusive identification of the mollusc species to which a pearl corresponds, unlike other methods currently available in gemmology today. Furthermore, DNA analysis has the potential to reveal the geographic origin of cultured or natural pearls (Figure 6) based on more specific fingerprinting. For corals, species determination may considerably contribute toward resource conservation efforts and also provide more information on the provenance of historic items. As such, this research is relevant to the work of international customs officials within the context of biogenic gem materials protected by CITES. With ivory, origin determination based on DNA analysis has already been proven possible (Wasser et al., 2004). However, the available methodology requires large amounts of sample material and is thus not appropriate for jewellery or other items that cannot be destructively tested. Ongoing research and specifically next-generation sequencing (see Glossary) enables the screening of a large number of DNA sequences from smaller samples

at lower costs, subsequently reducing the amount of sample material required. DNA fingerprinting is, therefore, becoming less destructive and more useful for biogenic gem materials.

DNA fingerprinting as a tool in gemmology further illustrates the importance of multidisciplinary research collaborations (in this case, with marine biology and genetics scientists) to develop new gem-testing techniques for the 21st century.

REFERENCES

Al-Saadi A., 2013. Population Structure and Patterns of Genetic Variation in a Pearl Oyster (*Pinctada radiata*) Native to the Arabian Gulf. Master's thesis, School of Earth, Environmental and Biological Sciences, Queensland University of Technology, Brisbane, Australia, 110 pp.

Allemand D. and Bénazet-Tambutté S., 1996. Dynamics of calcification in the Mediterranean red coral, *Corallium rubrum* (Linnaeus) (Cnidaria, Octocorallia). *Journal of Experimental Zoology*, **276**(4), 270–278, http://dx.doi.org/10.1002/(sici)1097-010x(19961101)276:4%3C270::aid-jez4%3E3.0.co;2-l.

Anderson B.W., 1932. The use of X rays in the study of pearls. *British Journal of Radiology*, **5**(49), 57–64, http://dx.doi.org/10.1259/0007-1285-5-49-57.

Arnaud-Haond S., Bonhomme F. and Blanc F., 2003a. Large discrepancies in differentiation of allozymes, nuclear and mitochondrial DNA loci in recently founded Pacific populations of the pearl oyster *Pinctada margaritifera*. *Journal of Evolutionary Biology*, **16**(3), 388–398, http://dx.doi.org/10.1046/j.1420-9101.2003.00549.x.

Arnaud-Haond S., Monteforte M., Blanc F. and Bonhomme F., 2003b. Evidence for male-biased effective sex ratio and recent step-by-step colonization in the bivalve *Pinctada mazatlanica*. *Journal of Evolutionary Biology*, **16**(5), 790–796, http://dx.doi.org/10.1046/j.1420-9101.2003.00603.x.

Arnaud-Haond S., Blanc F., Bonhomme F. and Monteforte M., 2005. Recent foundation of Mexican populations of pearl oysters (*Pteria sterna*) revealed by lack of genetic variation on two mitochondrial genes. *Journal of the Marine Biological Association of the United Kingdom*, **85**(2), 363–366, http://dx.doi.org/10.1017/S0025315405011288h.

Barton H.A., Taylor N.M., Lubbers B.R. and Pemberton A.C., 2006. DNA extraction from low-biomass carbonate rock: An improved method with reduced contamination and the low-biomass contaminant database. *Journal of Microbiological Methods*, **66**(1), 21–31, http://dx.doi.org/10.1016/j.mimet.2005.10.005.

Glossary*

Deoxyribonucleic acid (DNA): Contains all the information an organism needs to develop, live and reproduce. It is formed by the four nucleobases (or 'bases') adenine (A), cytosine (C), guanine (G) and thymidine (T). The order of the bases (e.g. ATCGGTT…) codifies the specific instructions for any living organism.

DNA sequencing: The reading of nucleobases (A, C, G and T) in DNA. One can choose to sequence an entire genome (whole/full genome sequencing) of a tested sample or just sequence a few targeted nucleobases that are useful for distinguishing different species (DNA fingerprinting).

Genome: An organism's full set of DNA, including all of its genes.

Microsatellite: Repetitive DNA sequences that can be used as genetic markers to measure levels of relatedness between species or individuals. They can be used for genetic population studies and thus may offer more information on the geographic origin of individuals from a species.

Next-generation sequencing (NGS): Allows massive parallel sequencing of DNA, enabling a rapid and cost-effective way to sequence large amounts of genetic regions and whole genomes of organisms. With its ultra-high throughput, NGS has revolutionised genomic research.

DNA amplification and polymerase chain reaction (PCR): A method for amplifying DNA sequences. The technique involves using short DNA sequences called primers (see below) to select the portion of a genome for amplification. In PCR, sample temperature is repeatedly increased and decreased to help a DNA replication enzyme synthesise the target DNA sequence. As such, PCR can produce thousands to millions of copies of the target sequence in several hours, which can then be analysed. For example, it allows the identification of specific DNA sequences using visual inspection (e.g. gel electrophoresis) or they may be read through sequencing.

Primer: A primer is a short DNA sequence that serves as a starting point for DNA synthesis by PCR. Primers are selected according to the sequence region targeted for DNA amplification. These are, for example, regions in the genome of various oyster species (specific genetic markers) for which differences allow species determination.

Restriction fragment length polymorphism (RFLP): A technique based on variations in the DNA sequence (e.g. from different species) recognised by restriction enzymes. The resulting restriction fragments are separated according to their length by gel electrophoresis. The length (in base pairs) can differ between individuals and species such that the positions of gel bands can be used to separate samples from different species.

* Sources: National Human Genome Research Institute glossary (www.genome.gov/glossary), National Center for Biotechnology Information Probe glossary (www.ncbi.nlm.nih.gov/probe/docs/glossary) and Wikipedia.

Charpentier V., Phillips C.S. and Méry S., 2012. Pearl fishing in the ancient world: 7500 BP. *Arabian Archaeology and Epigraphy*, **23**(1), 1–6, http://dx.doi.org/10.1111/j.1600-0471.2011.00351.x.

Comps M., Herbaut C. and Fougerouse A., 2000. Abnormal periostracum secretion during the mineralization process of the pearl in the blacklip pearl oyster *Pinctada margaritifera*. *Aquatic Living Resources*, **13**(1), 49–55, http://dx.doi.org/10.1016/s0990-7440(00)00134-0.

Comstock K.E., Ostrander E.A. and Wasser S.K., 2003. Amplifying nuclear and mitochondrial DNA from African elephant ivory: A tool for monitoring the ivory trade. *Conservation Biology*, **17**(6), 1840–1843, http://dx.doi.org/10.1111/j.1523-1739.2003.00358.x.

Cuif J.-P. and Dauphin Y., 1996. Occurrence of mineralization disturbances in nacreous layers of cultivated pearls produced by *Pinctada margaritifera* var. *cumingi* from French Polynesia. Comparison with reported shell alterations. *Aquatic Living Resources*, **9**(2), 187–193, http://dx.doi.org/10.1051/alr:1996022.

Cunha R.L., Blanc F., Bonhomme F. and Arnaud-Haond S., 2010. Evolutionary patterns in pearl oysters of the genus *Pinctada* (Bivalvia: Pteriidae). *Marine Biotechnology*, **13**(2), 181–192, http://dx.doi.org/10.1007/s10126-010-9278-y.

Dauphin Y., Brunelle A., Cotte M., Cuif J.P., Farre B., Laprévote O., Meibom A., Salomé M. and Williams C.T., 2009. A layered structure in the organic envelopes of the prismatic layer of the shell of the pearl oyster *Pinctada margaritifera* (Mollusca, Bivalvia). *Microscopy and Microanalysis*, **16**(1), 91–98, http://dx.doi.org/10.1017/s1431927609991115.

Debreuil J., Tambutté É., Zoccola D., Deleury E., Guigonis J.M., Samson M., Allemand D. and Tambutté S., 2012. Molecular cloning and characterization of first organic matrix protein from sclerites of red coral, *Corallium rubrum*. *Journal of Biological Chemistry*, **287**(23), 19367–19376, http://dx.doi.org/10.1074/jbc.M112.352005.

Edwards H.G.M. and Farwell D.W., 1995. Ivory and simulated ivory artefacts: Fourier transform Raman diagnostic study. *Spectrochimica Acta Part A: Molecular and Biomolecular Spectroscopy*, **51**(12), 2073–2081, http://dx.doi.org/10.1016/0584-8539(95)01455-3.

Edwards H.G.M., Hassan N.F.N. and Arya N., 2006. Evaluation of Raman spectroscopy and application of chemometric methods for the differentiation of contemporary ivory specimens I: Elephant and mammalian species. *Journal of Raman Spectroscopy*, **37**(1–3), 353–360, http://dx.doi.org/10.1002/jrs.1458.

Elen S., 2002. Identification of yellow cultured pearls from the black-lipped oyster *Pinctada margaritifera*. *Gems & Gemology*, **38**(1), 66–72, http://dx.doi.org/10.5741/gems.38.1.66.

Farn A.E., 1986. *Pearls: Natural, Cultured and Imitation*. Butterworth-Heinemann, London, 150 pp.

Galopim de Carvalho R., 2018. Getting your facts right. *Gems&Jewellery*, **27**(1), 28–29.

Grillo M.C., Goldberg W.M. and Allemand D., 1993. Skeleton and sclerite formation in the precious red coral *Corallium rubrum*. *Marine Biology*, **117**(1), 119–128, http://dx.doi.org/10.1007/bf00346433.

Hänni H.A., 2012. Natural pearls and cultured pearls: A basic concept and its variations. *Australian Gemmologist*, **24**(11), 258–266.

Hayward L.G., 1990. The origin of the raw elephant ivory used in Greece and the Aegean during the Late Bronze Age. *Antiquity*, **64**(242), 103–109, http://dx.doi.org/10.1017/s0003598x00077334.

Henn U., 2006. Korallen im Edelstein- und Schmuckhandel [Corals in the gem and jewellery trade]. *Gemmologie: Zeitschrift der Deutschen Gemmologischen Gesellschaft*, **55**(3/4), 77–104 (in German with English abstract).

Karampelas S., Fritsch E., Rondeau B., Andouche A. and Métivier B., 2009. Identification of the endangered pink-to-red *Stylaster* corals by Raman spectroscopy. *Gems & Gemology*, **45**(1), 48–52, http://dx.doi.org/10.5741/gems.45.1.48.

Karampelas S., Fritsch E., Gauthier J.-P. and Hainschwang T., 2011. UV-Vis-NIR reflectance spectroscopy of natural-color saltwater cultured pearls from *Pinctada margaritifera*. *Gems & Gemology*, **47**(1), 31–35, http://dx.doi.org/10.5741/gems.47.1.31.

Kono M., Hayashi N. and Samata T., 2000. Molecular mechanism of the nacreous layer formation in *Pinctada maxima*. *Biochemical and Biophysical Research Communications*, **269**(1), 213–218, http://dx.doi.org/10.1006/bbrc.2000.2274.

Krzemnicki M.S., Friess S.D., Chalus P., Hänni H.A. and Karampelas S., 2010. X-ray computed microtomography: Distinguishing natural pearls from beaded and non-beaded cultured pearls. *Gems & Gemology*, **46**(2), 128–134, http://dx.doi.org/10.5741/gems.46.2.128.

Krzemnicki M.S., Cartier L.E. and Hajdas I., 2017. Radiocarbon age dating of 1,000-year-old pearls from the Cirebon shipwreck (Java, Indonesia). *Journal of Gemmology*, **35**(8), 728–736, http://dx.doi.org/10.15506/jog.2017.35.8.728.

Ledoux J.B., Garrabou J., Bianchimani O., Drap P., Féral J.P. and Aurelle D., 2010. Fine-scale genetic structure and inferences on population biology in the threatened Mediterranean red coral, *Corallium rubrum*. *Molecular Ecology*, **19**(19), 4204–4216, http://dx.doi.org/10.1111/j.1365-294X.2010.04814.x.

Levi-Kalisman Y., Falini G., Addadi L. and Weiner S., 2001. Structure of the nacreous organic matrix of a bivalve mollusk shell examined in the hydrated state using cryo-TEM. *Journal of Structural Biology*, **135**(1), 8–17, http://dx.doi.org/10.1006/jsbi.2001.4372.

Li L. and Chen Z., 2001. Cultured pearls and colour-changed cultured pearls: Raman spectra. *Journal of Gemmology*, **27**(8), 449–455, http://dx.doi.org/10.15506/JoG.2001.27.8.449.

Lind C.E., Evans B.S., Elphinstone M.S., Taylor J.J. and Jerry D.R., 2012. Phylogeography of a pearl oyster (*Pinctada maxima*) across the Indo-Australian Archipelago: Evidence of strong regional structure and population expansions but no phylogenetic breaks. *Biological Journal of the Linnean Society*, **107**(3), 632–646, http://dx.doi.org/10.1111/j.1095-8312.2012.01960.x.

Maisels F., Strindberg S., Blake S., Wittemyer G., Hart J., Williamson E.A., Aba'a R., Abitsi G., Ambahe R.D., Amsini F., Bakabana P.C., Hicks T.C., Bayogo R.E., Bechem M., Beyers R.L., Bezangoye A.N., Boundja P., Bout N., Akou M.E., Bene L.B., Fosso B., Greengrass E., Grossmann F., Ikamba-Nkulu C., Ilambu O., Inogwabini B.-I., Iyenguet F., Kiminou F., Kokangoye M., Kujirakwinja D., Latour S., Liengola I., Mackaya Q., Madidi J., Madzoke B., Makoumbou C., Malanda G.-A., Malonga R., Mbani O., Mbendzo V.A., Ambassa E., Ekinde A., Mihindou Y., Morgan B.J., Motsaba P., Moukala G., Mounguengui A., Mowawa B.S., Ndzai C., Nixon S., Nkumu P., Nzolani F., Pintea L., Plumptre A., Rainey H., de Semboli B.B., Serckx A., Stokes E., Turkalo A., Vanleeuwe H., Vosper A. and Warren Y., 2013. Devastating decline of forest elephants in central Africa. *PLoS ONE*, **8**(3), article e59469, 13 pp., http://dx.doi.org/10.1371/journal.pone.0059469.

Mann S., 2001. *Biomineralization: Principles and Concepts in Bioinorganic Materials Chemistry*. Oxford University Press, Oxford, 198 pp.

Mannes D., Hanser C., Krzemnicki M., Harti R.P., Jerjen I. and Lehmann E., 2017. Gemmological investigations on pearls and emeralds using neutron imaging. *Physics Procedia*, **88**, 134–139, http://dx.doi.org/10.1016/j.phpro.2017.06.018.

Meyer J.B., Cartier L.E., Pinto-Figueroa E.A., Krzemnicki M.S., Hänni H.A. and McDonald B.A., 2013. DNA fingerprinting of pearls to determine their origins. *PLoS ONE*, **8**(10), article e75606, 11 pp., http://dx.doi.org/10.1371/journal.pone.0075606.

Nudelman F., Gotliv B.A., Addadi L. and Weiner S., 2006. Mollusk shell formation: Mapping the distribution of organic matrix components underlying a single aragonitic tablet in nacre. *Journal of Structural Biology*, **153**(2), 176–187, http://dx.doi.org/10.1016/j.jsb.2005.09.009.

Peng K., Wang J., Sheng J., Zeng L. and Hong Y., 2012. Molecular characterization and immune analysis of a defensin from freshwater pearl mussel, *Hyriopsis schlegelii*. *Aquaculture*, **334–337**, 45–50, http://dx.doi.org/10.1016/j.aquaculture.2011.12.039.

Revol V., Hanser C. and Krzemnicki M., 2016. Characterization of pearls by X-ray phase contrast imaging with a grating interferometer. *Case Studies in Nondestructive Testing and Evaluation*, **6**, 1–7, http://dx.doi.org/10.1016/j.csndt.2016.06.001.

Rolandi V., Brajkovic A., Adamo I., Bocchio R. and Landonio M., 2005. Gem corals: Classification and spectroscopic features. *Australian Gemmologist*, **22**(7), 285–298.

Santangelo G., Carletti E., Maggi E. and Bramanti L., 2003. Reproduction and population sexual structure of the overexploited Mediterranean red coral *Corallium rubrum*. *Marine Ecology Progress Series*, **248**, 99–108, http://dx.doi.org/10.3354/meps248099.

Saruwatari K., Suzuki M., Zhou C., Kessrapong P. and Sturman N., 2018. DNA techniques applied to the identification of *Pinctada fucata* pearls from Uwajima, Ehime Prefecture, Japan. *Gems & Gemology*, **54**(1), 40–50, http://dx.doi.org/10.5741/GEMS.54.1.40.

Shi J., Hong Y., Sheng J., Peng K. and Wang J., 2015. *De novo* transcriptome sequencing to identify the sex-determination genes in *Hyriopsis schlegelii*. *Bioscience, Biotechnology, and Biochemistry*, **79**(8), 1257–1265, http://dx.doi.org/10.1080/09168451.2015.1025690.

Smith C.P., McClure S.F., Eaton-Magaña S. and Kondo D.M., 2007. Pink-to-red coral: A guide to determining origin of color. *Gems & Gemology*, **43**(1), 4–15, http://dx.doi.org/10.5741/gems.43.1.4.

Strack E., 2006. *Pearls*. Rühle-Diebener-Verlag, Stuttgart, Germany, 707 pp.

Taylor J. and Strack E., 2008. Pearl production. In P.C. Southgate and J.S. Lucas, Eds., *The Pearl Oyster*, Elsevier, Oxford, 273–302, http://dx.doi.org/10.1016/b978-0-444-52976-3.00008-5.

Tsounis G., Rossi S. and Gili J.-M., 2010. Identifying population decline in *Corallium rubrum* by using historical information. In E. Bussoletti, D. Cottingham, A. Bruckner, G. Roberts and R. Sandulli, Eds., *Proceedings of the International Workshop on Red Coral Science, Management, and Trade: Lessons from the Mediterranean*, Naples, Italy, 23–26 September 2009, 33–39.

van der Merwe N.J., Lee-Thorp J.A., Thackeray J.F., Hall-Martin A., Kruger F.J., Coetzee H., Bell R.H.V. and Lindeque M., 1990. Source-area determination of elephant ivory by isotopic analysis. *Nature*, **346**(6286), 744–746, http://dx.doi.org/10.1038/346744a0.

Wada K.T. and Tëmkin I., 2008. Taxonomy and phylogeny. In P.C. Southgate and J.S. Lucas, Eds., *The Pearl Oyster*, Elsevier, Oxford, 37–75, http://dx.doi.org/10.1016/b978-0-444-52976-3.00002-4.

Wasser S.K., Shedlock A.M., Comstock K., Ostrander E.A., Mutayoba B. and Stephens M., 2004. Assigning African elephant DNA to geographic region of origin: Applications to the ivory trade. *Proceedings of the National Academy of Sciences*, **101**(41), 14847–14852, http://dx.doi.org/10.1073/pnas.0403170101.

Wasser S.K., Brown L., Mailand C., Mondol S., Clark W., Laurie C. and Weir B.S., 2015. Genetic assignment of

large seizures of elephant ivory reveals Africa's major poaching hotspots. *Science*, **349**(6243), 84–87, http://dx.doi.org/10.1126/science.aaa2457.

Wittemyer G., Northrup J.M., Blanc J., Douglas-Hamilton I., Omondi P. and Burnham K.P., 2014. Illegal killing for ivory drives global decline in African elephants. *Proceedings of the National Academy of Sciences*, **111**(36), 13117–13121, http://dx.doi.org/10.1073/pnas.1403984111.

Yin Z., Zhang P., Chen Q., Luo Q., Zheng C. and Li Y., 2013. A comparison of modern and fossil ivories using multiple techniques. *Gems & Gemology*, **49**(1), 16–27, http://dx.doi.org/10.5741/gems.49.1.16.

Ziegler S., Merker S., Streit B., Boner M. and Jacob D.E., 2016. Towards understanding isotope variability in elephant ivory to establish isotopic profiling and source-area determination. *Biological Conservation*, **197**, 154–163, http://dx.doi.org/10.1016/j.biocon.2016.03.008.

The Authors

Dr Laurent E. Cartier FGA[1,2], Dr Michael S. Krzemnicki FGA[1], Dr Bertalan Lendvay[1,3] and Dr Joana B. Meyer[4]

[1] Swiss Gemmological Institute SSEF, Aeschengraben 26, 4051 Basel, Switzerland. Email: gemlab@ssef.ch

[2] Institute of Earth Sciences, University of Lausanne, 1015 Lausanne, Switzerland

[3] University of Zürich, Institute of Forensic Medicine, Zürich, Switzerland

[4] Swiss Federal Research Institute WSL, Zürcherstrasse 111, 8903 Birmensdorf, Switzerland

Acknowledgements

We thank Prof. Bruce McDonald (ETH Zürich, Switzerland) for his initial support of this project; Prof. Dr Henry Hänni (GemExpert, Basel, Switzerland) for supplying Figure 2 and for many discussions on pearls; Dr Christoph Sperisen (Swiss Federal Institute for Forest, Snow and Landscape Research, Birmensdorf, Switzerland); Dr Massimiliano Cardinale (Justus Liebig University Giessen, Germany) for useful input; and Andy Müller (Hinata Trading, Kobe, Japan) for his generous donation of many pearl samples for this and other research projects at SSEF.

The Fire Within

"For in them you shall see the living fire of the ruby, the glorious purple of the amethyst, the sea-green of the emerald, all glittering together in an incredible mixture of light."

– Roman Elder Pliny, 1st Century AD

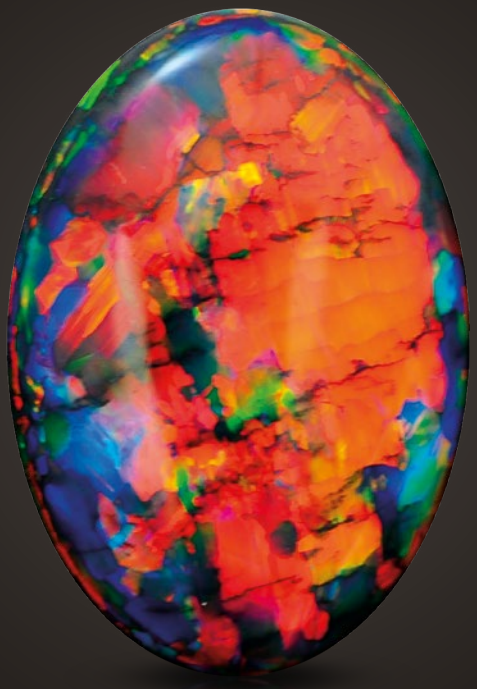

Black Opal 15.7 Carats

Suppliers of Australia's finest opals to the world's gem trade.

CODY OPAL

Level 1 - 119 Swanston Street Melbourne Australia

T. +61 3 9654 5533 E. info@codyopal.com

www.codyopal.com

ICA
INTERNATIONAL COLORED GEMSTONE ASSOCIATION
MEMBER

JOG

Conferences

15TH ANNUAL SINKANKAS SYMPOSIUM—TANZANITE & TSAVORITE

On 14 April 2018 the 15th Annual Sinkankas Symposium was held at the Gemological Institute of America (GIA) in Carlsbad, California, and was co-hosted by the Gemological Society of San Diego. Approximately 160 people were treated to informative presentations by 11 speakers (Figure 1), as well as a beautiful display of tanzanite and tsavorite crystal specimens and gemstones that was assembled for the event. Abstracts of the presentations are available on the conference website at www.sinkankassymposium.net. The symposium was moderated by **Robert Weldon** (GIA, Carlsbad), who also delivered a poem that he wrote specifically for the event.

Dr Raquel Alonso-Perez (Harvard University, Cambridge, Massachusetts, USA) examined the geology of East Africa's Mozambique Belt in order to explain why tanzanite and tsavorite form in the same region. Both gems are Ca-Al silicates that are associated with graphitic gneiss and other metamorphic rocks. While tanzanite forms during retrograde metamorphism, tsavorite may crystallise during either prograde or retrograde events.

Robert Gessner (Gessner Gems, Beverly Hills, California) described his experience mining tanzanite at Merelani Block C in north-eastern Tanzania, where he was employed by TanzaniteOne. The mineralisation is hosted by fractured boudins formed by calc-silicate minerals that are concentrated along the axes of complex fold structures.

Nathan Renfro (GIA, Carlsbad) reviewed the internal features of tanzanite and tsavorite, both of which typically host relatively few inclusions. Tanzanite may contain ribbon-like growth tubes, 'fingerprints', fractures (sometimes with epigenetic residues), lamellar twinning, growth zoning, and crystals of graphite and hematite. Inclusions in tsavorite may consist of 'fingerprints', colourless crystals (possibly diopside), etch tubes and platelets, rare three-phase inclusions, and crystals of graphite and pyrite.

Stuart Robertson (Gemworld International Inc., Glenview, Illinois, USA) reviewed tanzanite price trends, and emphasised how the management of supply is critical to the sustainability of a single-source gem

Figure 1: Speakers at the 15th Annual Sinkankas Symposium gather together with a life-size bronze sculpture of Richard T. Liddicoat Jr. From left to right: Nathan Renfro, Meg Berry, Stuart Robertson, Will Larson, Shane McClure, Bill Larson, Judith and Bruce Bridges, Raquel Alonso-Perez, George Rossman and Robert Gessner. Photo by Jim Parrish.

material such as tanzanite. Viewed in the context of its rarity, the current wholesale prices of tanzanite may prove to be one of the biggest bargains in coloured stones.

Father-and-son team **Bill and Will Larson** (Pala International, Fallbrook, California) conveyed their experience with collecting tanzanite and tsavorite crystals. Bill chronicled the history of his involvement with procuring fine specimens, and Will showed a video of his 2012 visit to a tanzanite mine at Merelani Block C. The period from 2008 to 2011 was good for obtaining tanzanite crystals since the market for cut stones was relatively slow. Nevertheless, both matrix specimens and good undamaged crystals of tanzanite are very rare.

Bruce and Judith Bridges (Bridges Tsavorite, Tucson, Arizona, USA) described the history of the discovery and mining of tsavorite in Kenya. The mother-and-son team shared stories of life in their mining camp with husband/father Campbell Bridges before he was tragically murdered in 2009. Although the price of tsavorite has increased greatly since that time, new Tanzanian mining regulations are making it very difficult for foreign investment to continue.

Meg Berry (Megagem, Fallbrook) described the process of cutting a suite of fancy-colour zoisite. She used a dichroscope to orient each piece of rough in order to attractively blend the pleochroic colours while taking into account the shape/yield of the resulting gemstones. She prefers a crown angle of 25°–30° for zoisite, and her yields generally ranged from 25% to 30%.

Shane McClure (GIA, Carlsbad) covered the treatments and imitations of tanzanite and tsavorite. Both gem varieties can be clarity enhanced by filling surface-reaching fractures with oil. Tsavorite is not subjected to any other treatments, while tanzanite is commonly heat treated at 500–700°C to produce its attractive blue-to-violet colouration from brown starting material. Tanzanite has been imitated by various materials including synthetic sapphire, yttrium aluminium garnet (YAG), synthetic forsterite and high-RI glass, whereas tsavorite is only rarely imitated with high-RI laboratory-grown products such as YAG and CZ-like materials.

Dr George Rossman (California Institute of Technology, Pasadena) examined the colour causes of tanzanite and tsavorite. In tanzanite, V is the dominant trace element, and other chromophores include Cr, Mn and Fe, but the exact mechanism that causes its colour remains elusive. Tsavorite colouration is much more straightforward, being caused mainly by V^{3+}, together with some contribution from Cr^{3+} when present in sufficient amounts.

Brendan M. Laurs FGA

SWISS GEMMOLOGICAL SOCIETY

On 7–8 May 2018, the Swiss Gemmological Society (SGS) held its 76th annual conference at Hotel de la Paix in Lugano, southern Switzerland. In attendance were approximately 70 SGS members and guests (Figure 2). The meeting was chaired by **Hans Pfister** (SGS president), **Michael Hügi** (SGS director) and **Dr Michael Krzemnicki** (Swiss Gemmological Institute SSEF, Basel). The main theme of the conference was diamonds from southern Africa, although a variety of additional topics was covered.

Mike Brook (Debswana, Gaborone, Botswana) profiled Botswana's diamonds, including their prospecting history, localities, mining, production and incorporation into jewellery. Today, Botswana is the world's second largest diamond producer by value and there are currently eight operating mines. Good governance practises since 1966 have allowed the significant diamond revenues accrued by Botswana's government to directly benefit the nation (once one of the poorest in the world), transforming it into a middle-income economy with one of the largest gross domestic products on the African continent. **Dr Jurgen Jacob** (Namdeb Diamond Corporation Pty Ltd, Oranjemund, Namibia) reviewed the characteristics of Namibia's diamond megaplacer, which has so far produced more than 100 million carats. Several geological factors contributed to its formation as the world's most spectacular placer diamond deposit, including: a fertile craton that has hosted numerous diamondiferous kimberlite intrusions throughout geological time; the presence of a single exit point at the mouth of the Orange River; a low volume of diluting sediments; extensive regional uplift followed by a long period of erosion; a relatively high-energy marine depositional environment that helped separate the diamonds from the other sediments, combined with northward prevailing winds and longshore currents that helped remove sand from the diamondiferous gravels; and the relatively young age of the sediments so they are unlithified and easy to mine. A brief history of mining over the past 110 years was given, as well as current challenges and innovations which should enable mining in this area to continue well into the future, both of the onshore and offshore deposits. **This author** covered recent mining of some alluvial diamond deposits in South Africa (see *The Journal*, Vol. 35, No. 6, 2017, pp. 484–485).

In other diamond presentations, **Gilles Walthert** (Edigem Ltd, Lucerne, Switzerland) examined the current diamond market. He summarised 2017 reports from Bain & Co. (see *The Journal*, Vol. 36, No. 1, 2018, p. 3) and

from De Beers (see p. 88 of this issue of *The Journal*), and then examined factors that affect diamond pricing, including physical properties ('4 Cs'), the presence of fluorescence, the stone's cut grade and whether it exemplifies a 'critical weight', the seller's situation and the gem's charm (particularly for fancy cuts). **Michael Hügi** discussed synthetic diamonds (Figure 3), which are becoming more common in the jewellery trade—2 million carats in 2017. He reviewed the diagnostic features of natural and synthetic diamonds that are seen with standard gemmological equipment, and also examined the marketing strategies being promulgated by mining companies and synthetics producers. He indicated that it is essential to have well-educated sales staff who should emphasise the exclusiveness of natural diamond.

Coloured stone overviews were delivered in two presentations. **Antoinette Starkey** (Antoinette Starkey Pierres Précieuses, Geneva, Switzerland) provided a coloured stone market report. She indicated that increasing demand for alternative gem varieties to ruby, emerald and sapphire are boosting the prices of those less-common stones. Overall, price increases are evident for top-quality gemstones of all varieties. **Dr Michael Krzemnicki** reviewed various gem materials that recently have come through SSEF's laboratory, including emeralds and sapphires from Ethiopia; sapphires from Bemainty, Madagascar with unstable padparadscha-like colouration; rubies from Mozambique that have undergone low-temperature heat treatment; fissure-filled rubies and Paraíba tourmalines; a glued jadeite bangle; grandidierite from Madagascar; 'mini-Ming' cultured pearls; saltwater natural pearls mixed with beadless freshwater cultured pearls that had been 'aged' to hide their presence; various types of fake pearls; and an opalised dinosaur vertebra.

Coloured stone localities were covered by several speakers. **Dr Klaus Schollenbruch** (Gübelin Gem Lab, Lucerne) described his May 2017 trip to Bemainty, Madagascar, where sapphire mining had slowed since the initial rush in late 2016. He estimated that 1,000–2,000 miners were active in each of two mining areas near Bemainty, and sapphire production was low. He then compared the gemmological properties of these sapphires with those from Kashmir, and found some significant differences in their inclusions and trace-element compositions. **Dr Lore Kiefert** (Gübelin Gem Lab, Lucerne) provided an update on emeralds from Ethiopia. The main emerald-producing area near the Kenticha tantalum deposit was closed by government authorities in December 2016 and reopened in 2017 after the formation of a local mining cooperative. The hillside was cleared of vegetation and soil using heavy machinery, but only small amounts of emerald were found. Another Ethiopian emerald deposit is located 150 km further south, approaching the Kenyan border.

Figure 2: Participants assemble for a poolside photo during the 2018 Swiss Gemmological Society conference. Photo by Michael Hügi.

Figure 3: Michael Hügi lectures on synthetic diamonds at the Swiss Gemmological Society conference. Photo by B. M. Laurs.

It is being worked by Gemfields, and so far most of the production has consisted of pale-coloured emerald and green beryl. **Alexander Klumb** (Swiss Gemmological Institute SSEF, Basel) summarised an October 2017 field trip by three SSEF gemmologists to Paraíba tourmaline mines in Brazil. They witnessed mining, sorting, cutting and trading activities in both Paraíba (São José da Batalha) and Rio Grande do Norte States (Mulungu mine near Parelhas), and they also learned about the geological context of the mining areas and collected research samples. At the time of their visit, Mulungu was the only mine producing significant quantities of Paraíba tourmaline, although mostly in smaller sizes.

Judy Tu (Swiss Gemmological Institute SSEF, Taipei, Taiwan) reviewed gem materials of Taiwan, which consist of nephrite, chrysocolla chalcedony, aragonite, rhodonite and precious coral. In the 1960s, Taiwan was an important nephrite producer (>1,200 tonnes/year), but by 1983 mining had mostly stopped. For nearly a century, precious coral has been fished from waters around Taiwan (eventually extending across the Pacific Ocean to Midway Island), with most production occurring from 1976 to the 1990s. Nowadays, Taiwanese government regulations limit harvesting to 200 kg per vessel per year, for a total of up to 60 tonnes. **Dr Karl Schmetzer** (Petershausen, Germany) recounted some little-known history of the Chivor emerald mine in Colombia. German gem merchant Fritz Klein re-opened Chivor in 1912, together with Colombian miner Francisco Restrepo, who rediscovered the mine in the late 19th century after it had lain forgotten in the jungle for about 200 years. Restrepo died in 1914, and Klein stopped his mining operations because of the outbreak of World War I. In the early 1920s, Klein was hired for two periods by an American company (Colombian Emerald Syndicate Ltd) that had bought the mining titles of Chivor in 1919. **Prof. Dr Henry Hänni** (GemExpert, Basel) and co-authors studied 'Sannan Skarn', a green ornamental stone from the Muslim Bagh area of Pakistan. SEM-EDS analysis revealed that the rock mainly consists of a groundmass of anorthite and diopside that contains crystals of green Cr-bearing hydrogrossular composed of 58 mol.% grossular, 33 mol.% uvarovite, 7 mol.% andradite and 1 mol.% pyrope.

Jörg Gellner (Gellner GmbH & Co. KG, Wiernsheim, Germany) reviewed the various types of cultured pearls, as well as their localities and production in 2017. He then explored quality criteria for cultured pearls that he defined according to the '5 Cs': size, shape, shade, surface/spot level and shine. For each category, he assigned different value factors according to specific characteristics that resulted in price premiums or discounts.

Dr Walter Balmer (Chulalongkorn University, Bangkok, Thailand) described a March–April 2018 SGS trip to Sri Lanka. SGS excursions to gem mining regions are organised every 2–3 years and are open to a maximum of 12 people who are SGS members or their close relatives/spouses. Rather than being buying trips, the excursions provide an opportunity to gain first-hand knowledge of the history, mining and culture of a gem-producing region, while also building friendships. **Martin Julier** (Bucherer Gem Lab, Lucerne) described his involvement with the BusinessKind aid project in Myanmar. He first visited Myanmar in 2007 as a gem merchant, and in 2008 he became interested in social work when he personally witnessed the devastation caused by Cyclone Nargis. BusinessKind has organised the manufacture of bed nets and citronella candles to help prevent malaria, and also provides employment training. Its most recent project, Thone Pan Hla, is Myanmar's first female garment factory workers' association.

Brendan M. Laurs FGA

Gem-A Notices

Gifts to the Association

Gem-A is most grateful to the following for their generous donations which will support continued research and teaching:

Eric Braunwart, Columbia Gem House Inc., Vancouver, Washington, USA, for a variety of imitation gem materials.

Dr Rui Galopim de Carvalho, for donating two books to Gem-A's library: *Precious Stones in Sacred Art in Portugal* by Rui Galopim de Carvalho and *O Santo Lenho da Sé de Évora* by Rui Galopim de Carvalho, Artur Goulart de Melo Borges and Gonçalo Vasconcelos e Sousa.

Farooq Hashmi, Intimate Gems, Glen Cove, New York, USA, for an assortment of rough garnet from the Democratic Republic of Congo.

William Hasselrot, for a monetary donation.

Ronda Hipwell, for a monetary donation.

Syed Iftikhar Hussain, Syed Trading Co., Islamabad, Pakistan, for three afghanite crystals from Afghanistan.

Dr Jaroslav Hyršl, Prague, Czech Republic, for a 'zebra garnet' cabochon from Peru.

Charles Mark, Elizabeth, Colorado, USA, for a piece of rough Larimar from the Caribbean.

John Osborne, for a monetary donation.

Lorne Stather, for donating four books to Gem-A's library: *Birthstones of the Month* by Joan Frank, *Carving Shells and Cameos* by Carson I. A. Ritchie, *Consumer Guide to Coloured Gemstones* by David Federman and *Diamants* by Hubert Bari and Violaine Sautter.

Estelle Weiner, for diamond manufacture models.

Tak Yi Yung, for a monetary donation.

NAJ and Gem-A Field Trip to Sri Lanka

1–16 October 2018
Collaborative National Association of Jewellers and Gem-A field trip to Sri Lanka accompanied by gem experts Colin and Hillary Winters. For more information, contact lindsey.straughton@naj.co.uk.

Gem-A Open Evening

18 July 2018
Tour Gem-A's headquarters and meet our tutors. http://gem-a.com/event/rsevents/event/25-gem-a-open-evening.

Gemstone Photographer of the Year Competition 2018

Gem-A's annual photography competition returns this summer 2018 for all members and students of Gem-A. There are three categories for entry: '**Internal**' (including photomicrography, gemscapes and unusual inclusions), '**External**' (unusually cut or faceted gemstones, carvings and *objets d'art*) and '**Humanity in Gems**' (life around gemstones, including mining, dealing, and gemmologists at work or studying).

Please submit all entries to editor@gem-a.com, specifying your membership/student number and category of entry. For files larger than 10 MB, please submit via Dropbox or WeTransfer.

A member award and a student award, and honourable mentions for each category, will be announced at the 2018 Gem-A Conference. Closing date for entries is Friday 31 August 2018.

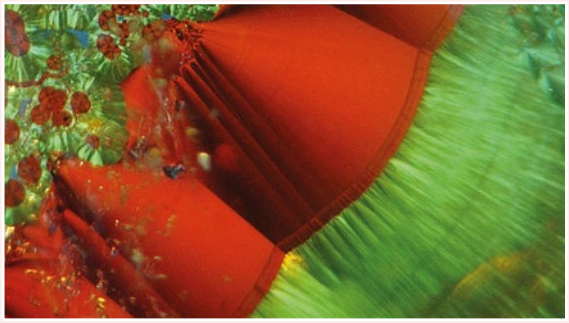

Iron oxide in quartz from Brazil. Image by Oliver Segura.

Learning Opportunities

CONFERENCES AND SEMINARS

Sainte-Marie-aux-Mines 55th Mineral & Gem Show
21–24 June 2018
Sainte-Marie-aux-Mines, France
www.sainte-marie-mineral.com/english/modules/cultural-activities
Note: Includes a seminar programme

Northwest Jewelry Conference
10–12 August 2018
Seattle, Washington, USA
www.northwestjewelryconference.com

22nd Meeting of the International Mineralogical Association
13–17 August 2018
Melbourne, Victoria, Australia
www.ima2018.com/program
Sessions of interest:

- Mantle Xenoliths, Kimberlites and Related Magmas: The Diamond Trilogy
- Pegmatite Mineralogy, Geochemistry, Classification and Origins
- Recent Advances in our Understanding of Gem Minerals
- Sciences Behind Gemstone Treatments

Dallas Mineral Collecting Symposium
24–26 August 2018
Dallas, Texas, USA
www.dallassymposium.org

Scandinavian Gem Symposium 2018
25–26 August 2018
Kisa, Sweden
www.sgs.gemology.se/#home

Japan Jewellery Fair
28–30 August 2018
Tokyo, Japan
www.ubmjapan-group.com/jjf/en/seminar
Note: Includes seminar programme

IJL London
2–4 September 2018
London
www.jewellerylondon.com/Whats-On/Seminars
Note: Includes a seminar programme

29th International Conference on Diamond and Carbon Materials
2–6 September 2018
Dubrovnik, Croatia
www.elsevier.com/events/conferences/international-conference-on-diamond-and-carbon-materials

Hong Kong Jewellery & Gem Fair
12–18 September 2018
Hong Kong
http://exhibitions.jewellerynet.com/9jg/en-us/specialevents
Note: Includes a seminar programme

Fabergé Museum International Academic Conference: Jewellery Art of the 19th & Early 20th Centuries
20–22 September 2018
St Petersburg, Russia
https://fabergemuseum.ru/en/news/article/118

Mallorca Gemquest
22–23 September 2018
Sóller, Mallorca, Spain
www.mallorcagemquest.com

2018 GIA Symposium: New Challenges. Creating Opportunities
7–9 October 2018
Carlsbad, California, USA
http://discover.gia.edu/symposium

ASMOSIA XII—Association for the Study of Marble & Other Stones in Antiquity International Conference
8–14 October 2018
Izmir, Turkey
www.asmosia2018.com

II World Emerald Symposium
12–14 October 2018
Bogotá, Colombia
www.regonline.com/builder/site/Default.aspx?EventID=2137425

2018 Friends of Mineralogy, Pacific Northwest Chapter Symposium—Minerals of California
19–21 October 2018
Kelso, Washington, USA
http://pnwfm.org/2017/12/19/2018-symposium-minerals-of-california

Canadian Gemmological Association Gem Conference 2018
19–21 October 2018
Vancouver, British Columbia, Canada
http://canadiangemmological.com/events-conferences/upcoming-conferences

The Munich Show: Mineralientage München
26–28 October 2018
Munich, Germany
https://munichshow.com/en/the-munich-show/public-days/highlights
Note: Includes a seminar programme

Singapore Jewellery & Gem Fair
26–29 October 2018
Singapore
www.singaporejewellerygemfair.com/JewelTalk
Note: Includes seminar programme

Gem-A Conference 2018
3–4 November 2018
London
https://gem-a.com/event/conference

The Geological Society of America 130th Annual Meeting
4–7 November 2018
Indianapolis, Indiana, USA
http://community.geosociety.org/gsa2018/home
Session of interest: Gemological Research in the 21st Century—Characterization, Exploration, and Geological Significance of Diamonds and Other Gem Minerals

Swiss Geoscience Meeting
30 November–1 December 2018
Bern, Switzerland
https://geoscience-meeting.ch/sgm2018
Note: Includes a gemmology session

Gem-A Midlands Branch Conference
23 February 2019
Birmingham
Email louiseludlam@hotmail.com

Inhorgenta Munich
22–25 February 2019
Munich, Germany
www.inhorgenta.com
Note: Includes a seminar programme

American Gem Society Conclave
8–10 April 2019
Seattle, Washington, USA
www.americangemsociety.org/page/conclave2019

European Gemmological Symposium 2019
24–26 May 2019
Idar-Oberstein, Germany
Email info@dgemg.com

EXHIBITIONS

Australia and New Zealand

The Language of Things: Meaning and Value in Contemporary Jewellery
Until 24 June 2018
The Dowse Art Museum,
Lower Hutt, New Zealand
http://dowse.org.nz/exhibitions/detail/the-language-of-things

Cartier: The Exhibition
Until 22 July 2018
National Gallery of Australia, Canberra, Australia
https://nga.gov.au/cartier

Lustre: Pearling & Australia
Until 22 July 2018
National Museum of Australia, Canberra, Australia
www.nma.gov.au/exhibitions/lustre-pearling-and-australia

Europe

De Calder à Koons, Bijoux d'Artistes. La Collection Idéale de Diane Venet
Until 8 July 2018
Musée des Arts Décoratifs, Paris, France
http://tinyurl.com/ydb28ru8

Grant MacDonald: International Silversmith
Until 25 July 2018
Goldsmiths' Hall, London
https://grantmacdonald.com/exhibition

Designers and Jewellery 1850–1940: Jewellery and Metalwork from the Fitzwilliam Museum
31 July–11 November 2018
The Fitzwilliam Museum, Cambridge
http://tinyurl.com/ybvy7oj6

Eva's Beauty Case & Adam's Necessaire. Schmuck und Styling im Spiegel der Zeiten
Until 12 August 2018
Braunschweigisches Landesmuseum, Braunschweig, Germany
http://3landesmuseen.de/Eva-s-Beauty-Case-Adams-Necessaire.1649.0.html

Jewellery by Giò Pomodoro – The Sign and the Ornament
Until 2 September 2018
Museo del Gioiello, Vicenza, Italy
http://tinyurl.com/y7bdzt4h

The Splendour of Power
Until 30 September 2018
Museet på Koldinghus, Kolding, Denmark
www.koldinghus.dk/uk/exhibitions-2017/the-splendour-of-power-2018.aspx

Brussels Horta & Wolfers. Reopening of the Wolfers Frères Jewellery Store, 1912
Until 30 December 2018
Cinquantenaire Museum, Brussels, Belgium
www.kmkg-mrah.be/expositions/horta-wolfers

East Meets West – Jewelled Splendours of the Art Deco Era. The Prince and Princess Sadruddin Aga Khan Collection
Until 6 January 2019
Schmuckmuseum Pforzheim, Germany
www.schmuckmuseum.de/en/current.html

BVLGARI. Tribute to Femininity. Magnificent Roman Jewels
7 September 2018–13 January 2019
The Moscow Kremlin Museums, Russia
www.kreml.ru/en-Us/exhibitions/moscow-kremlin-exhibitions/bvlgari-tribute-to-femininity

From Zeus to Earth and from Chile to Neapolis
1 October–31 December 2018
Ilias Lalounis Jewelry Museum, Athens, Greece
http://lalaounis-jewelrymuseum.gr/en/exTdetails.asp?exid=39

North America

American Jewelry from New Mexico
Until 14 October 2018
Albuquerque Museum, New Mexico, USA
www.cabq.gov/culturalservices/albuquerque-museum/exhibitions/american-jewelry

Fabergé and the Russian Crafts Tradition: An Empire's Legacy
Until 24 June 2018
The Walters Art Museum, Baltimore, Maryland, USA
https://thewalters.org/event/faberge-and-the-russian-crafts-tradition-an-empires-legacy

A Modern Gem and Jewelry Collection
Until July 2018
Flandrau Science Center & Planetarium, University of Arizona, Tucson, Arizona, USA
https://flandrau.org/exhibits/somewhere-rainbow

Past is Present: Revival Jewelry
Until 19 August 2018
Museum of Fine Arts, Boston, Massachusetts, USA
https://mfa.org/news/past-is-present-revival-jewelry

Peacock in the Desert: The Royal Arts of Jodhpur, India
Until 19 August 2018
Museum of Fine Arts, Houston, Texas, USA
https://mfah.org/exhibitions/peacock-in-desert-royal-arts-jodhpur-india

Centuries of Opulence: Jewels of India
Until 10 October 2018
GIA Museum, Carlsbad, California, USA
www.gia.edu/gia-museum-exhibit-centuries-opulence-jewels-india

Crowns of the Vajra Masters: Ritual Art of Nepal
Until 16 December 2018
The Met Fifth Avenue, New York, New York, USA
https://metmuseum.org/exhibitions/listings/2017/crowns-of-vajra-masters

Fabergé Rediscovered
Until 13 January 2019
Hillwood Estate, Museum & Gardens, Washington DC, USA
http://hillwoodmuseum.org/faberge-rediscovered

Beadwork Adorns the World
Until 3 February 2019
Museum of International Folk Art, Santa Fe, New Mexico
http://internationalfolkart.org/exhibition/3348/beadwork-adorns-the-world

East Meets West: Jewels of the Maharajas from the Al Thani Collection
3 November 2018–24 February 2019
Legion of Honor Museum, San Francisco, California, USA
http://legionofhonor.famsf.org/exhibitions/east-meets-west

OTHER EDUCATIONAL OPPORTUNITIES

Gem-A Workshops and Courses
Gem-A, London
https://gem-a.com/education/courses/workshops

American Society of Appraisers—Appraising Gems & Jewelry for Advanced Assignments: Development and Report Writing
23 August 2018
McLean, Virginia, USA
www.appraisers.org/Education/View-Course?CourseID=72

Pearls as One – Pearl Specialist Course
Online pearl course from The Cultured Pearl Association of America (CPAA), supported in part by Swiss Gemmological Institute SSEF. Gem-A members have been granted complimentary access (normally US$599) to the course by SSEF and CPAA. Sign up at www.pearlsasone.org using discount code 'Gem-A' at the payment menu.

Lectures with Gem-A's Midlands Branch
Fellows Auctioneers, Augusta House, Birmingham
Email louiseludlam@hotmail.com

- Craig O'Donnell—Styles & Stones
  28 September 2018
- Paul Phillips—Photography & Micro Photography
  26 October 2018
- Vanessa Paterson—Amber
  30 November 2018

Lectures with The Society of Jewellery Historians
Society of Antiquaries of London, Burlington House, London
www.societyofjewelleryhistorians.ac.uk/current_lectures

- Tara Kelly—Purchasing the Past: Consumers of Irish Facsimile Jewellery, 1840–1940
  26 June 2018
- Christopher Thompson Royds—My Work as a Jeweller
  25 September 2018
- Anna Tabakhova—Clasps: 4000 Years of Fasteners in Jewellery
  23 October 2018
- Helen Ritchie—Designers and Jewellery: Jewellery and Metalwork from the Fitzwilliam Museum 1850–1940
  27 November 2018
- Martin Henig—Personal Cameos of Roman Date in the Content Family Collection
  22 January 2019
- Jack Ogden—TBA
  26 February 2019
- Peter Semrád—The Story Behind 'Hungarian' Opals
  26 March 2019
- Beth Wees—TBA
  25 June 2019

New Media

Magnificent Green – On the Trail of the Legendary Colombian Emerald

By Adolf Peretti and Thierry Falise, 2017. GRS Gemresearch Swisslab AG, Lucerne, Switzerland, http://gemresearch.ch/product/magnificent-green-on-the-trail-of-the-legendary-colombian-emerald, 337 pages, illus., ISBN 978-3906905099. US$150.00 hardcover

Books on single gem varieties are few and far between, so the addition of a book specifically on Colombian emeralds is quite a treat. Co-author Dr Adolph Peretti, who attended more than 40 gem and jewellery auctions between 1994 and 1998, has created a unique database of some of the rarest and highest-quality emeralds ever offered on the international market. Many of the Colombian emerald jewels he studied are pictured in this book, and they represent masterpieces of jewellery art.

On first impression *Magnificent Green* looks like a 'coffee-table' book, with lots of beautiful pictures but not a lot of serious content to offer. So, I was pleasantly surprised by the quality of information that coincided with wonderful photos of the mines and the emeralds—rough, cut and in jewels—which are depicted throughout the book. Detailed maps and extracts from geological reports help to further enlighten the reader on the origins and formation of Colombian emeralds. Rare photographs capture the open-cut Muzo mine workings from 1872, and other historical photos illustrate different mines in the early years of the 20th century.

The authors lead the reader through historical and modern accounts of the people for whom emeralds are their daily existence. The indigenous Colombian inhabitants were the first to appreciate the green stones. By the time the Spanish arrived in the 16th century, the locals had been trading emeralds for centuries, calling them 'Stones of Earth' and believing that they were associated with fertility. The Spanish conquistadors brought these New World emeralds back to Europe, revealing to gem merchants of the time that the term *Oriental* emerald was a false attribution, and proving that most of the fine-quality emeralds in collections originated from South America, not Asia. Mining in 16th-century Colombia was difficult, carried out by enslaved indigenous people as well as African slaves who rarely survived more than a few years before succumbing to brutal overseers, disease or starvation. Besides reviewing this important back history, the book also brings the reader up to date in regard to current activities. Muzo is presently the most productive mine in the region and has been run by an American company since 2009. Chivor, after being lost for 200 years, is now again producing vivid green emeralds as well. Cunas, Coscuez and Gachalá too are all still being exploited.

Throughout the book the authors weave together tales of famous jewels, antique and modern, and brief portraits of the renowned jewellers who created them. Some of the antique pieces include the jewelled mirror of King Louis XIV, the 'Sun King' of France; La Lechuga, an 18 carat gold liturgical monstrance set with 1,485 Muzo emeralds along with numerous natural pearls, diamonds, amethysts, rubies and one sapphire; and the 'Crown of the Andes', a 17th-century gold and emerald crown made to adorn a statue of the Virgin Mary in Popayan, Colombia and acquired by the Metropolitan Museum of Art in New York City in 2015. These are just a few of the historical jewels that are described. Also included is a helpful timeline of events in Colombia compared with developments in the rest of the world from roughly 2000 BC to the present day, which helps put Colombian emeralds into a global context.

Although there is a discussion of emerald quality and how the gemmological properties of Colombian emeralds help make them so special, the human stories interested me the most. Conflicts were common in the region during most of the 20th century, but were somewhat resolved in 1990 with a negotiated peace agreement between prominent emerald families. But with the 2013 death of

Victor Carranza, a key figure in the peace negotiations, violence once again became a concern. (In one place the book indicates that Carranza died of cancer, but elsewhere it states that Carranza was murdered. There are other inconsistencies in the book, but they do not detract from the main narrative.) In 2009 Carranza had agreed to work with the American company Minería Texas Colombia (MTC) to modernise mining and management in the emerald region, effectively cutting out the independent prospectors (*guaqueros*) who traditionally searched through the tailings produced by the various mining activities. That, combined with general political and social unrest in Colombia, made for a dangerous situation. A new peace agreement was suggested in 2015 through the gathering of 400 people, including the Catholic Church, civil society and the armed forces, but sadly it never came to fruition. Currently, MTC is working to set an example and encourage other emerald mines to run their operations to American standards. Health and safety measures have been greatly upgraded, and salaries, benefits and living conditions are being improved. The inclusion of women in the Colombian emerald industry is common in most areas of business, and with improved social and safety measures this should become even more prevalent in the future.

An Appendix at the end of the book includes a selection of laboratory reports on Colombian emeralds sold through international auction houses; all the reports were created by GRS Gemresearch Swisslab AG, run by Dr Peretti. In addition, information has been compiled including the auction house, date of sale, auction location and brief description of the item, but no selling prices are included, which would have been helpful.

This book is unusual (and is to be commended) in having been created, in part, to fund a charitable organisation known as Clay Hands, which plans to use the proceeds of the book's sale to sponsor the building of a school in Muzo that will be called 'GRS Muzo School for Young Talents'. Furthermore, in an effort to marry different communication formats, there are several QR matrix codes throughout the book, and scanning them with a smartphone links the reader to informative videos. It is nice to see modern technology combined with the age-old comfort of a handheld book. Overall, *Magnificent Green* weaves together an excellent compilation of the many different aspects that comprise Colombian emeralds and the complex and quickly changing industry that surrounds them. The charitable aspect is an added bonus.

Jo Ellen Cole GG
Cole Appraisal Services
Los Angeles, California, USA

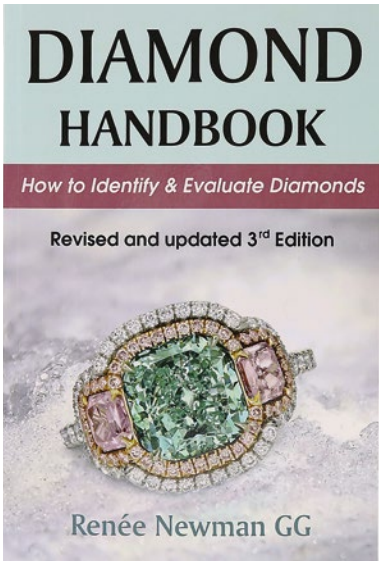

Diamond Handbook, 3rd edn.

By Renée Newman, 2018. International Jewelry Publications, Los Angeles, California, USA, www.reneenewman.com/handbook.htm, 168 pages, illus., ISBN 978-0929975535. US$19.95 softcover.

This third edition of the *Diamond Handbook* by Renée Newman provides a welcome update to her series. Information has been added in the chapters titled Fancy Color Diamonds, Diamond Fluorescence, Diamond Treatments, Recutting Diamonds and Antique Cuts & Jewelry. Overall, the content follows the first (2005) and second (2010) editions, but there are some significant deletions and additions.

Two chapters from previous editions have been deleted: Judging Light Performance—a topic with little consensus in the trade—and Diamond Grading Reports. This reviewer is disappointed to see this latter chapter being omitted, since it will be missed by the novice hoping to learn about diamonds and avoid being cheated by unscrupulous sellers using unreliable grading reports. The Synthetic Diamonds chapter has been reworked and expanded, adding more explanation of advanced testing and the newest instrumentation currently available on the market. New to this third edition is a chapter titled Diamond Imitations, which includes the separation of black diamonds from other black stones. In addition, more high-quality images have been added to the chapter called Judging Fancy Color Diamonds, making this complicated subject a little easier to understand.

Charles I. Carmona GG
Guild Laboratories Inc.
Los Angeles, California, USA

Other Book Titles

DIAMOND

The Diamond: All About Diamonds
By Michael Kummer, 2018. Self-published, 77 pages, ISBN 978-1982959692. US$29.99 softcover or US$8.88 Kindle edition.

Diamonds: An Early History of the King of Gems
By Jack Ogden, 2018. Yale University Press, New Haven, Connecticut, USA, 408 pages, ISBN 978-0300215663. US$40.00 hardcover.

COLORED STONES

Bradwell's Images of Blue John Stone
By Vicky Turner and Gary Ridley, 2018. Bradwell Books, Sheffield, 32 pages, ISBN 978-1912060641. £4.99 softcover.

Caractérisation de la Tourmaline et des Minéraux Associés de Sahatany [Characterisation of Tourmaline and Associated Minerals of Sahatany (Madagascar)]
By Haingo Raherisoa, 2017. Self-published at Éditions Universitaires Européennes, 168 pages, ISBN 978-6202268776. €64.90 softcover (in French).

Spacerocks: A Collectors' Guide to Meteorites, Tektites and Impactites
By David Bryant, 2018. Self-published at Heathland Books, 168 pages, ISBN 978-1999741723. US$35.00 softcover.

GEM LOCALITIES

Diamond Exploration and Prospectivity of Western Australia
By Mark T. Hutchison, 2018. Geological Survey of Western Australia, Report 179, Perth, Australia, 70 pages, ISBN 978-1741687736. Free PDF download.

Gemstones of Western Australia, 2nd edn.
By J. Michael Fetherston, Susan M. Stocklmayer and Vernon C. Stocklmayer, 2017. Geological Survey of Western Australia, Mineral Resources Bulletin 25, Perth, Australia, 356 pages, ISBN 978-1741686890. A$60.00 softcover or free PDF download.

JEWELLERY HISTORY

The Archaeology of Portable Art—Southeast Asian, Pacific, and Australian Perspectives
Ed. by Michelle Langley, Mirani Litster, Duncan Wright and Sally K. May, 2018. Routledge, New York, New York, USA, 342 pages, ISBN 978-1138237766. US$140.00 hardcover or US$54.95 eBook.

Collecting and Collectors: From Antiquity to Modernity
Ed. by Alexandra Carpino, Tiziana D'Angelo, Maya Muratov and David Saunders, 2018. Archaeological Institute of America, Selected Papers on Ancient Art and Architecture, Vol. 4, Boston, Massachusetts, USA, 267 pages, ISBN 978-1931909365. US$24.95 softcover.

JEWELLERY AND *OBJETS D'ART*

Fabergé Rediscovered
By Wilfried Zeisler, 2018. Hillwood Estate, Museum & Gardens, Washington DC, USA, 224 pages, ISBN 978-1911282167. US$44.95 hardcover.

Figures and Faces: The Art of Jewelry
By Patrick Mauriès and Évelyne Possémé, 2018. Thames & Hudson, New York, New York, USA, 128 pages, ISBN 978-0500021811. US$24.95 hardcover.

Masterpieces in Miniature: Engraved Gems from Prehistory to the Present
By Claudia Wagner and John Boardman, 2018. Philip Wilson Publishers Ltd, London, 272 pages, ISBN 978-1781300626. £40.00 hardcover.

New Brooches: 400 + Contemporary Jewelry Designs
Ed. by Nicolás Estrada, 2018. Promopress, Barcelona, Spain, 240 pages, ISBN 978-8416851225. €25.98 hardcover.

Precious Indian Weapons and Other Princely Accoutrements [The al-Sabah Collection]
By Salam Kaoukji, 2017. Thames & Hudson, London, 504 pages, ISBN 978-0500970805. £45.00 hardcover.

Literature of Interest

COLOURED STONES

Chatoyancy in sillimanite. H. Killingback, *Gems&Jewellery*, **27**(1), 2018, 20–22.

Distinguishing "synthetic" and natural moldavite. R. Hanus and J. Hyršl, *Journal of Gems & Gemmology*, **20**(1), 2018, 14–25.

Emeralds from Ethiopia. R. Schluessel and N.H. Schuessel [*sic*], *GemGuide*, **37**(2), 2018, 4–8.

Feasibility study on quality evaluation of jadeite-jade color green based on GemDialogue color chip. Y. Guo, X. Zong and M. Qi, *Multimedia Tools and Applications*, 2018, 16 pp., http://dx.doi.org/10.1007/s11042-018-5753-7.

On the formation of gemstones and geology of gem deposit. G. Shi, Y. Liu, Y. Yuan, X. Zhao, Y. Liu, S. Song and R. Zhang, *Earth Science Frontiers*, **24**(6), 2017, 142–151 (in Chinese with English abstract).

Gold Sheen sapphires – From gold mine to market. C. Unninayar, *InColor*, No. 38, 2018, 92–95.*

Insight on gem opal formation in volcanic ash deposits from a supereruption: A case study through oxygen and hydrogen isotopic composition of opals from Lake Tecopa, California, U.S.A. E. Martin and E. Gaillou, *American Mineralogist*, **103**(5), 2018, 803–811, http://dx.doi.org/10.2138/am-2018-6131.

Iridescence in metamorphic "rainbow" hematite. X. Lin, P.J. Heaney and J.E. Post, *Gems & Gemology*, **54**(1), 2018, 28–39, http://dx.doi.org/10.5741/GEMS.54.1.28.*

Major and trace element geochemistry of emerald from several deposits: Implications for genetic models and classification schemes. C. Aurisicchio, A.M. Conte, L. Medeghini, L. Ottolini and C. De Vito, *Ore Geology Reviews*, **94**, 2018, 351–366, http://dx.doi.org/10.1016/j.oregeorev.2018.02.001.

Mineral chemistry composition and structural characteristics of jadeite from Burma, Kazakhstan and Russia. Y. Zou, Y. Liang, Y. Liu, D. Wang and L. Yang, *Bulletin of the Chinese Ceramic Society*, **36**(S1), 2017, 144–152 (in Chinese with English abstract).

Provenance classification of nephrite jades using multivariate LIBS: A comparative study. J. Yu, Z. Hou, S. Sheta, J. Dong, W. Han, T. Lu and Z. Wang, *Analytical Methods*, **10**(3), 2018, 281–289, http://dx.doi.org/10.1039/c7ay02643a.

The role of evaporites in the formation of gems during metamorphism of carbonate platforms: A review. G. Giuliani, J. Dubessy, D. Ohnenstetter, D. Banks, Y. Branquet, J. Feneyrol, A.E. Fallick and J.-E. Martelat, *Mineralium Deposita*, **53**(1), 2017, 1–20, http://dx.doi.org/10.1007/s00126-017-0738-4.

Understanding Chinese jade in a world context. G.L. Barnes, *Journal of the British Academy*, **6**, 2018, 1–63, http://dx.doi.org/10.5871/jba/006.001.

X-ray diffraction study of emerald from Mingora and Charbagh deposits, Swat Valley, northwest Pakistan. M.A. Badar, S. Hussain, S. Niaz and S. Rehman, *Journal of Himalayan Earth Sciences*, **50**(1A), 2017, 13–24.*

DIAMONDS

Chameleon diamonds: Thermal processes governing luminescence and a model for the color change. K.S. Byrne, J.E. Butler, W. Wang and J.E. Post, *Diamond and Related Materials*, **81**, 2018, 45–53, http://dx.doi.org/10.1016/j.diamond.2017.10.014.

Crystal morphological evolution of growth and dissolution of curve-faced cubic diamonds from placers of the Anabar diamondiferous region. A.D. Pavlushin, D.A. Zedgenizov and K.L. Pirogovskaya, *Geochemistry International*, **55**(12), 2017, 1193–1203, http://dx.doi.org/10.1134/s0016702917090051.

Diamant – Eigenschaften, Bedeutung, Nomenklatur [Diamond – Properties, importance, nomenclature]. T. Lind, *Gemmologie: Zeitschrift der Deutschen Gemmologischen Gesellschaft*, **66**(3/4), 2017, 1–8 (in German).

Diamaten – wie alt und woher [Diamonds – How old and where from]? G. Brey and H. Höfer, *Gemmologie: Zeitschrift der Deutschen Gemmologischen Gesellschaft*, **66**(3/4), 2017, 9–26 (in German with English abstract).

Evidence for large scale fractionation of carbon isotopes and of nitrogen impurity during crystallization of gem quality cubic diamonds from placers of north Yakutia. V.N. Reutsky, A.A. Shiryaev, S.V. Titkov, M. Wiedenbeck and N.N. Zudina, *Geochemistry International*, **55**(11), 2017, 988–999, http://dx.doi.org/10.1134/s001670291711009x.

Die Farbe und Farbursache von unbehandelten und behandelten natürlichen und synthetischen Diamanten [The color and color cause of untreated and treated natural and synthetic diamonds]. T. Hainschwang, *Gemmologie: Zeitschrift der Deutschen Gemmologischen Gesellschaft*, **66**(3/4), 2017, 27–58 (in German with English abstract).

The internal structure of yellow cuboid diamonds from alluvial placers of the northeastern Siberian Platform. A. Ragozin, D. Zedgenizov, K. Kuper, V. Kalinina and A. Zemnukhov, *Crystals*, **7**(8), 2017, article 238, 12 pp., http://dx.doi.org/10.3390/cryst7080238.*

Let there be light [diamond optics and cut performance]. M. Cowing, *Gems&Jewellery*, **27**(1), 2018, 24–27.

Mineral inclusions in diamonds may be synchronous but not syngenetic. F. Nestola, H. Jung and L.A. Taylor, *Nature Communications*, **8**, 2017, article 14168, 6 pp., http://dx.doi.org/10.1038/ncomms14168.*

Nanosculptures on round surfaces of natural diamonds. A.A. Chepurov, S.S. Kosolobov, D.V. Shcheglov, V.M. Sonin, A.I. Chepurov and A.V. Latyshev, *Geology of Ore Deposits*, **59**(3), 2017, 256–264, http://dx.doi.org/10.1134/s1075701517030023.

Natural-color green diamonds: A beautiful conundrum. C.M. Breeding, S. Eaton-Magaña and J.E. Shigley, *Gems & Gemology*, **54**(1), 2018, 2–27, http://dx.doi.org/10.5741/GEMS.54.1.2.*

Non-destructive in situ study of plastic deformations in diamonds: X-ray diffraction topography and μFTIR mapping of two super deep diamond crystals from São Luiz (Juina, Brazil). G. Agrosì, G. Tempesta, G. Della Ventura, M. Cestelli Guidi, M. Hutchison, P. Nimis and F. Nestola, *Crystals*, **7**(8), 2017, article 233, 11 pp., http://dx.doi.org/10.3390/cryst7080233.*

Chapter 17: Popa–Loimye Arc, correlations with Tibet, and alluvial diamonds in Myanmar. A. Mitchell, *Geological Belts, Plate Boundaries, and Mineral Deposits in Myanmar*, Elsevier, Amsterdam, The Netherlands, 2018, 473–482, http://dx.doi.org/10.1016/b978-0-12-803382-1.00017-1.

Prospecting history leading to the discovery of Botswana's diamond mines: From artefacts to Lesedi La Rona. M.C.J. de Wit, *Mineralogy and Petrology*, 2018, 16 pp., http://dx.doi.org/10.1007/s00710-018-0556-0.

The relationship between platelet size and the B′ infrared peak of natural diamonds revisited. L. Speich, S.C. Kohn, R. Wirth, G.P. Bulanova and C.B. Smith, *Lithos*, **278–281**, 2017, 419–426, http://dx.doi.org/10.1016/j.lithos.2017.02.010.

SEM and EPMA analyses of metallic inclusions in diamonds – Probing the earth's deep mantle. E.S. Bullock, E.M. Smith and S.B. Shirey, *Microscopy and Microanalysis*, **23**(S1), 2017, 2286–2287, http://dx.doi.org/10.1017/s1431927617012090.*

Is space our next diamond resource? A. Galmiche, *Gems&Jewellery*, **27**(1), 2018, 32–35.

Tracking sources of selected diamonds from southern Africa based on carbon isotopic and chemical impurities. A.T. Kidane, M. Koch-Müller, M. Wiedenbeck and M.J. de Wit, *South African Journal of Geology*, **120**(3), 2017, 371–384.

The uniquely high-temperature character of Cullinan diamonds: A signature of the Bushveld mantle plume? N.M. Korolev, M. Kopylova, Y. Bussweiler, D.G. Pearson, J. Gurney and J. Davidson, *Lithos*, **304–307**, 2018, 362–373, http://dx.doi.org/10.1016/j.lithos.2018.02.011.

Xenoliths of eclogites with diamonds from the Yubileinaya kimberlite pipe, Yakutia. Z.V. Spetsius, I.N. Bogush and A.S. Ivanov, *Doklady Earth Sciences*, **478**(1), 2018, 88–91, http://dx.doi.org/10.1134/s1028334x1801018x.

GEM LOCALITIES

Bazhenovskoe deposit (Central Urals, Russia)—Mineralogy of Rodingites [facetable grossular and vesuvianite]. Y.V. Erokhin, *Mineralogical Almanac*, **22**(3), 2017, 3–25 and 30–129.

Expedition to Ethiopia's sapphire fields. A. Lucas, W. Vertriest, D. Girma, T. Abay and B. Bekele, *InColor*, No. 38, 2018, 26–34.*

Exploring gemstones in northern part of Myanmar. H.L. Aung and T.T. Zin, in J.W. Lin., J.S. Pan, S.C. Chu and C.M. Chen., Eds., *Genetic and Evolutionary Computing*, ICGEC 2017, Advances in Intelligent Systems and Computing, **579**, Springer, Singapore, 2018, 182–188, http://dx.doi.org/10.1007/978-981-10-6487-6_22.

Fluid inclusion studies on emeralds from Malipo area, Yunnan Province, China. W. Huang, T. Shui and P. Ni, *Acta Mineralogica Sinica*, **37**(1/2), 2017, 75–83 (in Chinese with English abstract).

FTIR spectra and LA-ICP-MS research of growth zones in sapphire bands from Changle, Shandong Province. X. Li, Z. Yang, S. Huang, Y. Chen, X. Zeng and W. Zhou, *Spectroscopy and Spectral Analysis*, **38**(2), 2018, 407–412 (in Chinese with English abstract).

Gemmological and geochemical characteristic of zircon megacryst related to Cenozoic alkaline basalt from eastern China. H. Ai, X. Zhao, Q. Chen, Q. Long and J. Qin, *Journal of Gems & Gemmology*, **20**(1), 2018, 1–13 (in Chinese with English abstract).

Gemological characteristics and coloration mechanism research of Sri Lanka Elahera mining pyropes. L. Tao, X. Hu, Y. Tong and Y. Zhao, *Bulletin of the Chinese Ceramic Society*, **36**(S1), 2017, 179–183 (in Chinese with English abstract).

Chapter 14: Jade mines–Loimaw uplift. A. Mitchell, *Geological Belts, Plate Boundaries, and Mineral Deposits in Myanmar*, Elsevier, Amsterdam, The Netherlands, 2018, 439–460, http://dx.doi.org/10.1016/b978-0-12-803382-1.00014-6.

Microstructural, Raman, EPMA and X-ray tomographic study of the Odisha's beryl (emerald) sample. P.R. Jena and P.K. Mishra, *Journal of Geology & Geophysics*, **6**(3), 2017, article 288, 7 pp., http://dx.doi.org/10.4172/2381-8719.1000288.*

Mineral identification of black-jade gemstone from Aceh Indonesia. Ismail, A. Nizar and Mursal, *Journal of Physics: Conference Series*, **1011**, 2018, article 012001, 6 pp., http://dx.doi.org/10.1088/1742-6596/1011/1/012001.*

Mineralogical characteristics and colouration mechanism of blue opals from Peru. Y. Xing, L. Qi and H. Wang, *Rock and Mineral Analysis*, **36**(6), 2017, 608–613 (in Chinese with English abstract).

Chapter 7: Mogok metamorphic belt. A. Mitchell, *Geological Belts, Plate Boundaries, and Mineral Deposits in Myanmar*, Elsevier, Amsterdam, The Netherlands, 2018, 201–251, http://dx.doi.org/10.1016/b978-0-12-803382-1.00007-9.

Chapter 18: Myanmar orogens and flysch, potential for mineral discoveries, and Shan scarps and jade mines cross sections. A. Mitchell, *Geological Belts, Plate Boundaries, and Mineral Deposits in Myanmar*, Elsevier, Amsterdam, The Netherlands, 2018, 483–495, http://dx.doi.org/10.1016/b978-0-12-803382-1.00018-3.

Petrochemistry, mineral chemistry, and pressure–temperature model of corundum-bearing amphibolite from Montepuez, Mozambique. A. Fanka and C. Sutthirat, *Arabian Journal for Science and Engineering*, **43**, 2018, 1–17, http://dx.doi.org/10.1007/s13369-018-3172-8.

Raman and FTIR spectra of nephrites from the Złoty Stok and Jordanów Śląski (the Sudetes and Fore-Sudetic Block, SW Poland). I. Korybska-Sadło, G. Gil, P. Gunia, M. Horszowski and M. Sitarz, *Journal of Molecular Structure*, **1166**, 2018, 40–47, http://dx.doi.org/10.1016/j.molstruc.2018.04.020.

Some characteristics of Nanyaseik area corundum and other assorted gemstones in Myanmar. H.L. Aung and T.T. Zin, in J.W. Lin., J.S. Pan, S.C. Chu and C.M. Chen, Eds., *Genetic and Evolutionary Computing*, ICGEC 2017, Advances in Intelligent Systems and Computing, **579**, Springer, Singapore, 2018, 173–181, http://dx.doi.org/10.1007/978-981-10-6487-6_21.

Spectroscopic characteristics of natural variscite from Yunnan. Z. Wei and J. Di, *Acta Petrologica et Mineralogica*, **37**(1), 2018, 169–174 (in Chinese with English abstract).

The spessartine–almandine garnet from Val Codera pegmatite, Central Alps, Italy: A new insight on the crystallochemistry and a 3D image analysis of its inclusions. V. Diella, R. Bocchio, N. Marinoni, A. Langone, I. Adamo and N. Rotiroti, *Rendiconti Lincei. Scienze Fisiche e Naturali*, 2018, 9 pages, http://dx.doi.org/10.1007/s12210-018-0697-4.

Study of impurity in blue spinel from the Luc Yen mining area, Yen Bai Province, Vietnam. L.T.T. Huong, T. Haeger and L. Phan, *Vietnam Journal of Earth Sciences*, **40**(1), 2017, 47–55, http://dx.doi.org/10.15625/0866-7187/40/1/10915.*

Trace-element compositions of sapphire and ruby from the eastern Australian gemstone belt. J. Wong, C. Verdel and C.M. Allen, *Mineralogical Magazine*, **81**(6), 2018, 1551–1576, http://dx.doi.org/10.1180/minmag.2017.081.012.

INSTRUMENTATION

Application of near infrared spectroscopy in the study of gems. X. Li, L. Yu and E. Zu, *Spectroscopy and Spectral Analysis*, **38**(1), 2018, 54–57 (in Chinese with English abstract).

Let there be light – Light sources for colored gemstones. K. Feral, *Gemmology Today*, May 2018, 64–70, www.worldgemfoundation.com/GTMay2018.*

The value of simple, portable instruments – Part 3. How to use a loupe. A. Matlins, *Gemmology Today*, May 2018, 38–40, www.worldgemfoundation.com/GTMay2018.*

MISCELLANEOUS

50th anniversary of "The Diamond Fund of Russian Federation" exhibition. E.G. Gapanyuk, *Mineralogical Almanac*, **23**(1), 2018, 4–23.

Bring on blockchain? M. Hoare, *Gems&Jewellery*, **27**(1), 2018, 38–39.

Collecting engraved gems. H.J. Rambach, *GemGuide*, **37**(2), 2018, 13–18.

Getting your facts right [gemmological nomenclature]. R. Galopim de Carvalho, *Gems&Jewellery*, **27**(1), 2018, 28–29.

Taiwan's new Jurassic Museum. C. Unninayar, *InColor*, No. 38, 2018, 12–13.*

Yield of the earth [mineralogical stamp collection]. P.R. Cheer, *Gems&Jewellery*, **27**(1), 2018, 36–37.

NEWS PRESS

5,000-year-old cosmetics, jewelry show rise of ancient Jericho. P. Bohström, *National Geographic*, 19 December 2017, https://news.nationalgeographic.com/2017/12/jericho-ancient-archaeology-egypt-bible.*

Biggest fake Native American art conspiracy revealed [counterfeit jewellery]. M. Cornell, *National Geographic*, 15 March 2018, https://news.nationalgeographic.com/2018/03/native-american-indian-art-fake-forgery-hopi-zuni0.*

Blockchain used to track gems to counter blood diamonds and fakes. T. Shapshak, *Forbes*, 10 May 2018, www.forbes.com/sites/tobyshapshak/2018/05/10/blockchain-used-to-track-gems-to-counter-blood-diamonds-and-fakes/#537cbf3d18f6.*

De Beers to pilot digital programme in Sierra Leone to sell ethically sourced diamonds. H. Sanderson, *Financial Times*, 19 April 2018, www.ft.com/content/8ff2414c-43d6-11e8-93cf-67ac3a6482fd.

Does destroying ivory save elephants? Experts weigh in. J. Actman, *National Geographic*, 2 August 2017, https://news.nationalgeographic.com/2017/08/wildlife-watch-ivory-crush-elephant-poaching.*

Hong Kong moves to ban all sales of ivory by 2021. T. May, *New York Times*, 31 January 2018, www.nytimes.com/2018/01/31/world/asia/hong-kong-elephant-ivory.html.*

ORGANIC GEMS

Amber through the eyes of a geologist. B. Kosmowska-Ceranowicz, *InColor*, No. 38, 2018, 58–61.*

Baltic amber—The artistic context. A. Sobecka and M. Kosior, *InColor*, No. 38, 2018, 66–68.*

Baltic amber (succinite) gemstones and the main aspects of identification: An outline. E. Wagner-Wysiecka and M. Kosior, *InColor*, No. 38, 2018, 54–56.*

Burmese amber: Evidence of Gondwanan origin and Cretaceous dispersion. G. Poinar, *Historical Biology*, 2018, 6 pp., http://dx.doi.org/10.1080/08912963.2018.1446531.

CITES and products of endangered and threatened species used in jewelry. C.I. Carmona, *InColor*, No. 38, 2018, 80–84.*

Chapter 13: Hukawng basin, the amber mines, and the Orbitolina limestone. A. Mitchell, *Geological Belts, Plate Boundaries, and Mineral Deposits in Myanmar*, Elsevier, Amsterdam, The Netherlands, 2018, http://dx.doi.org/10.1016/b978-0-12-803382-1.00013-4.

Inclusions in Baltic amber. E. Sontag, *InColor*, No. 38, 2018, 62–65.*

Precious corals. R. Galopim de Carvalho, *InColor*, No. 38, 2018, 70–78.*

A review of preservational variation of fossil inclusions in amber of different chemical groups. V.E. McCoy, C. Soriano and S.E. Gabbott, *Earth and Environmental Science Transactions of the Royal Society of Edinburgh*, **107**(2–3), 2018, 203–211, http://dx.doi.org/10.1017/s1755691017000391.

So, what is ivory? M. Campbell Pedersen, *InColor*, No. 38, 2018, 86–91.*

PEARLS

The boom in pearls. J. Heebner, *GemGuide*, **37**(3), 2018, 10–13.

DNA techniques applied to the identification of *Pinctada fucata* pearls from Uwajima, Ehime Prefecture, Japan. K. Saruwatari, M. Suzuki, C. Zhou, P. Kessrapong and N. Sturman, *Gems & Gemology*, **54**(1), 2018, 40–50, http://dx.doi.org/10.5741/GEMS.54.1.40.*

Energy-resolved neutron tomography of an unconventional cultured pearl at a pulsed spallation source using a microchannel plate camera. G. Vitucci, T. Minniti, D. Di Martino, M. Musa, L. Gori, D. Micieli, W. Kockelmann, K. Watanabe, A.S. Tremsin and G. Gorini, *Microchemical Journal*, **137**, 2018, 473–479, http://dx.doi.org/10.1016/j.microc.2017.12.002.

Fiji cultured pearls—A vision for a blue industry. L.E. Cartier and J. Hunter, *InColor*, No. 38, 2018, 44–47.*

From tissue to bead—The transformation of the Chinese cultured freshwater pearl industry. J. Shepherd, *InColor*, No. 38, 2018, 48–52.*

Impact of spat shell colour selection in hatchery-produced *Pinctada margaritifera* on cultured pearl colour. C. Ky, M. Sham Koua and G. Le Moullac, *Aquaculture Reports*, **9**, 2018, 62–67, http://dx.doi.org/10.1016/j.aqrep.2017.12.002.

Quantitative discrimination of pearls using polarization-sensitive optical coherence tomography. J.H. Lee, J.G. Shin, H.Y. Kim and B.H. Lee, *Applied Optics*, **57**(9), 2018, 2197–2201, http://dx.doi.org/10.1364/ao.57.002197.*

Resurrecting an industry [cultured pearls from the United Arab Emirates]. C. Van Eerde, *Gems&Jewellery*, **27**(1), 2018, 12–14.

SOCIAL STUDIES

Agrarian distress and gemstone mining in India: The political economy of survival. A.R. Chowdhury and K. Lahiri-Dutt, in K. Lahiri-Dutt, Ed., *Between the Plough and the Pick*, ANU Press, Acton, Australia, 2018, 89–115, http://dx.doi.org/10.22459/BPP.03.2018.*

"As long as it sparkles!": The diamond industry in nineteenth-century Amsterdam. S. Coenen Snyder, *Jewish Social Studies*, **22**(2), 2017, 38–73, http://dx.doi.org/10.2979/jewisocistud.22.2.02.

Rice, sapphires and cattle: Work lives of women artisanal and small-scale miners in Madagascar. L. Lawson, in K. Lahiri-Dutt, Ed., *Between the Plough and the Pick*, ANU Press, Acton, Australia, 2018, 171–192, http://dx.doi.org/10.22459/BPP.03.2018.*

Social insecurity, stability and the politics in West Africa: A case study of artisanal and small-scale diamond mining in Guinea, 1958–2008. P. Diallo, *The Extractive Industries and Society*, **4**(3), 2017, 489–496, http://dx.doi.org/10.1016/j.exis.2017.04.003.

Tanzanite: Commodity fiction or commodity nightmare? K.C. Donahue, in K. Lahiri-Dutt, Ed., *Between the Plough and the Pick*, ANU Press, Acton, Australia, 2018, 63–88, http://dx.doi.org/10.22459/BPP.03.2018.*

Timely rubies. Temporality and Greenlandic gems. N. Brichet, *The Extractive Industries and Society*, **5**(2), 2018, 267–273, http://dx.doi.org/10.1016/j.exis.2018.03.001.

SYNTHETICS

Influences of each stage time on diamond in the synthesis process. W. Yin, J. Shao, H. Jiang, H. Mao, J. Yang, Y. Zhang and Y. Yao, *Superhard Material*

Engineering, **29**(6), 2017, 41–45 (in Chinese with English abstract).

Preparation of "natural" diamonds by HPHT annealing of synthetic diamonds. C. Fang, Y. Zhang, Z. Zhang, C. Shan, W. Shen and X. Jia, *CrystEngComm*, **20**(4), 2018, 505–511, http://dx.doi.org/10.1039/c7ce02013a.

Progress research on deposition of large size single crystal diamond. Z. Zhang, W. Lu and D. Zuo, *Journal of Synthetic Crystals*, **46**(12), 2017, 2417–2421 and 2437 (in Chinese with English abstract).

Synthetische Diamanten – eine aktuelle Betrachtung [Synthetic diamonds – A current observation]. U. Henn, T. Stephan, C.C. Milisenda, F. Schmitz and S. Müller, *Gemmologie: Zeitschrift der Deutschen Gemmologischen Gesellschaft*, **66**(3/4), 2017, 59–76 (in German with English abstract).

TREATMENTS

Enhanced lapidary materials: Lapis and gold in quartz. H. Serras-Herman, *GemGuide*, **37**(3), 2018, 4–9.

FWHM calculation of zircon gem-materials before and after thermal enhancement. P. Wattananurak, N. Monarumit, R. Chooyoung, K. Won-In, S. Chotikaprakhan and S. Satitkune, *Key Engineering Materials*, **737**, 2017, 599–603, http://dx.doi.org/10.4028/www.scientific.net/KEM.737.599.

Identification characteristics of the irradiated blue diamond. H. Zhu, T. Li, F. Yan, P. Wang and X. Zhao, *Superhard Material Engineering*, **29**(6), 2017, 62–64 (in Chinese with English abstract).

Identification of HPHT-treated hydrogen-rich diamonds by optical absorption and photo luminescence spectroscopy techniques. Z. Song, T. Lu, J. Su, J. Ke, S. Tang, J. Li, Gao-bo and J. Zhang, *Rock and Mineral Analysis*, **37**(1), 2018, 64–69 (in Chinese with English abstract).

Reinheitsveränderungen bei Diamanten [Clarity enhancement of diamonds]. U. Henn, T. Stephan and F. Schmitz, *Gemmologie: Zeitschrift der Deutschen Gemmologischen Gesellschaft*, **66**(3/4), 2017, 77–84 (in German with English abstract).

Spectroscopic characteristics of treated-color natural diamonds. M. Wang, G. Shi, J.C.C. Yuan, W. Han and Q. Bai, *Journal of Spectroscopy*, 2018, article 8153941, 10 pp., http://dx.doi.org/10.1155/2018/8153941.*

COMPILATIONS

***G&G* Micro-World.** Beryl crystal in fluorite • Diamond with interesting etch channels • Omphacite-chromite inclusion in diamond • Agate-like banding in opal • Dendritic inclusion in Cambodian sapphire • Green crystals in yellow sapphires • Celestial inclusion scene in sapphire • Pink tourmaline in spodumene • Cr-diopside in diamond. *Gems & Gemology*, **54**(1), 2018, 66–73, www.gia.edu/gg-issue-search?ggissueid=1495261209900&articlesubtype=microworld.*

Gem News International. Tucson 2018 • Gems from Arnoldi International • Updates on Namibian/Russian demantoid and Brazilian/Colombian emerald • Liddicoatite exhibit • Mexican and Australian opal outlook • Blue/brown Indonesian opal • Cultured pearl update • Secondary gem market • Oregon sunstone • Kenyan tsavorite mining • Arkansas turquoise • Vibrant colors on display • Carvings by Michael Dyber • Recutting by Rex Guo • Jewellery by Erica Courtney and Paula Crevoshay • Responsible practices • Supply chain transparency • Buccellati design award • Aquamarine from Pakistan • Phenakite from the Ural Mountains, Russia • Freshwater pearls from Texas • Very small akoya cultured pearls • Irradiated, annealed blue type Ia diamond • Microscope upgrade kit • International Diamond School • Gem-A photography award. *Gems & Gemology*, **54**(1), 2018, 74–110, www.gia.edu/gg-issue-search?ggissueid=1495261209900&articlesubtype=gni.*

Lab Notes. Fracture-filled diamond with 'rainbow' flash effect • HPHT-treated diamond fraudulently represented as untreated • Cat's-eye demantoid and brown andradite with horsetail inclusions • Orange pyrope-spessartine-grossular • Plastic opal imitation from Kyocera • Pearlfish natural blister pearl in *Pinctada maxima* shell • Five CVD synthetic diamonds over 3 ct • Fancy Deep brown-orange CVD synthetic diamond. *Gems & Gemology*, **54**(1), 2018, 56–64, www.gia.edu/gg-issue-search?ggissueid=1495261209900&articlesubtype=labnotes.*

**Article freely available for download, as of press time*

The Gem-A Conference 2018

BOOKING NOW OPEN!

If you are a Gem-A member or student, you will receive an email with a code to unlock special member and student rates.

To book, go to Eventbrite:
gem-a-conference-2018.eventbrite.com

- Discover an amazing line-up of **speakers** from all corners of gemmology
- Network with **industry leaders** during the Conference and at the Saturday evening dinner
- Learn from speakers and **fellow delegates**
- Attend **exclusive workshops** and enjoy guided trips including private viewings
- Be part of our **global community** of gemstone and diamond enthusiasts and professionals
- The Conference concludes with the **Gem-A Graduation** and Presentation of Awards!

3-4 November
etc. venues
County Hall,
London, UK

Every kind of bird resorts to a fruitful tree

— Sri Lankan Proverb

Pala International

PalaGems.com / PalaMinerals.com

+1 800 854 1598 / +1 760 728 9121

Padparadscha Sapphire from Sri Lanka • 6.02 ct • 11.10 x 8.06 x 7.17 mm

Bloom from Pala International Grounds • Photo: Mia Dixon